University of Alberta

Vitrinite Upgrading and Phosphorus Removal For Teck Coals

by

Seyed Ali Khakbazan Fard

A thesis submitted to the Faculty of Graduate Studies and Research
in partial fulfillment of the requirements for the degree of

Master of Science

in

Chemical Engineering

Department of Chemical and Materials Engineering

Spring 2013
Edmonton, Alberta

This thesis is dedicated to my wife: Sepideh Emam

Her love, patience, support and understanding have lightened up my spirit to finish this study and this thesis.

Abstract

The efficiency of gravity based separation and froth flotation techniques on vitrinite macerals upgrading and ash removal for two bituminous coals (Fording River and Coal Mountain Operation) has been investigated. Efficiency of these techniques for phosphorus removal for Fording River sample has also been evaluated. Density-based separation of Fording River sample revealed that highest vitrinite recovery can be achieved for < 425 µm size and < 1.45 $g.cm^{-3}$ density and phosphorus is more concentrated in heavier densities. Using Air dense medium fluidized bed, clean coal with low ash and phosphorus content has been achieved for both samples. Vitrinite upgrading in clean coal was achieved for > 2.36 mm particle size of Fording River and entire particle size range for Coal Mountain Operation sample. Using Denver cell, the effects of flotation kinetics and change in the pulp pH on the vitrinite upgrading in clean froth for both coals have been determined.

Acknowledgement

I would like to acknowledge my supervisors Dr. Qingxia Liu and Dr. Rajender Gupta for their guidance, patience and encouragement throughout the course of this thesis. My gratitude also expands to TECK Resources Limited for the financial support and all members of Canadian Centre for Clean Coal/Carbon and Mineral Processing Technologies (C^5MPT) and the staff in the Department of Chemical and Material Engineering for their kind assistance throughout my graduate studies.

Table of Contents

List of Tables

List of Figures

List of Nomenclatures

A_C	Ash content of clean coal
A_T	Ash content of tailing
A_t	Cross sectional area of the bed
d_{sv}	Mean particle size of ADMFB medium
d_p	Geometric diameter based on screen analysis (μm)
E_p	Separation efficiency for fluidized bed
$F.E.I$	Flotation efficiency index
g	Acceleration of gravity (9.81 m/s)
H_{mf}	Bed depth
ΔP	Pressure drop between two points in the bed
m	Weight of the bed
R	Recovery of clean coal
$Re_{p,mf}$	Reynolds number of particles at minimum fluidizing conditions
u_{cf}	Complete fluidization velocity
u_{mb}	Minimum bubbling velocity
u_{mf}	Superficial gas velocity at minimum fluidization conditions (cm/s)
V_D	London-van der Waals dispersion energy
V_E	Electrostatic interaction energy V_E
V_H	Hydrophobic interaction energy
V_T	Total surface energy between an air bubble and a hydrophobic solid particle V_T
ε	Fluidized bed void
ε_{mf}	Void fraction at minimum fluidizing conditions (dimensionless)
μ	Viscosity of gas (kg/m·s)

ρ	Average density of the fluidized bed
ρ_g	Gas density (kg/m^3)
ρ_f	Density of fluid
ρ_s	Solid density (kg/m^3)
ρ_P	Medium solids density
φ_s	Sphericity of a particle (dimensionless)

Chapter1. Introduction

Metallurgical coke has been traditionally used as the support for the iron burden in blast furnaces as well as the reducing agent for reduction of iron ore to iron (Tillman et al., 2012). However, properties of the metallurgical coke have a significant impact on the quality of the resultant steel. The level of impurities such as ash, sulphur, phosphorus and volatile matter in coal is one the factors which affects the performance of metallurgical coke in the blast furnace (Díez et al., 2002). A high ash coke produces high volume of slag in the blast furnace and as a result the furnace productivity worsens (Strassburger, 1969). Moreover, high ash content in original coal has a negative effect on the physical strength of the coke (CSR and CRI indexes) (Stepanov, Gilyazetdinov, Popova, & Makhortova, 2005). High level of phosphorus in coke also reduces the hardness of the steel and makes the final product brittle (Chaudhary, 1999). Therefore, it is necessary to reduce the level of such impurities in the coal.

Another important factor which affects the performance of the metallurgical coke in blast furnace is the petrographic composition of the original coal. It has been well demonstrated that vitrinite-rich coals yield in cokes of higher physical strength due to higher reactivity of vitrinite in carbonization process (Suárez-Ruiz and Crelling 2008).

In industry, heavy medium vessels and heavy medium cyclones have been used for cleaning of coarse coal and hydro-cyclone have been utilized for the fine coal (- 0.5 mm) beneficiation (Zhou, 1986). However, in recent years, use of dry cleaning methods for cleaning of coal has been investigated. Lower operating and construction cost as well as lack of need for water are the main advantages of these methods (Zhenfu & Qingru, 2001b).

The main objective of this project was to improve the coking quality of two western Canadian coals (Fording River and Coal Mountain Operation) by upgrading the vitrinite content and reducing the ash and phosphorus level in the studied coals either by means of density separation or surface properties-based methods.

The project was conducted in three phases. In the first phase of this project, the distribution of ash, phosphorus and macerals in different particle size ranges and different density fractions of the Fording River coal were analyzed. For that purpose, sink float tests have been conducted for different particles sizes of Fording River sample at selected density cut-points (range from 1.39 $g.cm^{-3}$ to 2.00 $g.cm^{-3}$) using CsCl solution as the heavy medium. The collected samples were analyzed for ash, phosphorus and macerals distribution.

In the second phase of the project, use of air dense medium fluidized bed as a dry density based separator for vitrinite upgrading and ash and phosphorus removal for both coal samples in > 1 mm size fraction has been evaluated. Since most of the vitrinite in coal is concentrated in the low densities (< 1.6 $g.cm^{-3}$), a low density fluidized bed has been designed using silica sand as the dense medium.

In the last phase of the project, potential of froth flotation technique for separation of high vitrinite and low ash and phosphorus froth for both studied coal samples has been tested. Effect of particle size on the efficiency of flotation has been evaluated. In addition, effect of change in the pulp pH on the ash, phosphorus and vitrinite content of the froth has been studied. Moreover, the effect of flotation time on the froth maceral content has been tested. Finally, for the Coal Mountain Operation sample, the effect of collector dosage on the efficiency of ash separation has been investigated.

Chapter2. Literature Review

Coal is a sedimentary rock which forms through million years of carbonification process of plants debris. As the world second source of energy, Coal reserves are found all over the world with the largest one in the Unites States (U.S Energy Information Administration, 2011). Canada has 8.7 billion tons of proved reserves of coal with 6.6 billion tons recoverable with current technology. Canada is also the second largest exporter of coking coal. Around 40% of its total annual coal production belongs to metallurgical coal Most of the exported coal exploits from British Columbia and Alberta provinces mines (Natural Resources Canada, 2010).

Metallurgical coke is the carbonaceous residue results from destructive distillation of coal in an inert environment in temperatures up to 1400 K. Around 90% of the produced metallurgical coke is utilized in blast furnaces to produce steel (Díez et al., 2002). The metallurgical coke plays three important roles in the process of steel making. As a reducing agent, it reduces iron ore to iron. Also as a fuel it provides energy for chemical reactions. Thirdly, it acts as a support in blast furnace to bear the iron burden in blast furnace and have reasonable porosity to allow the passage of slag and metal downward and hot air upward the blast furnace (Díez et al., 2002; Tillman et al. , 2012). The first two roles (reducing agent, energy provider for chemical reactions) can be fulfilled by other sources like oil, gas, plastics and coal. However, none of those materials can be utilized as the permeable support in blast furnaces (Díez et al., 2002). Over past few decades, significant effort has been put to enhance the blast furnace performance not only by means of increase in the calorific value of the coke but also by improving the strength and thermoplastic properties of coke. Presence of impurities in coke (such as moisture, volatile matter, ash, sulphur, phosphorus, and alkali contents) deteriorates calorific value, the reducing capability and permeability of coke in blast furnace. From above mentioned impurities, ash and sulphur have

more impact on the reduction of coke productivity and increase in the volume of slag in the blast furnace (Díez et al., 2002). Table 2.1 listed some of the specification that metallurgical coke should meet in order to use in blast furnaces for Canadian plants.

Table 2.1 Requirements of metallurgical coke for Canadian plants (Gransden et al., 1991)

Coke property	Canadian standard
Ash (%)	< 8.0
Volatile matter (%)	< 1.0
Sulphur (%)	< 0.7
Alkali oxides (%)	< 0.2
Phosphorus pentoxide(%)	0.27
Coke stability (ASTM)	60

Moreover, physical properties of coke (e.g. DI 50/15 ASTM stability, CSR, CRI) which are functions of its size and mechanical strength also influenced the role of coke as a permeable support in the blast furnace. Coke properties are mainly affected by the original coal properties as well as the conditions of carbonization process (Miller, 2010). Therefore, it is crucial for the original coal to meet the requirements for the chemical and physical properties before utilization in coke making. Table 2.2 lists typical ranges of some chemical properties for coking coal.

Table 2.2 Required coal properties for coke production (Miller, 2010)

Coal parameter	Typical values
Volatile matter, wt.% (dry, ash free)	24-28
Ash content, wt.%	<10
Sulphur content, wt.%	~ 0.5
H/C ratio	0.725
O/C ratio	0.04
Heating value Btu/lb (moist, mineral matter free)	~15500
Vitrinite reflectance,%	~1.25
Maximum fluidity, dial divisions per minute	~1000

Thermoplasticity (fluidity) of the resultant metallurgical coke can be predicted based on the petrographic composition of the coal. Petrographic composition of the coal consists of macerals (organic) and minerals (inorganic) constituents. In the following sections of this chapter, macerals and minerals properties will be discussed and effect of their distribution in coal on the resultant coke will be studied. Moreover, the effect of presence of phosphorus as an undesired element in coal in blast furnace performance will be investigated.

2.1 Petrographic constituents of coal

2.1.1 Macerals

Coal mainly constitutes of organic (macerals) and inorganic (minerals) components. Based on the morphology, level of reflectivity and the plant of origin, macerals are generally divided in to three main groups: vitrinite, liptinite and inertinite. Each of the individual macerals has its own chemical and physical properties (Ward, 1984).

Vitrinite macerals are originated from decomposition of stems, roots and leave of plants. They are also products of colloidal humic gels carbonification. They have the highest oxygen content among the macerals (Ward, 1984). They have the moderate thermoplastic properties among macerals which make them suitable to use for making good quality metallurgical coke (Honaker, Mohanty, & Crelling, 1996).Vitrinite appears medium gray in reflected light which is in contrast to the darker liptinite and lighter inertinite macerals (Ward, 1984). Vitrinite reflectance is a parameter that is commonly used to determine the rank of the coal for geological classification and also predict coal coking properties (Jiménez, Iglesias, Laggoun-Défarge, & Suárez-Ruiz, 1998). The vitrinite density varied in the range of 1.30 - 1.45 g/cm^3 and this range may change with the rank and type of the coal (Holuszko, 1979).

Liptinite macerals are originated from the exterior layer or exine of spores and pollens as well as the leaf cuticle materials, resins, algae, waxes and fats (Ward, 1984). They have higher aliphatic (paraffin) content As compared with vitrinite macerals (Holuszko, 1979). Liptinite has the highest hydrogen content, calorific value and reactivity among the macerals (Thomas, 2002). As a result, it produces considerable amount of gas and tar during carbonization. Coals which are rich in liptinite are preferable for hydrogenation. For low rank coals, liptinite has lower reflectivity as compared with vitrinite. As rank of the coal increases, the liptinite reflectance increases and approaches vitrinite reflectance in low-volatile bituminous coal (Holuszko, 1979). Coal strength is also enhanced by increase in the liptinite content of the coal (Falcon, 1978). The liptinite density varies in the range of 1.00 - 1.25 g/cm^3 (Dyrakacz, Bloomquist, Ruscic, & Horwitz, 1983).

Inertinite macerals have the same source materials as the vitrinite group but they differ in their properties due to the oxidation of those source materials in early stage of coalification (Ward,

1984). The name “Inertinite” was chosen for this group due to the fact that inertinite macerals are mostly inert in hydrogenation and carbonization processes. This behavior is attributed to their low hydrogen content (Thomas, 2002). However, one the inertinite macerals called “semi-fusinite” shows some degree of reactivity in the carbonization process. Therefore, the term “semi-inert” has been proposed by some workers to describe this maceral (Ward, 1984). Inertinite macerals have higher specific gravities as compared with other maceral groups (Holuszko, 1979).

Each of the individual macerals is a value-added product that has its own specific application. Liptinite macerals are considered as the most valuable macerals. Concentrates of liptinite macerals can be used to produce resins and waxes (Honaker et al., 1996). It has been reported that a product with 85% resinite content can have a market value of 1000 $/ton (Miller, Jensen, Yu, & Yea, 1992).Vitrinite concentrates also can be utilized as a solid fuel and be sold at the same price as a liquid hydrocarbon fuel with same thermal value (Yang, 1990) . Fig 2.1 shows the potential application of all macerals (Honaker et al., 1996).

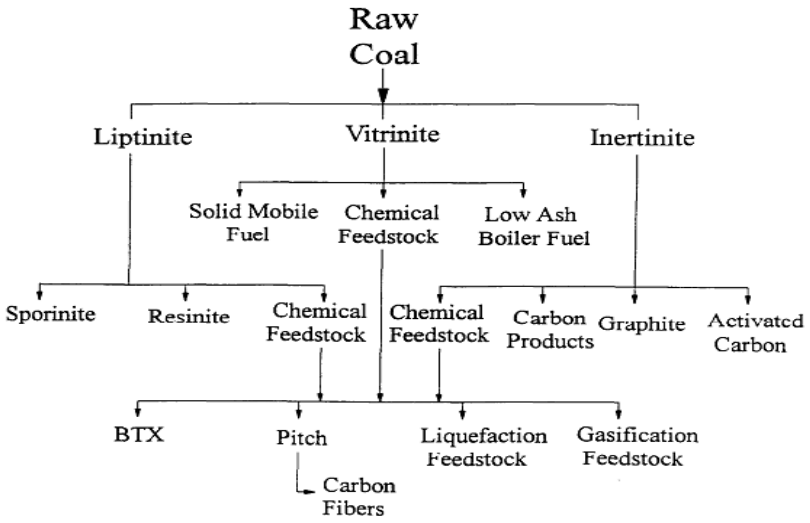

Fig 2.1 Potential application of maceral concentrates (Honaker et al., 1996)

2.1.2 Mineral matters

The mineral matter in coal consists mainly of clays (e.g. kaolinite and montmorillonite) , quartz and carbonate minerals like calcite ,dolomite, gypsum, and pyrite (Jia, Harris, & Fuerstenau, 2000). According to Mackowsky (Mackowsky, 1983), coal mineral matters are classified in to three types: detrital, syngenetic, and epigenetic. Those minerals which were deposited by natural currents of wind or water in swamps are called detrital. Illite clay, part of the quartz minerals and zircon are examples of detrital minerals. Minerals which were formed inside coal peat at the time of accumulation of plant debris are called syngenetic. Part of the pyrite in the coal, micron-size crystals of quartz, hematite and kaolinite are the examples of syngenetic minerals. Epigenic minerals were formed mainly long after the early stage of coalification (peat formation), when it reached its present rank. Most of the calcite and part of the pyrite in coal are categorized in epigenic minerals (Harvey & Ruch, 1984).

Among macerals, vitrinite has been considered to have the lowest mineral matter content while fusinite has the greatest potential for secondary mineral deposition and is more associated with minerals. This characteristic of fusinite is attributed to its cellular structure (Holuszko, 1979).

2.2 Effect of coal petrographic composition on coke thermoplastic properties

Based on the reactivity in carbonization process, coal petrographic constituents can be classified as reactive and inert components. Reactive component are those who can be easily fluidized during the coking process while inert materials are those who remain less reactive or non-reactive during the carbonization process (Tillman et al., 2012). Among coal macerals, vitrinite is the primary reactive component with moderate thermoplastic properties (fluidity) (Suárez-Ruiz

and Crelling 2008). During carbonization process in a reducing atmosphere, vitrinite easily fluidizes and forms in to a plastic mass, devolatilizes and solidifies into a porous structure. Liptinite exhibit higher fluidity and reactivity than vitrinite. However, it contributes more to by-products formation rather than coke formation due to its higher volatile content. On the other hand, inertinite has lower fluidity as compared with other macerals and hence is less reactive. Mineral matters are also considered non-reactive during the carbonization process (Tillman et al., 2012). In general, vitrinite works as binders in coke structure while inert components only act as fillers to reinforce the coke cell wall (Suárez-Ruiz & Crelling, 2008). Presence of large amount of inertinite macerals in original coal results in formation of weak spots in the produced coke and reduces the strength of coke (Díez et al., 2002). Therefore, finding the optimum ratio of inert to reactive components in coking coal or blends of coking coals is the key factor to obtain good metallurgical coke. One of the earliest models to predict North American coals macerals reactivity is Schapiro model (Schapiro & Gray, 1964)**.** This model assumes vitrinite, liptinite and one third of the semi-fusinite in the coal to be reactive and the rest which include other inertinite group macerals (such as fusinie, micrinite macrinite and inertodetrinite) and mineral matter to be inert (Gransden et al., 1991). Using macerals content distribution and vitrinite reflectance data, the optimum ratio of reactive to inert component for each vitrinoid type are determined and the composition balance index (CBI) is calculated. Composition balance index (CBI) is defined as the ratio of the inert component in the given coal to the optimum inert components which belong to the strongest possible coal from the same rank. In addition, strength index (SI) or rank index (RI) also can be determined. RI indicates the effect of rank and type of coal on coke strength. Using these two parameters, the ASTM stability factor can be determined which is used as an indicator of the coke strength (Díez et al., 2002). However, this classification cannot be applied

to all coals due to differences in reactivity of macerals from one type of coal to another one (Gupta, Shen, Lee, & O'Brien, 2012). For Cretaceous coals from Western Canada which are rich in semifusinite but have low micrinite and exinite content, the coke strength values predicted based on Schapiro model are lower than those experimentally obtained (Gransden et al., 1991). To resolve this issue, a new model developed by (Carr & Jorgensen, 1975) which assumed half of the semifusinite reactive. This model was developed for coals with greater than 20% semifusinite content (Gransden et al., 1991). Another model also proposed by (Pearson, Price 1985), which used a new parameter called "cut-off'' reflectance or reactive ''cut-off'' value ($R_{cut\text{-}off}$) to separate reactive and non-reactive macerals in a random reflectogram of macerals. $R_{cut\text{-}off}$ was successfully correlated to vitrinite reflectance for 76 coals with Romax ranging from 0.89 to 1.63%. Using coke microscopy, a range of 33-50% has been determined for the reactivity of semifusinite in recent years. The reactive proportion changed from coal to coal but 50% reactive semifusinite is accepted for western Canadian coals (Díez et al., 2002)

2.3 Effect of phosphorus content on blast furnace performance

In order to improve the performance of blast furnaces it is necessary to reduce the level of phosphorus in coke. Almost all of the phosphorus in coal remains in the resulting coke and significant portion of it is carried from coke to the Iron produced in blast furnaces and the resultant steel (Ward, Corcoran, Saxby, & Read, 1996). High concentration of phosphorus in steel leads to segregation of grain boundaries and makes the steel brittle. It also reduces the weldability of steel (Chaudhary, 1999). However, presence of phosphorus in certain levels is harmless and even enhances the fluidity of casting (Chaudhary, 1999). The average phosphorus content of world coal reserves is around 0.05% (Chaudhary, 1999; Ward et al., 1996). However, a few coal seams (e.g. Permian coals from India and Australia and Cretaceous coals from

western Canada) have higher phosphorus content (Ryan & Grieve, 1996; Ward et al., 1996). Numerous researchers investigated the phosphorus distribution in coal to find out whether it has organic or inorganic affinity. Organic/inorganic affinity is a term which is frequently used to describe the mode of occurrence of a certain element in organic and inorganic parts of the coal (Ryan, Grieve 1996). One simple accepted way to determine the mode of occurrence of an element in coal is to plot the element concentration versus ash content as density increases. If the slope of the curve is positive, the studied element has organic affinity in coal (Ryan, Grieve 1996). One problem associated with this method is the uncertainty about the consistent distribution of phosphorus in all ash increments (Nicholls 1968). The second approach is to compare the element (in this case phosphorus) concentration of different density fractions obtained from gravitational sink-float tests (Gluskoter et al., Ruch et al. 1977). The elements with organic affinity should appear more frequently in lighter density fractions while those which are associated with mineral matter should appear in the heavier density fractions of coal. This method was built upon the assumption of mineral grains liberation prior to the separation.

Generally, the phosphorus in coal (and especially in high rank coals) was considered to be prevalently associated with mineral matter (Burchill, Howarth, Richards, & Sword, 1990). However small or uncertain proportion of phosphorus in coal assumed to have organic affinity (Swaine, 1990). Using washability analysis, (Gluskoter et al., 1977) found that for some coals phosphorus has inorganic affinity but in the majority of coal seems is associated with organic part of coal. Using ionic potential to divide elements in to organic and inorganic affinities, (Powell, 1987) suggested that P^{+3} ions have organic and P^{+5} ions have inorganic association in coal. In another study, the distribution of different elements in a lignite coal from North Dakota was investigated and it was concluded that phosphorus in the studied coal has uncertain or

inorganic affinity (Karner, Schobert, Falcone, & Benson, 1986). (Ward et al., 1996) studied the occurrence of phosphorus minerals in Australian coals and found that most of the phosphorus-bearing minerals were finely associated with particular macerals rather than minerals. In a recent paper, the effect of particle size on phosphorus content of a South African coal seam was studied (Claassens, 2009). It was observed that decrease in particle size had a less obvious effect on the phosphorus removal from coal than on the ash removal. Moreover, Apatite was described as the most common form of phosphorus bearing mineral in South African coal. (Grieve, 1992) studied some of the British Columbia coking coals. It was found that the phosphorus is mainly associated with inorganic part. Low temperature ash mineralogy of raw coal samples and correlation of phosphorus with fluorine in different seams were also presented to confirm this finding. An extensive study on British Columbia coking coals also had been done by (Ryan & Grieve, 1996). Even though the report confirmed the predominant association of phosphorus with inorganic parts for most of the studied coals, it pointed out that washing (density separation by means of sink-float) did not reduce the phosphorus content of the by coal more than 30 %. Based on this observation, it has been concluded that phosphorus does not follow ash in the cleaning process. The author suggested that blending with run-of-mine coal may help to control the phosphorus in the clean coal.

The phosphorus minerals in coal can be classified in to three main groups: apatite (which is a mineralized calcium phosphate (Burchill et al., 1990), cranadallite which is associated with aluminum and monazite which is associated with rare earth elements (Ryan & Grieve, 1996). Among them, apatite group minerals frequently reported in western Canadian coals (Grieve, 1992). Based on the relationship between phosphorus and fluorine, it has been speculated that the

apatite is presented in the form of the flour-apatite ($Ca_5 F (PO_4)_3$) in coal (Burchill et al., 1990; Grieve, 1992).

2.4 Coal Beneficiation

"Coal beneficiation" is a term that is used to describe all processes which are associated with preparing coal for specific applications (Mak, 2007). Coal beneficiation processes have been used traditionally to upgrade the quality of raw coal by reducing the ash and sulfur content of the coal. Besides that, coal cleaning and beneficiation reduce the cost of coal transportation and disposal, improve the combustion efficiency and prevent the slag formation in furnace (Gupta, 1990).

Coal beneficiation methods can be categorized in to physical, chemical and biological methods. Physical methods are used to remove the inorganic sulfur and ash from the coal. The chemical and biological methods are mostly considered as the supplementary treatment to physical methods to remove the inorganic sulfur from treated coal (Gupta, 1990).

All physical methods are working based on the differences in the physical properties (like density, surface properties, magnetic susceptibility, electric resistivity, etc) between macerals and minerals and among macerals themselves. As a general rule, larger than 500 μm coal particles are subjected to density based coal beneficiation processes while fine size coal particles (smaller than 500 μm) are mainly subjected to processes which are based on differences in surface properties (like hydrophobicity) between macerals and minerals and among the macerals. Coal beneficiation methods can be classified as dry and wet cleaning methods (Gupta, 1990).

2.4.1 Wet cleaning methods

Wet beneficiation methods include: Froth flotation, oil agglomeration, heavy medium vessels, heavy medium cyclones, hydro cyclones, jigs, spirals and concentrating tables (Gupta, 1990; Zhou, 1986). Traditionally, heavy medium vessels have been used for coarse coal (6.3 – 200 mm). Also, heavy medium cyclones can be used for the purpose of Intermediate-size coal (6.3 - 0.5 mm) separation and hydro-cyclone can be applied for fine coal (- 0.5 mm). All of these three methods are based on the principle of using a wet medium for gravity separation (Zhou, 1986). Jigs are also gravity-based separators in which water is used for the purpose of pulsating and washing (Zhou, 1986). The main disadvantage of wet cleaning methods is the additional cost associated with clean coal dewatering after these processes (Choung, Mak, & Xu, 2006).

2.4.1.1 Wet density-based method for separation macerals

Massive research has been done on the use of density gradient centrifugation (DGC) and Continuous flow centrifugation (CFC) as wet density-based separation methods for lab-scale separation and isolation of individual macerals in fine coals (Bloomquist, & Horwitz, Dyrkacz, 1981; Dyrkacz & Horwitz, 1982; Dyrkacz, Bloomquist, & Ruscic, 1984; Karas, Pugmire, Woolfenden, Grant, & Blair, 1985; C. Choi & Dyrkacz, 1989; Dyrkacz & Bloomquist, 1992a; Dyrkacz & Bloomquist, 1992b; Dyrkacz, Ruscic, & Fredericks, 1992). The methodology of maceral separation using DGC and CFC techniques was described by (Dyrkacz, 1994) in details. In first stage, coal is ground to less than 10 μm to ensure the complete liberation of macerals and mineral matter of coal. In second stage, the mineral matter of coal is removed using strong acids like HF and HCl. Finally, the mineral free coal is added to a centrifuge at which a density gradient is created with layers of different density from lightest one at top to the heaviest one at the bottom. It has been observed that using aqueous CsCl or Ca $(NO3)_2$ as the medium along

with Brij-35 as the surfactant, the coal particles are completely wetted and dispersed in solution and macerals isolation considerably improved (Dyrkacz & Horwitz, 1982). Using continuous flow centrifugation (CFC), larger amount of coal can be handled and higher separation efficiencies can be achieved (Dyrkacz & Bloomquist, 1992a). (Choi, Dyrkacz, & Stock, 1987) investigated the effect of macerals alkylation prior to use of DGC technique. Alkylation alters the density of macerals. It also changes the reactivity of sub-macerals and provides an opportunity to identify and separate sub-macerals of the same maceral group (e.g. Fusinite in inertinite group) which is not possible by simple density separation methods.

2.4.1.2 Froth flotation

Froth flotation is the most efficient process in industry for fine coal beneficiation (Honaker et al., 1996). It utilizes the differences in surface properties between macerals and minerals and among macerals as a driving force to separate them from each other (Piñeres & Barraza, 2011). As a general rule, hydrophilic minerals and some of the macerals which are weakly hydrophobic move downward to the tailing while more hydrophobic macerals move upward toward the froth layer (Piñeres & Barraza, 2012). The floatability of coal in this process is also rank dependent. As rank of the coal increases, its floatability increases through bituminous range (Hower, Frankie, Wild, & Trinkle, 1984). The main challenges in using this technique for coal beneficiation are: (i) poor selectivity of high rank coals (with high froth recoveries) with respect to macerals due to entrainment of mineral matter in froth zone and (ii) low froth recoveries for low rank coals and oxidized coals (Polat, Polat, & Chander, 2003). To address these problems, it is necessary to optimize the parameters which affect the flotation condition. Those parameters can be classified in to 4 main groups: materials, chemicals, operational and equipment (Polat et al., 2003). Fig 2.2 listed examples of each of those groups. Those parameters which are needed

to be regularly adjusted due to daily-basis fluctuations are presented as level I parameters. Those which are selected with in the design stage are listed in level II parameters and parameters which cannot be controlled because of practical limitation and material characteristics are categorized in level III parameters (Polat et al., 2003).

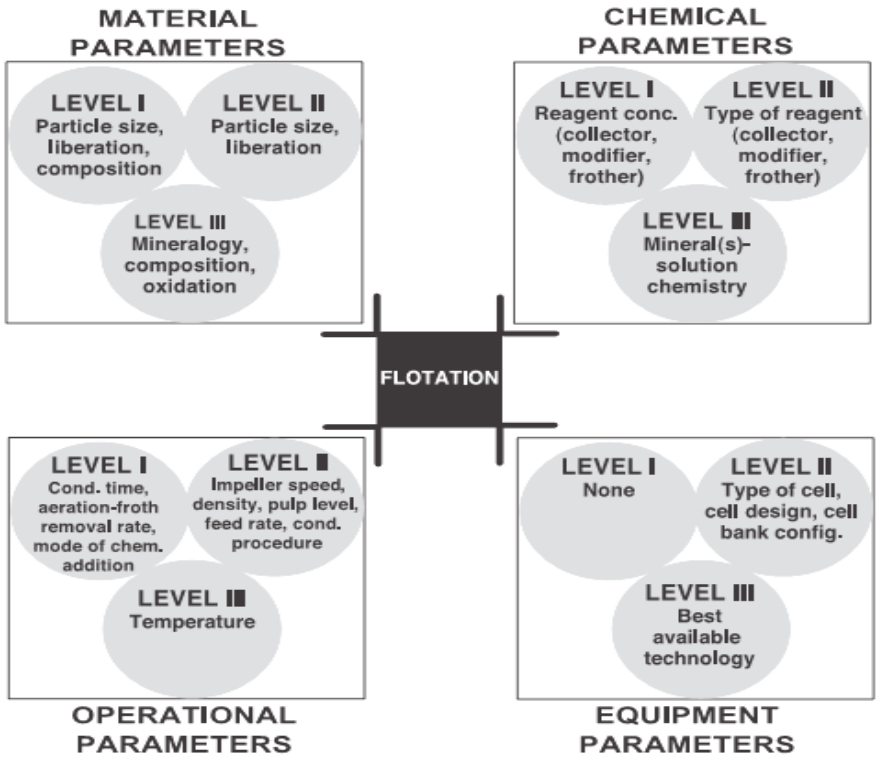

Fig 2.2 Froth flotation process parameters (Polat et al., 2003)

2.4.1.2.1 Effect of coal particle size on froth flotation

Generally, it has been proven that the flotation rate and hence froth recovery increase with increase in coal particle size until it reaches a maximum and further increase beyond that size lead to decrease in flotation rate and froth recovery. This behavior is attributed to the low particle-bubble collision probability in fines and high particle bubble detachment probability in large particle sizes (Al Taweel et al., 1986) . However, it is quite difficult to establish an exact relationship between the particle size and flotation rate due to the aggregation problem

associated with fines flotation which prevent identifying the effect of original particle size on the flotation rate (Polat et al., 2003).

2.4.1.2.2 Effect of collector addition on froth flotation

Collectors are water insoluble hydrocarbons which used to improve the bubble-particle adhesion. They have affinity toward hydrophobic surfaces (Kawatra & Eisele, 2001). Increase in the collector concentration in pulp results in higher froth recovery and also increase in particle - particle interaction which leads to the coal agglomeration. It also has been reported that collector addition improves the floatability of all particles in all sizes and densities but the effect is more significant for mineral matters (Naik, Reddy, & Misra, 2005). As a result, increase in the collector dosage results in lower combustible recovery (Naik et al., 2005). The most commonly accepted collectors in coal flotation are kerosene and fuels oil. Low viscosity which helps them to be dispersed easily over coal particles and their low cost make them advantageous over other collectors (Kawatra & Eisele, 2001; Garand, 1993)

2.4.1.2.3 Effect of frother addition on coal flotation

Water soluble reagents (frothers) have been frequently used in froth flotation process to reduce the bubble size, stabilize the froth layer and enhance the particle-bubble collision and adhesion (Polat et al., 2003). The reduction in bubble size with addition of frother to the pulp is attributed to decrease in liquid-vapor interface surface tension (Naik et al., 2005). Some of the frothers which commonly utilized in coal flotation are: methyl isobutyl carbinol (MIBC), polypropylene glycol, methyl ethers (e.g., Dowfroth 250) and phenol and cresylic acid (Polat et al., 2003). It has been experimentally established that increase in the frother dosage result in higher froth recovery but in the expense of less selective flotation and lower combustible recovery (Naik et al., 2005;

Piñeres & Barraza, 2012). In the presence of collector, frother also plays an important role in the collector emulsification and attachment of oil droplet to coal particle surface (Laskowski, 1993).

2.4.1.2.4 Maceral separation using selective froth flotation

Contact angle is the main indicator of the hydrophobicity of coal macerals. A low contact angle for a coal or individual maceral means low hydrophobicity and low floatability (Ofori, Firth, Obrien, McNally, & Nguyen, 2010). Based on the contact angle measurements which have been done on the varieties of north-American coals, it has been established that the hydrophobicity of the coal macerals decreases in the order of liptinite, vitrinite and inertinite (Arnold & Aplan, 1989). Contact angle and hydrophobicity also varies among macerals of the same group. Among liptinite macerals, sporinite (contact angle = 90°) is obviously less hydrophobic than resinite (contact angle = 120°)(Honaker et al., 1996). Table 2.3 shows the typical contact angle values for macerals in north-American coals (Honaker et al., 1996).

Table 2.3 Contact angles of macerals for North-American coal

Maceral group	Liptinite	Vitrinite	Inertinite
Contact angle (°)	90 – 130	60 – 70	25 - 40

For a successful particle-bubble attachment to happen, the total surface interaction energy between particle and bubble should be attractive. Therefore, providing a process environment at which desired particles have attractive surface interaction energy and undesired particles have repulsive surface interaction energy with bubbles significantly improves the selectivity of flotation towards the desired particles. As a modification to the Deraguin-Landau-Verwey-Overbeek (DLVO) theory, Xu and Yoon(Xu & Yoon, 1989; Xu & Yoon, 1990) suggested that the total surface energy (V_T) between an air bubble and a hydrophobic solid particle (such as coal) can be calculated using following formula:

$$V_T = V_E + V_D + V_H \qquad (2-1)$$

Where : V_E is the electrostatic interaction energy, V_D is the London-van der Waals dispersion energy and V_H is the hydrophobic interaction energy. V_D and V_E are repulsive in nature and hinder the particle bubble attachment for most of the bubble-particle interactions whereas V_H is attractive and promotes the particle bubble attachment. If the sum of repulsive energies (V_D and V_E) is small enough to be overcome by attractive energy (V_H), then the hydrophobic particle becomes floatable. On the other hand, if the sum of the repulsive energies becomes larger than hydrophobic interaction energy, the particle is rejected to the tailing.

The electrostatic interaction energy is mainly a function of ζ-potential (electrokinetic potential) and for coal particles; ζ-potential is strongly dependent on the concentration of H^+ and OH^- ions. Consequently, increase in the coal slurry pH can make the electrostatic interaction energy strongly repulsive and render the coal particle unfloatable. The more hydrophobic is a maceral, the higher is the value of ζ-potential needed to overcome the hydrophobic interaction energy and make it unfloatable (Honaker et al., 1996). Therefore, it is possible to change the floatability of different macerals and hence separate them from each other by changing pH.

Using conventional column flotation, Miller *et al.* achieved very high resinite maceral recovery for a western U.S coal seam by increase in the pH up to 12 (Miller et al., 1992). Since resinite has the highest hydrophobicity among all macerals (Arnold & Aplan, 1989), its floatability is not decreased by increase in the pH of medium. However the rest of the macerals are depressed at a pH value as high as 12. As a result, the resinite content of the studied coal significantly upgraded from 7% to 80% with 95% resinite recovery for -75μm feed coal (Miller et al., 1992; Yu, Bukka, & Miller, 1994). Fig 2.3 displays the effect of change in the ζ-potential values of each individual

macerals on the energy barrier which rises from interaction between the maceral and the air bubble. As seen from this figure, at ζ-potential values around -50 mV, the energy barrier for vitrinite and inertinite macerals become strongly large which render those macerals unfloatable while this energy barrier for liptinite macerals is still small and this condition allows selective flotation of liptinite rather than other macerals. In the same way, at ζ-potential values around -30 mV, both liptinite and vitrinite become floatable while the energy barrier for inertinite macerals is too large to be overcome by hydrophobic interaction energy Therefore, they become unfloatable.

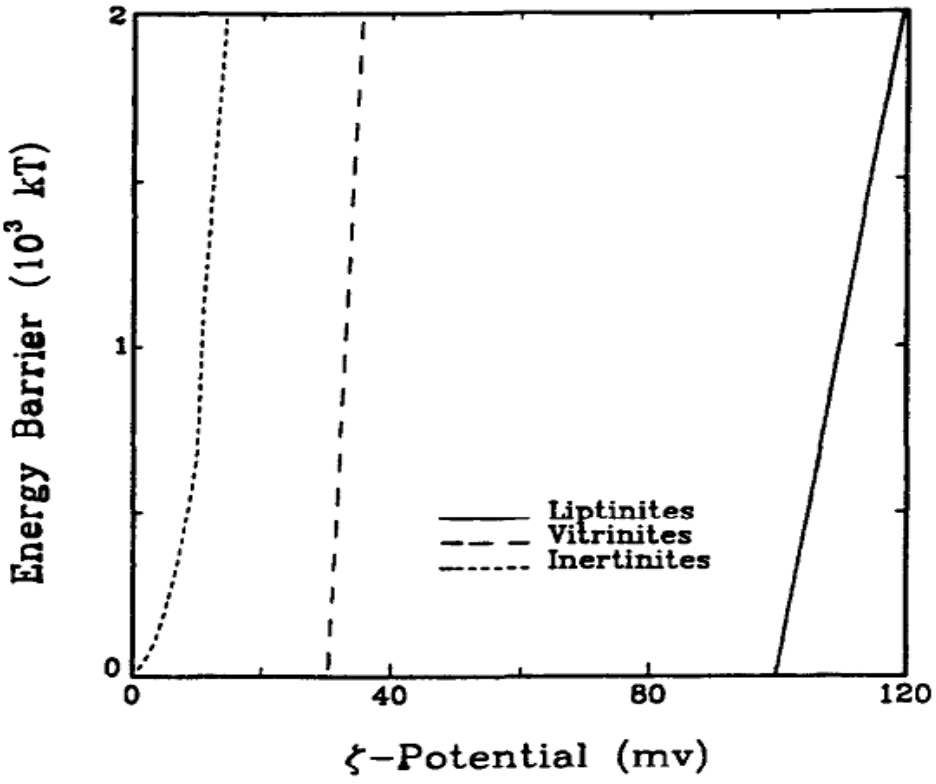

Fig 2.3 Effect of ζ-potential on the energy barrier for individual macerals
Bubble and particle diameter = 100 and 5 μm, respectively (Honaker et al., 1996)

Contrary to (Miller et al., 1992) results, the finding of (Honaker et al., 1996) showed that increase in pH from 8 to 11 resulted in reduction of liptinite floatability .However, vitrinite

floatability remained almost unchanged and inertinite floatability reduced around 50%. This difference can be attributed to the type of liptinite macerals in their studied coal. In the study conducted by Miller et al., western U.S coal is mainly associated with resinite maceral. Resinite is considerably more hydrophobic as compared with sporinite which is the main liptinite maceral in the Illinois basin coals (studied by Hoanker *et al.*). The similarity in surface hydrophobicity between sporinite and vitrinite macerals have been reported as one of the main challenges in efficient maceral separation of Illinois basin coals using this method (Honaker et al., 1996).

(Yu et al., 1994) investigated the effect of ozone conditioning on the selective flotation of resinite from the rest of the coal. Resinite is mainly consists of aliphatic components while the rest of the coal is mainly consists of the aromatic structures which contain more oxygen functional groups as compared with resinite. As a result, oxidation of coal during ozone conditioning has less impact on the resinite structure. However; it significantly reduces the hydrophobicity of the rest of the coal. This phenomenon increases the difference in hydrophobicity between resinite and rest of the coal, reduces the coagulation of resinite and rest of the coal in the slurry and provides an opportunity for selective flotation of resinite in flotation.

2.4.2 Dry beneficiation methods

In dry cleaning methods, coal and mineral matter are separated based on their differences in physical properties (i.e. size, shape. density, color, magnetic susceptibilities, electrical conductivity, etc) (Dwari & Rao, 2007). Generally, dry beneficiation methods can be classified into three main categories: mechanical, electric and magnetic methods. Mechanical methods are more suitable for larger than 1mm coal size range while the two latter methods are more compatible to be used with less than 1mm coal particles (Gupta, 1990). Table 2.4 listed the

physical properties that have been utilized in different dry coal beneficiation processes (Dwari & Rao, 2007).

Table 2.4 Coal characteristics used in dry cleaning processes (Dwari & Rao, 2007)

Characteristics	Process
Appearance/Color	Sorting
Coefficient of Friction	None direct
Shape	Screening
Friability/Elasticity	Rotary breaker and differential crushing
Density	Pneumatic separations and fluidized bed separations
Magnetic susceptibility	Magnetic separation
Electrical resistivity	Electrostatic separation
Radioactivity	Sorting

Mechanical methods also include: screening, classifier, gravity separators (air fluidized bed, air table separation) and heavy media separation (Sahu, Biswal, & Parida, 2009). Dry cleaning methods have lower efficiency as compared with wet cleaning methods (Mak, 2007). However, they have several advantages over wet methods. Air which is normally used as the separating medium (or in combined with a solid dense medium) in dry beneficiation methods is abundant while, sources of water which is used as the separating medium in wet methods is limited. More than two-third of the known coal reserves around the world are located in areas where water resources are not sufficiently available. Extremely cold weather condition in some countries also limits the use of water in wet methods (Luo, Zhao, Chen, Tao, & Fan, 2004).

Some low rank coals like brawn coal tend to form slime in wet processes (Zhenfu & Qingru, 2001b) which causes difficulties in coal cleaning and leads to pollution of underground water. Use of dry methods eliminates this problem. Lack of need for Dewatering in dry methods reduces the total cost as compared with wet methods. Lower construction and operation cost (Zhenfu & Qingru, 2001b); lower energy consumption and environmental hazards production and lack of need for chemical reagents are other advantages of dry cleaning methods over wet methods (Van Houwelingen & De Jong, 2004). In recent years, use of Air-dense medium fluidized bed (ADMFB) as an efficient beneficiation method has been more investigated by researchers (Prashant, Xu, Szymanski, Gupta, & Boddez, 2010). It has been claimed that ADMFB has higher separation efficiency over other dry cleaning methods like jigs and air tables (Luo, Zhu, Fan, Zhao, & Tao, 2007). It also has lowest cost per heat unit delivered to the power station as compared with other dry cleaning methods (Sahu et al., 2009). Table 2.5 shows the cost comparison among different dry cleaning methods (Van Houwelingen & De Jong, 2004).

Table 2.5 Cost comparison among different dry coal cleaning processes (Sahu et al., 2009)

Process	Product quality, Kcal/kg	Yield,%	Process operating cost,$/t	Coal delivered to power station,$/Gcal
Conventional	5947.11	84.2	1.79	1.94
Rare earth magnetic separator	6281.50	68.4	1.55	2.16
Air dense medium fluidized bed	6281.50	80.6	1.91	1.91
Electrostatic separator at mine	6639.75	59.9	5.01	2.65
Electrostatic separator at power station	6639.75	59.9	1.42	2.51
Air table	6281.50	71.4	1.78	2.12

2.4.2 Air-Dense Medium Fluidized Bed

Air dense medium fluidized bed is working on the same principle as other density-based separation methods. A uniform pseudo fluid of air-solid suspension is utilized as the separating medium. The density of the medium can be modified by changing the void fraction and type (and consequently density) of the solids. In this process, those feed particles which have a higher density than that of the medium will sink down the bed, while the particles with lower densities will remain on the top of the bed, resulting in stratification of feed coal particles according to their density along the bed height. In case of coal, particles with higher mineral matter content will settle down while carbon-rich particles will remain on the top of the bed (Sahu, Tripathy, Biswal, & Parida, 2011).

In fluidization stage, the pressure drop between two points in the bed (ΔP) is equal to the difference between the hydrostatic heads between those points and can be calculated using following formula (Luo et al., 2007):

$$\Delta P = \frac{mg}{A_t} \qquad (2-2)$$

Where, m is the weight of the bed A_t is cross sectional area of the bed and g is gravitational acceleration. Formula $(2-2)$ also can be re-written as:

$$\Delta P = H_{mf}\left(1-\varepsilon_{mf}\right)\left(\rho_P - \rho_g\right) \qquad (2-3)$$

Where, H_{mf} is the bed depth, ε_{mf} is the bed void fraction, ρ_P is the medium solids density and ρ_g is the gas density. The average density of fluidized bed (ρ) can be calculated using following formula:

$$\rho = \frac{\Delta P}{H_{mf}} \qquad (2-4)$$

Using equation $(2-3)$, equation $(2-4)$ can be re-written as:

$$\rho = \left(1-\varepsilon_{mf}\right)\left(\rho_P - \rho_g\right) \qquad (2-5)$$

Assuming $\rho_P \gg \rho_g$, equation $(2-5)$ can be expressed as:

$$\rho = \left(1-\varepsilon_{mf}\right)\rho_P \qquad (2-6)$$

As seen from equation $(2-6)$, the bed density is a function of bed void and density of solid medium. Factors like shape and size distribution of solid medium particles and gas velocity mainly determine the bed void fraction (Luo et al., 2007).

The fluidization stage starts at a certain air velocity which is called minimum fluidization velocity (u_{mf}) and can be calculated using Kunni and Levenspiel formula (Prashant et al., 2010):

$$u_{mf} = \frac{d_p^2(p_s - p_g)g}{150\mu}\frac{\varepsilon_{mf}^3\varphi_s^2}{1-\varepsilon_{mf}} \quad \mathrm{Re}_{p,mf} < 20 \qquad (2-7)$$

Where $\mathrm{Re}_{p,mf}$ and Ar can be calculated using following equations respectively:

$$\mathrm{Re}_{p,mf} = [(33.7)^2 + 0.0408Ar]^{1/2} - 33.7 \qquad (2-8)$$

$$Ar = \frac{d_p^3 p_g(p_s - p_g)g}{\mu^2} \qquad (2-9)$$

Where: u_{mf} is the superficial gas velocity at minimum fluidization conditions (cm/s), d_p is the geometric diameter based on screen analysis (µm), ρ_s is solid density (kg/m^3) , ρ_g is Gas density(kg/m^3), g is acceleration of gravity (9.81 m/s), ε_{mf} is void fraction at minimum

fluidizing conditions (dimensionless), φ_s is sphericity of a particle (dimensionless), μ is viscosity of gas (kg/m·s) and $Re_{p,mf}$ is Reynolds number of particles at minimum fluidizing conditions (dimensionless). It has been well demonstrated that u_{mf} also varies with some other operating parameters such as gas pressure and bed height (Mak, 2007). However, Equation 2.7 can provide a rough estimation about u_{mf} in the absence of complete experimental data. Minimum fluidization velocity is lower than complete fluidization velocity (u_{cf}) at which all the particles are fully fluidized and minimum bubbling velocity (u_{mb}) at which, air bubbles begin to flow in the solid bed (Mak, 2007). Increase in velocity beyond u_{mb} results in back mixing of medium particles and instability of bed density. (Luo et al., 2007).

Based on the density and size of the materials, Geldart (Geldart, 1973), classified the behavior of the solid mediums in fluidized bed in to 4 different regimes:

Group C: Cohesive bed; fine particles which hardly fluidize due to the strong inter-particle forces

Group A: Aeratable bed; Particles with low mean particle size and/or low density which fluidize easily at low gas flow rates

Group B: Sand like bed; particles with mean particle size in the range of $40 < d_{sv} < 500$ μm and density in the range of $1.4\ g.cm^{-3} < \rho_s < 4\ g.cm^{-3}$. They readily fluidize near minimum fluidization velocity.

Group D: Spoutable bed; large and/or dense particles. These solids fluidize more easily in shallow beds. Large rising bubbles are formed in the fluidized bed (Mak, 2007; Mak, Choung, Beauchamp, Kelly, & Xu, 2008). Fig 2.4 displays different types of gas fluidization.

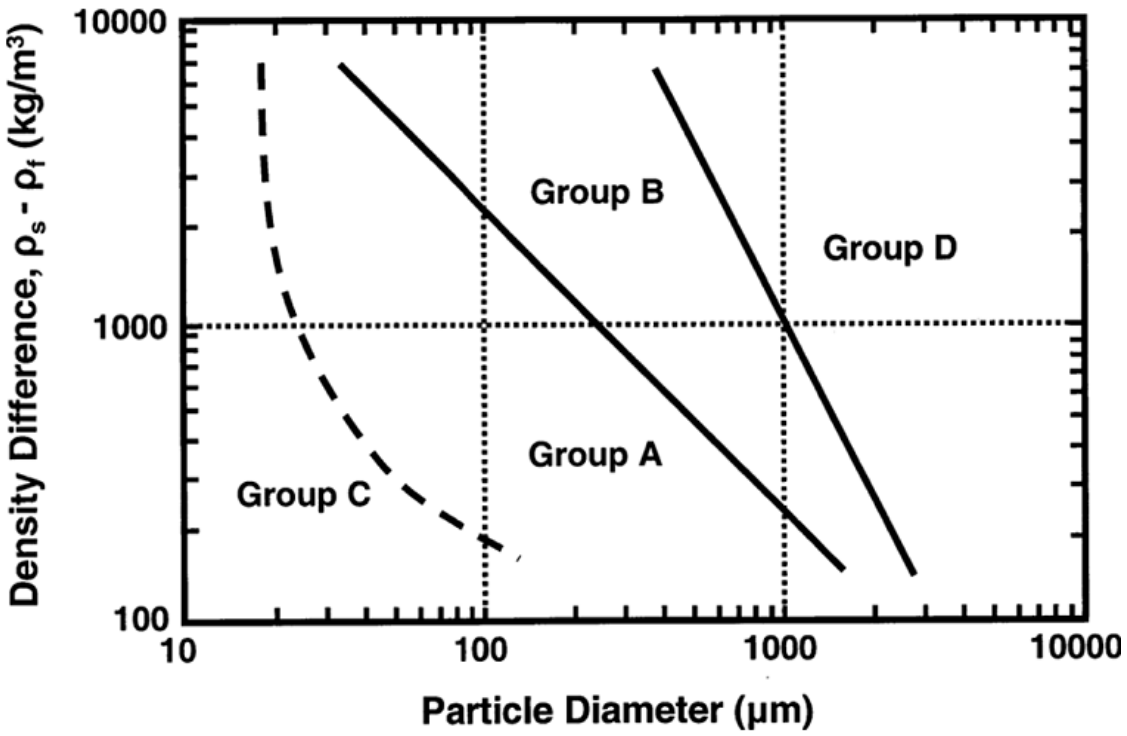

Fig 2.4 Types of gas fluidization (Geldart, 1986)

In order to achieve an efficient separation in ADMFB, the solid dense medium and the feed particles (i.e. Coal) should be selected from different Geldart groups. Moreover, the medium particles should fluidize easier than coal particles (Mak et al., 2008).

It has been demonstrated that air dense medium fluidized bed can be efficiently applied for coal cleaning in size range of 6 - 50 mm (Luo et al., 2007; Luo et al., 2003; Zhenfu & Qingru, 2001a; Zhenfu & Qingru, 2001b). Efficiency of separation is significantly reduced with further decrease in the coal feed size. This behavior is attributed to the back-mixing of medium particles during ADMFB operation which consequently leads to the re-mixing of the separated coal particles. The back mixing of medium particles is mainly caused by presence of large air bubble in the bed. (Luo et al., 2003; Mak et al., 2008; Zhenfu & Qingru, 2001a). When an air bubble rises in the fluidized bed since the pressure at the bottom of the bubble is slightly lower than nearby, some of

the medium solid particles are attached to it. The bubble continues to collect medium particles while moving upward. After weight of the collected medium particles reaches a certain value, they detach from the bubble and settle down. Therefore, solid medium particles which originally belonged to a lower point will move up to a relatively higher level and medium solids which are in emulsion phase will gradually settle down to fill the empty space that created by lifted medium particles. The circulation of medium solid particles in the bed is called back mixing (Luo et al., 2007). Fig 2.5 shows the steps that lead to the back mixing in fluidized bed.

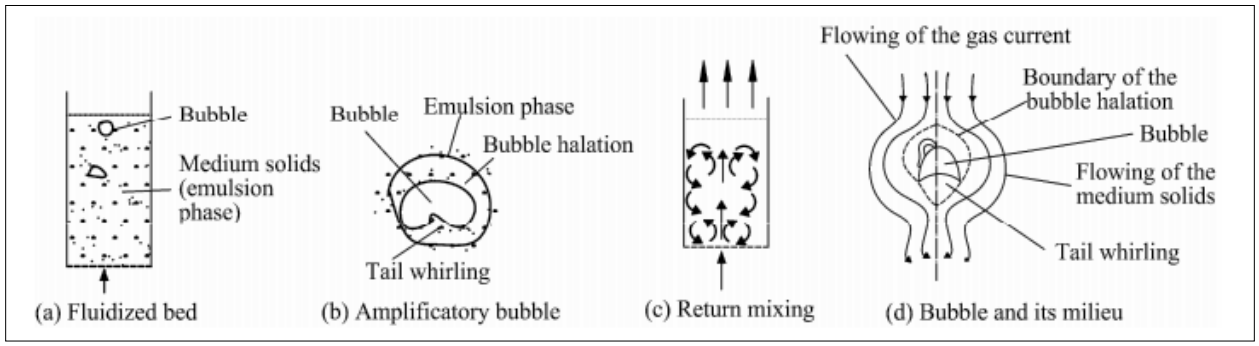

Fig 2.5.Bubble and flow pattern in fluidized bed (Luo et al., 2007)

It has been demonstrated that the back mixing of solids is minimized near minimum fluidization velocity but increase in air velocity to more than 1.3 times this velocity will significantly increase the back mixing. Even at minimum fluidization condition, re-mixing of extra-fine solid particles may happen as a result of entrainment in air flow. Use of small or medium size solid dense medium particles can minimize back mixing of medium solids. However, bed viscosity is increased by reduction in size of medium particles. Consequently, the efficiency of separation is reduced by increase in viscosity of the bed. Adhesion force among particles will also increase with reduce in solid medium particles size which consequently make the bed unstable (Mak, 2007).

In recent years extensive efforts have been put to reduce the lower limit of particle size in ADMFB down to 0.5 mm. Use of external energy field (like magnetic and electric field) or mechanical vibration in fluidized bed significantly reduces the air bubble size and minimizes the back mixing of medium particles and consequently stabilize the density of the fluidized bed for fine coal (6 - 0.5 mm) beneficiation (Jin, Tong, Schlaberg, & Zhang, 2005; Kleijn van Willigen, van Ommen, van Turnhout, & van den Bleek, 2005; Luo, Zhao, Chen, Fan, & Tao, 2002).

(Luo et al., 2003) achieved high separation efficiency (E_P=0.07) for 0.5 - 6 mm coal feed size using vibrated fluidized bed. (Fan, Luo, Tao, Zhao, & Chen, 2009) also studied the effect of vibration on separation of coal in the size range of 0.5 - 6 mm and found that the E_P value significantly reduces from 0.15 in absence of vibration to 0.0.6 - 0.08 in presence of it. Mechanical vibration enhances the contact between gas and solids, minimizes the formation of air bubbles and improves the fluidization of smaller dense medium particles which consequently enhanced the fluidization of fine coal (Luo et al., 2003).

(Choung et al., 2006) found that using a finer size of medium combined with an optimum air flow rate which is high enough to avoid bed collapse and not too high to avoid back-mixing, fine coal (down to 1mm) can be efficiently cleaned.

(Chen & Yang, 2003) studied the efficiency of ADMFB for > 50 mm feed coal. They found that in order to form a uniform and stable bed, the height of the fluidization chamber should be around 1.2 m which is significantly higher than height of the FB chambers used for coal beneficiation in 6 – 50 mm size range. Use of double-density air dense medium fluidized bed to obtain three products from the feed coal also has been investigated by number of researchers (Geldart & Wong, 1985; Luo et al., 2003; Wei, Chen, & Zhao, 2003). It has been observed that

using a proper bed structure and optimized operating parameters, two separating regions with two uniform densities can be formed along the bed height in the fluidization chamber. As a result, three different products (clean coal, middling and tailing) can be separated. Moreover, it has been noted that the fluidized bed viscosity should be kept as small as possible to obtain good fluidization performance. Magnetite powder and magnetic pearls were used respectively as the heavy and light dense mediums for the lower and upper parts of the bed. Specially structured bed with a middle part of pyramidal shape was designed at which, gas velocity decreased along the pyramidal part. Consequently, the lighter magnetic pearls fluidize at lower velocities than magnetite powder which prevent the axial mixing of medium particles along the bed (Luo et al., 2003; Wei et al., 2003).

(Zhenfu & Qingru, 2001b) investigated use of fine coal (0.45 – 0.9 mm) and magnetic powder mixture as the solid medium for 6 - 50 mm feed coal. They found that using this mixture, uniformly distributed medium with stable density can be obtained and feed coal can be separated with an E_P value of about 0.05.

(Luo et al., 2004) studied the effect of gas distributor on the performance of dense phase high density fluidized bed. They found that increase in the pressure drop of gas distributor above its critical value enhances the stability and uniformity of the bed density.

(Mak et al., 2008) investigated the potential of air dense medium fluidized bed to use for co-rejection of mercury along with mineral matters from three sub-bituminous coal seams from Alberta mines. They observed a strong linear relation between mineral matter rejection and mercury rejection using ADMFB for two of the mined seams.

Despite all the improvements achieved in operation for Air dense medium fluidized bed as an efficient dry cleaning method, it still has some deficiencies which need to be resolved. High moisture content in run-of-mine coal or dense medium solids deteriorates the performance of the ADMFB and affects the efficiency of separation due to the decrease in medium fluidity. The fluidized gas is also needed to be dried. Coating of dense medium particles on the surface of the feed particles is another problem which leads to the gradual consumption of medium over a long period of operation. Finally, generation of fine coal particles during ADMFB operation reduces the uniformity and stability of the bed density (Sahu et al., 2009).

Chapter3. Analysis of petrographic composition and phosphorus distribution of density separated coal fractions - Fording River sample

3.1 Experimental

3.1.1 Materials

A bituminous coking coal from Fording River mine in B.C, Canada, has been analyzed for the purpose of density separation and characterization. The overall proximate and ultimate analyses of the studied coal sample are measured based on D3172-07a and D3176 – 09 ASTM methods and displayed in table 3.1. Ultimate analysis (C, H, N and S) of coal samples was determined by using Carlo Erba CHNS-O EA1108 elemental analyzer. Proximate analysis was performed using programmable muffle furnace.

Table 3.1 Proximate and ultimate analysis of the Fording River Coal

Proximate analysis (wt.%)				Ultimate analysis (wt.%)				
Moisture	Ash	VM	FC	C	H	N	S	O[a]
2.17	12.22	23.13	62.48	79.4	4.48	1.46	0.61	1.83

[a]Oxygen by difference, VM : Volatile matter, FC: Fixed Carbon, C: Carbon, H: Hydrogen, N: Nitrogen, S: Sulfur, O: Oxygen

3.1.2 Particle Size distribution analysis

The particle size distribution analysis was performed on a Ro-Tap sieve shaker (obtained from W.S.Tyler) using U.S standard brass sieves. 300 g of each sample was used for each run. The sieving time was set on 15 minutes. After sieving, weight of the sample which remained on each sieve was measured. The particle size distribution obtained by dividing weight of the sample remained on each sieve by total weight of sample used in the analysis. In order to assure the repeatability this test repeated three times.

3.1.3 Coal sample preparation for sink-float tests

The coal feedstock had been screened in to 6 different sizes fractions (-75 μm, 75 - 212 μm, 212 - 425μm, 425 - 600 μm, 600 – 850 μm and +850 μm). The largest fraction sieved again to remove +2.5 mm fraction. The finest fraction has not been considered for the analysis due to the long settling time in sink-float tests. Spinning Riffler was used in coal samples preparation stage to provide representative samples for further analysis. All prepared coal samples were stored in a laboratory freezer at -18 °C to prevent oxidation.

3.1.4 Sink-float test

Heavy medium solutions for sink-float tests were prepared by adding appropriate amount of Solid Cesium Chloride solid (purchased from Fisher Scientific Canada) to distillated water. Brij35 (purchased from Sigma Aldrich Chemicals) was added as the surfactant at $8 g.l^{-1}$ concentration to prevent agglomeration of the coal particles. Medium solutions with following densities (1.38, 1.40, 1.45, 1.60, 1.78 and 2 $g.cm^{-3}$) were prepared for the purpose of the sink-float tests. The density of the medium solutions was measured using a picnometer (obtained from Fisher Scientific Canada). All the sink-float tests were conducted in 1 liter glass beakers. After putting the coal sample in the known density solution, 12 hours settling time was given to assure the separation between sink and float phases. Afterward, the float phase is collected in Erlenmeyer flask using vacuum. For the coarsest fraction (+850 μm), a strainer with opening of 0.5mm used to remove the float phase particles. The collected float particles were washed with distillated water, dried and weighted. The sink phase particles were also washed to remove the CsCl salt coated on the surface of coal particles and then moved to the next medium with higher density. This procedure was then repeated with liquid mediums of increasingly higher densities until the point at which most of the coal particle floated. The weight of the portion of sample

which floated in each density range and the portion which settled at the heaviest density was recorded.

3.1.5 Preparation of polished coal mounts

Lucite Powder was chosen as the pellet binder. A multiple Buehler Simplimet automatic pelletizer equipped with duplex mold was used to prepare ready-to-polish pellets. Automated polishing Buehler Ecomet/Automet polishing equipment was also used to polish mounts. The preparation of pellets for petrographic analysis had been performed in Pearson petrographic coal lab, B.C, Canada.

3.1.6 Maceral content analysis for sink-float collected samples

Maceral analysis of density fractions obtained from sink-float test at different size fractions was conducted using a Leitz MPV-2 photometer-orthoplan microscope with a X 32 oil immersion objective and X 10 eyepiece. 500 separate maceral points were counted for each sample analysis. All the petrographic analysis had been performed in Pearson petrographic coal lab, B.C, Canada. All the maceral content analyses were done only once for each density fraction of a certain size fraction..

3.1.7 Ash content analysis for sink-float collected samples

Ash content of the density fractions obtained from sink-float tests was measured based on the ASTM method D 3174. Using Porcelain mortar and pestle, coal samples were crushed and then sieved to obtain < 250 µm particle size. For each test, 1g of coal sample was placed in the crucible and the crucible weight after adding the coal was recorded using balance. The crucible then was placed in the thermally programmable furnace. Using a ramp program (10 °C/min), samples were heated up to 450 °C in the first hour and then up to 750 °C in the next hour and

stayed in the 750 °C for additional two hours. Then samples were kept in the furnace until temperature reduced to less than 200 °C. Afterwards, crucibles were taken out of the furnace and placed in the desiccator to prevent the absorption of moisture. After giving enough cooling time, crucibles were taken out of the desiccator and weighted. The ash content (wt.%) of samples was calculated using the following formula (3-1). In order to assure the repeatability of the result, each ash content test repeated at least three times.

Ash (wt. %) = [1- (weight of full crucible before test (g) – weight of full crucible after test (g))] x 100 (3-1)

3.1.8 Phosphorus content analysis

Phosphorus content measurement of density fractions were conducted in two steps. At first step, the phosphorus containing materials of the coal samples were digested by sequential adding of Sulfuric acid, Hydrogen peroxide and Hydrofluoric acid. Detail of the acidic digestion method had been described by (Bowman, 1988). At second step, the phosphorus content of the digested sample was measured using the Molybdenum Blue method. At this method, the intensity of the blue color produced from reaction between Molybdenum and Phosphorus was determined at 830 nm against a blank reagent using SmartChem Discrete Wet Chemistry Analyzer, Model 200 (Manufactured by Westco Scientific). The Molybdenum Blue method for phosphorus content determination had been described by (Carter, 1993) in details.

3.2 Results and Discussion

3.2.1 Particle size distribution

Table 3.2 shows the particle size distribution for the studied coal. The coal feedstock is more distributed in the coarsest and finest fractions respectively.

Table 3.2 Particle size distribution of Fording River coal

Particle size (μm)	-75	75 - 212	212 - 425	425 - 600	600 - 850	+850
Distribution (wt. %)	16	6	10	6	7	55

3.2.2 Sink-float tests results

Fig 3.1 shows the cumulative yield versus density curves for sink-float (S/F) tests at different size fractions. As seen from this Figure, no density fraction lighter than 1.38 $g.cm^{-3}$ has been observed for all studied sizes. The yield of sink-float at density of 1.45 $g.cm^{-3}$ is significantly reduced (around 50%) by increase in size above 850 μm. This can be attributed to the lower degree of macerals liberation in larger sizes. More than 89% of the feed coal in all size fractions floats at density of 1.80 $g.cm^{-3}$. This behaviour can be attributed to very low ash content of the raw sample in the studied size fractions (9 - 10% for < 850 μm). Since most of the ash in coal is concentrated in the heavy density fraction (> 1.80 $g.cm^{-3}$), low ash content in raw coal results in lower yield for heavy density fraction.

Fig 3.2 shows cumulative ash versus density curves for S/F tests at different size fractions. As shown in this figure, the ash content in density range of 1.38 - 1.45 $g.cm^{-3}$ is extremely low (less than 3%) for all studied sizes. In addition, the ash content of the largest size fraction (+850 μm) is significantly larger than smaller size fractions. As a result the overall ash content of this size fraction is around 13.2% while the overall ash content of smaller size fractions varies in the range of 9-10%.

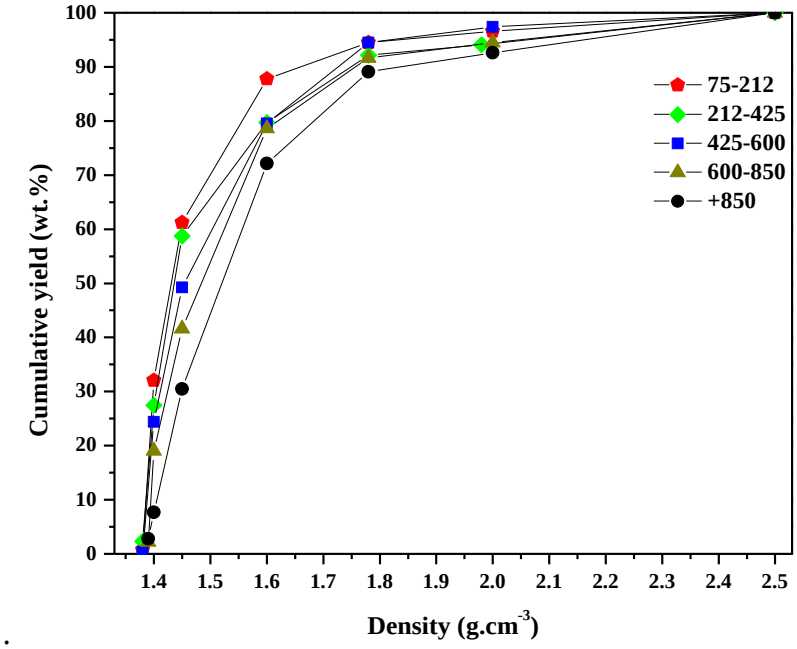

Fig 3.1 Cumulative yield vs. Density for S/F test at different size fractions

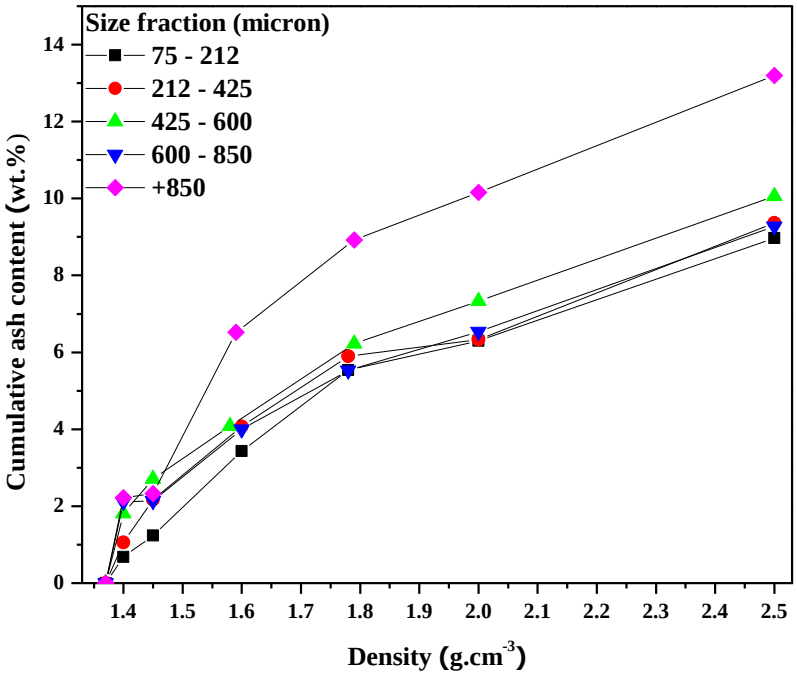

Fig 3.2 Cumulative ash vs. Density for S/F test at different size fractions

3.2.3 Petrographic analysis

Table 3.3 displays the petrographic analysis for all studied sizes at selected density fractions. Mineral matter (wt.%) has been calculated using Parr formula (Suárez-Ruiz, Crelling 2008) and then converted to volume basis using a density of 2.8 $g.cm^{-3}$ for mineral matter and 1.35 $g.cm^{-3}$ for organic components based on ASTM D2799–11 method. As shown in Table 3.3, the 1.38 - 1.45 $g.cm^{-3}$ density fraction is remarkably rich in vitrinite in all sizes, while for 1.45 - 1.60 $g.cm^{-3}$ density fraction, vitrinite content is significantly lower. It has also been noticed that vitrinite content of the 1.38 - 1.45 $g.cm^{-3}$ density fraction remains almost constant (~90%) with increase in size up to 600 µm but it is noticeably reduced by further increase in size. This change may be attributed to the liberation size characteristic of vitrinite in this coal. It has been noted that the inertinite content of heavy density fraction (> 1.78 $g.cm^{-3}$) is significantly reduced by increase in size beyond 425 µm. As presented in Table 3.3, the mean maximum reflectance of vitrinite in oil (Romax) is also reduced with increase in density for all size fractions.

As suggested by (Díez et al., 2002), vitrinite, liptinite and half of the semifusinite are assumed to be reactive. Therefore, the reactive portion of each density fraction is calculated for different sizes and presented in Table 3.3. It has been observed that significant reduction in reactivity of vitrinite-rich density fraction (1.38 - 1.45 $g.cm^{-3}$) happens when size of particle goes beyond 850 µm. This can be attributed to the significantly higher fusinite and mineral matter content and considerably lower vitrinite content of +850 µm particle size.

Fig 3.3 displays reflectance profiles for three different density fractions of 75 - 212 µm size fraction. As shown in this figure, the reflectance profile for the lightest density fraction (< 1.45 $g.cm^{-3}$) is distributed over a narrow range of reflectivity (0.9% – 1.75%) while further increase in density fraction to 1.45 – 1.60 $g.cm^{-3}$ results in distribution of reflectivity over a wider range

(0.85% – 2.5%) and even a wider range of reflectivity is observed for 1.60 - 1.78 g.cm^{-3} fraction. This behaviour can be interpreted based on the maceral distribution of each density fraction. The main peak in each of these reflectivity profiles is related to vitrinite macerals. For 1.60 – 1.78 g.cm^{-3} density fraction, high inertinite content (68 wt.%) results in a second peak at reflectivity of 1.45%. The area under the curve for the first peak in each curve represents the vitrinite content of that density fraction. As shown in Fig 3.3, this area is significantly larger for the lightest density fraction (< 1.45 g.cm^{-3}) as compared with heavier density fractions. This can be attributed to the considerable difference in vitrinite content between < 1.45 g.cm^{-3} density fraction (89.1 wt.%) and heavier density fractions (40.4 wt.% and 26.6 wt.% respectively).

Table 3.3 Petrographic analysis of density fractions for different size fractions

Size fraction (µm)	75 – 212				212 - 425				425 – 600				600 - 850	850 - 2500
Density fraction* (g.cm^{-3})	1.38 - 1.45	1.45 - 1.60	1.60 - 1.78	> 1.78	1.38 - 1.45	1.45 - 1.60	1.60- 1.78	> 1.78	1.38 - 1.45	1.45 - 1.60	1.60 - 1.78	> 1.78	1.38 - 1.45	1.38 - 1.45
Vitrinite (%)	89.10	40.4	26.6	12.2	90.9	30.4	29.9	12.0	88.1	46.2	29.6	12.6	79.0	63.0
Inertinite (%)	9.4	54.4	54.2	68	6.6	63.0	60.1	70.3	8.6	49.7	59.9	46.7	17.5	34.7
Liptinite (%)	0.4	0.4	1.1	0.2	0.8	1.5	0.4	0.3	1.2	0.6	0.9	0.3	2.0	0.7
Mineral matter (%)	1.1	4.8	18	24	1.7	5.1	9.6	26	2.1	3.5	9.6	28	1.5	1.6
Romax	1.19	1.16	1.11	-	1.19	1.17	1.16	-	1.18	1.16	1.14	-	1.18	1.16
Reactive (%)	93.5	62.3	45.4	34.1	93.7	54.9	49.2	34.8	92.0	64.2	51.30	31.5	89.5	76.4

*Due to minor variations in medium solution densities, displayed densities are nominal and subjected to ±0.02g.cm^{-3} error.

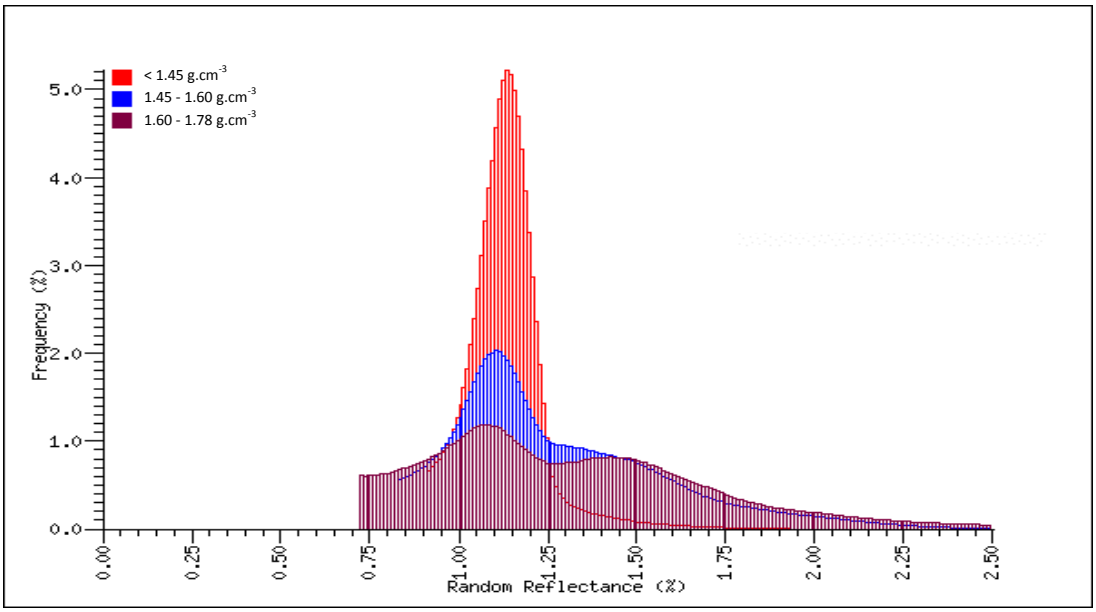

Fig 3.3 Reflectance profiles for three different density fractions of 75- 212 µm size fraction

Fig 3.4 displays the cumulative vitrinite content of different size fraction as a function of density. Using cumulative data, the effect of vitrinite content and yield of sink-float for each density fraction can be combined. The cumulative vitrinite content of 425 - 600 µm fraction is slightly lower than two finer fractions due to the lower sink-float yield at vitrinite rich density fraction (1.38 - 1.45g.cm^{-3}).

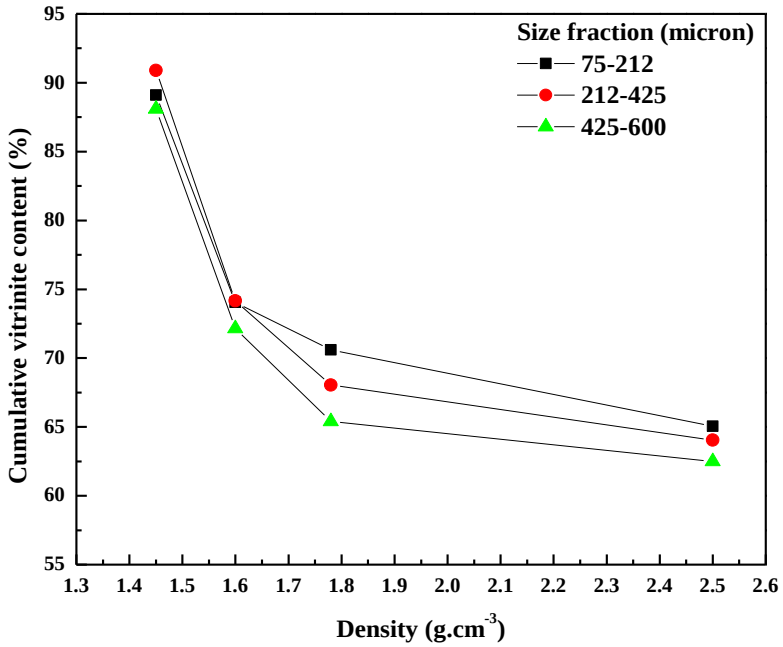

Fig 3.4 Cumulative vitrinite content vs. density for different size fractions

Assuming vitrinite recovery (wt.%) for a selected density fraction as the ratio of vitrinite recovered in this density fraction to the total vitrinite exists in the studied size fraction, this index is calculated for 1.38 - 1.45g.cm^{-3} density for all sizes and listed in Table 3.4. It can be noted that vitrinite recovery significantly reduces by increase in size above 425µm.

Size fraction (µm)	75 - 212	212 - 425	425 - 600	600 - 850	850 - 2500
Vitrinite recovery (Wt.%)	84.0	82.2	69.4	57.5	32.7

Table 3.4 Vitrinite recovery of different size fraction in 1.38 - 1.45g.cm^{-3} density fraction

Fig 3.5 (a) and (b) display the optical images taken from raw sample of 75 - 212 µm size fraction and 1.38 - 1.45 g.cm^{-3} density fraction of the same size. In the top half to the left of the Fig 3.5 (a), two uniformly grey vitrinite particles can be observed. The grain in the bottom section in the middle is inert semifusinite and the small bright white particles throughout are inertinite macerals. Moreover, the dark grey bits in the grain on the bottom right are liptinite sitting in a ground mass of vitrinite. Comparison of these two optical images easily shows the abundance of pure gray vitrinite particles and rarity of inertinite macerals in 1.38 - 1.45 g.cm^{-3} density range. No fusinite and macrinite macerals have been observed in this density range for < 212 µm size particles.

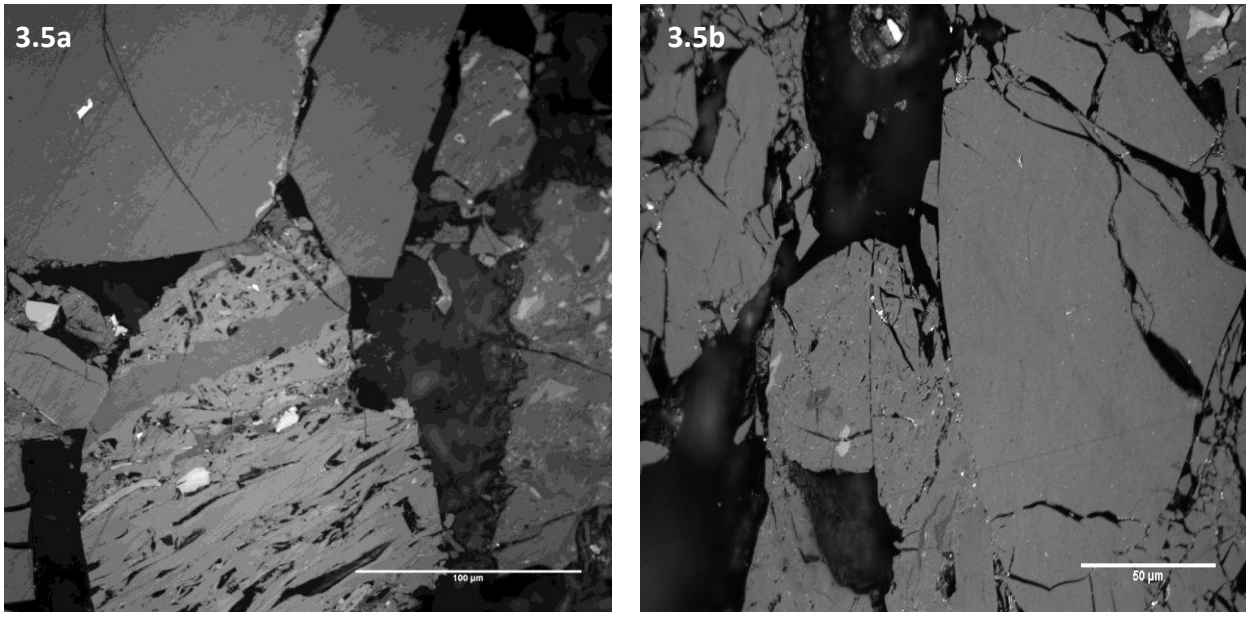

Fig 3.5 Petrographic images of 5a) raw and 5b) 1.38 - 1.45 g.cm^{-3} density fraction of 75 - 212 µm size fraction

3.2.4 Phosphorus content measurement of density fractions

Fig 3.6 shows the Phosphorus distribution in different density fractions for < 850 µm particle size. Based on the conducted experiments, the average phosphorus content of the fine fractions (< 850 µm) is around 0.18 %. Minor variations in phosphorus content (in the range of 0.17 - 0.19%) with particle size is observed for fines. However, the phosphorus content is significantly reduced down to 0.13% by further increase in size (up to 2.5 mm). This is contrary to (Claassens 2009, 99-111) findings that phosphorus content is increased with increase in coal particle size. This difference may be attributed to the nature and liberation size of phosphorus-bearing minerals in different coal seams. Moreover, as illustrated in Fig 3.6, the phosphorus distributed throughout all density fractions but less concentrated in < 1.60 g.cm^{-3} density fraction.

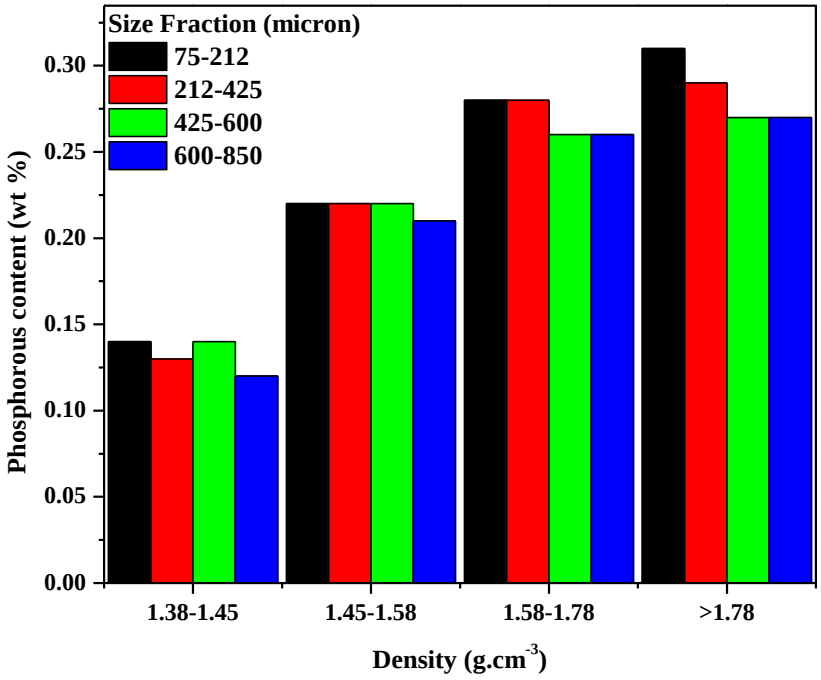

Fig 3.6 Phosphorus distribution in different density fractions of different sizes for Fording River

A significant increase in phosphorus content observed with increase in density cut-point from 1.45 g.cm^{-3} to 1.60 g.cm^{-3} for all studied sizes. This behaviour can be attributed to the fact that

phosphorus is more associated with inert components (inertinite and minerals) rather than vitrinite macerals. Using separation at density of 1.45 $g.cm^{-3}$, the phosphorus level can be reduced from 0.18% in raw coal to 0.12 – 0.14% in clean coal for the studied sizes. However, this phosphorus level is still higher than the desired level of phosphorus in coal for use in steel marketing industry (< 0.03 wt.%) (Ryan, Grieve 1996).

Chapter4. Air-Dense Medium Fluidized Bed (ADMFB)

4.1Experimental Details

4.1.1 Materials

4.1.1.1 Fluidizing Medium – Silica Sand

Silica sand particles (Density = 2620 kg/m^3) were used as the fluidizing medium. It was purchased in 30 - 50 mesh size from Sil Industrial Minerals, Canada. Upon receiving, the silica sand particles were sieved to obtain 355 - 500 μm size range. Based on particle size distribution, the average particle size for the selected size range was 390 μm. The minimum fluidization velocity for this medium is 0.149 m/s. It is calculated based on Kunni and Levenspiel formula (Prashant et al., 2010):

$$u_{mf} = \frac{d_p^2(p_s - p_g)g}{150\mu} \frac{\varepsilon_{mf}^3 \varphi_s^2}{1-\varepsilon_{mf}} \qquad (4-1)$$

Where : u_{mf} is the superficial gas velocity at minimum fluidization conditions (cm/s), d_p is the medium particle diameter (μm), ρ_s is solid medium density (kg/m^3) , ρ_g is gas density(kg/m^3), g is acceleration of gravity (9.81 m/s), ε_{mf} is void fraction at minimum fluidizing conditions (dimensionless), φ_s is sphericity of a particle (dimensionless) and μ is the gas viscosity (kg/m·s).

4.1.1.2 Coal Samples

Two Bituminous coal samples were obtained from Fording River and Coal Mountain Operation mines in B.C, Canada. Due to the high moisture content of the Coal Mountain Operation sample, it was air dried using vacuum dryer at 60 °C for 8 hours prior to use in ADMFB tests. The Fording River sample was screened into coarse (> 4.75 mm), intermediate (1.00 - 4.75 mm) and

fine fraction (< 1.00 mm). The fine fraction was not used for the ADMFB tests. The intermediate fractions were sieved into 4 different size fractions (-1 mm, 1 - 2.36 mm, 2.36 - 3.35 mm, 3.35 - 4.75 mm). The coarse fractions were also sieved into three different size fractions (4.75 - 13 mm, 13 - 25 mm, and +25 mm). The Coal Mountain Operations samples were also sieved into 4 different size fractions (-1 mm, 1 - 2 mm, 2 - 13 mm, 13 - 25 mm and +25 mm). The fraction of -1 mm was not used for ADMFB tests. Dry coal samples were stored in a laboratory freezer at -18 °C to prevent oxidation prior to tests. Particle size distribution and ash content analysis for the entire particle size range were done for both samples and the results are listed in Table 4.1 and 3.2. The variation of cumulative ash content with particle size for both samples is also presented in Fig 4.1. As seen from this Figure, the ash content of the Coal Mountain Operation samples is significantly higher than Fording River sample in all particle size ranges. The average ash content of Fording River and Coal Mountain Operation samples are 17.8% and 31.1%, respectively.

Table 4.1. Particle size distribution for the Fording River

Size fraction (mm)	< 1	1 - 2.36	2.36 - 3.35	3.35 - 4.75	4.75 - 13	13 - 25	+25
Yield (wt.%)	46.6	12.0	7.1	4.3	14.3	7.5	8.2
Ash content (wt.%)	10.0	13.8	16.0	17.1	27.0	35.0	39.0

Table 4.2. Particle size distribution for the Coal Mountain Operation

Size fraction (mm)	< 1	1 - 2	2 - 13	13 - 25	+25
Yield (wt.%)	30.9	16.3	31.4	12.0	9.4
Ash content (wt.%)	22.0	25.2	32.6	45.4	49.3

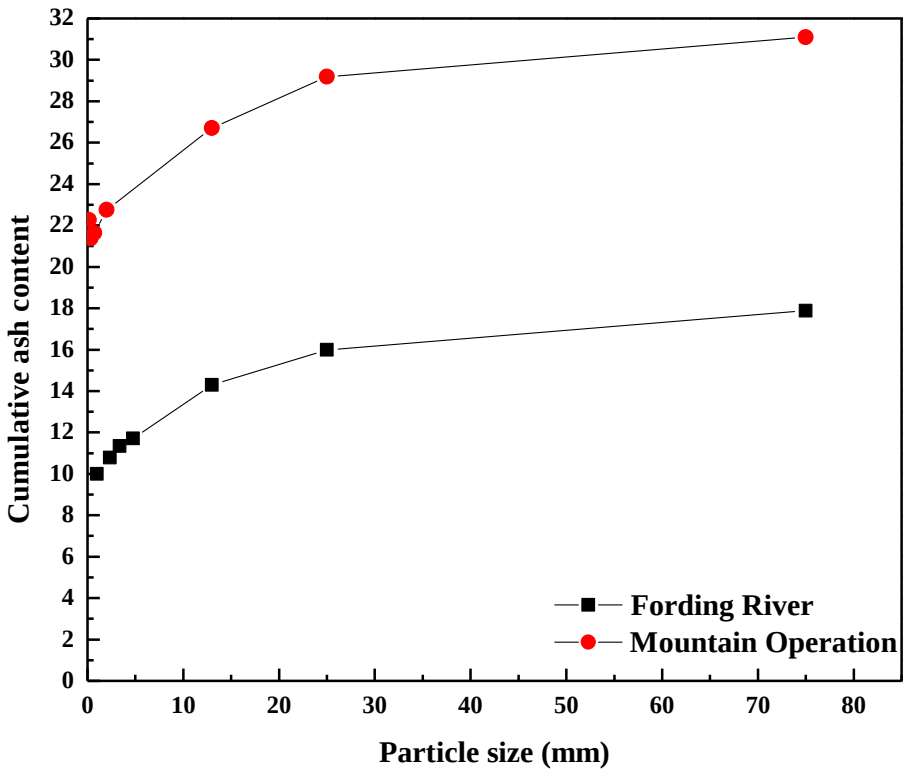

Fig 4.1 Variation of ash content with particle size for Fording River and Coal Mountain Operation samples

4.1.2 Experimental Setup

Fig 4.2 shows the schematic of batch ADMFB used in all experiments. A Plexiglas cylinder with inner diameter of 20 cm and height of 40 cm was connected to an air distributor plate and used to hold fluidizing medium. The air distributor plate was a porous metallic plate with 40μm opening size and 0.3 cm thickness obtained from the Matt Corporation in Farmington, Illinois. Fluidizing medium particles were feed to the fluidization chamber and the medium height in bed was measured by metric ruler. The ruler precision was 0.1 cm. The flow of the air to the fluidizing bed is controlled by a valve and measured by a rotameter purchased from Cole Palmer. The inlet air pressure kept constant at 40 psig.

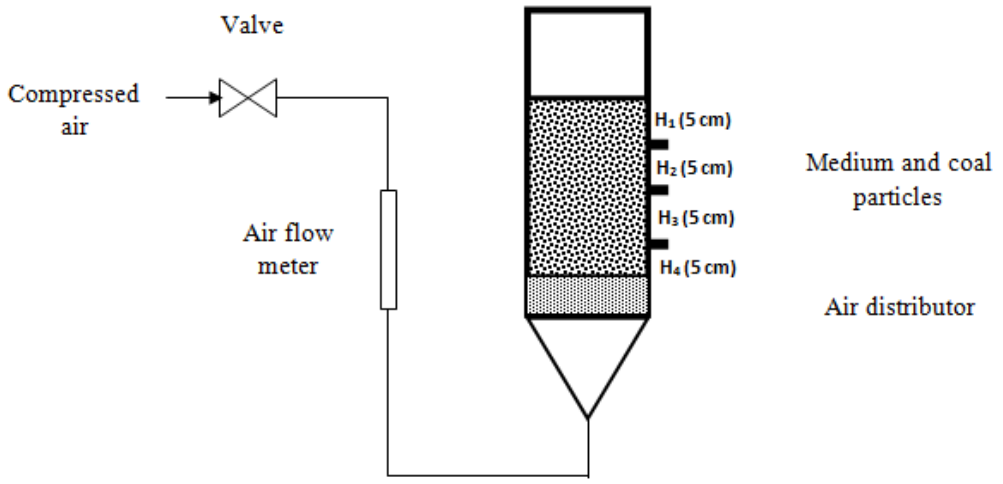

Fig 4.2 Schematic diagram of ADMFB (Prashant, Xu, Szymanski, Gupta, & Boddez, 2010)

4.1.3 Operation procedure

Before operating the ADMFB, medium particles were first introduced to the column. Afterwards, the valve was opened and the air velocity was regulated using rotameter. For all experiments, the air velocity was kept constant at 0.17 m/s. This velocity is slightly higher than minimum fluidization velocity for this fluidized bed which is calculated to be 0.149 m/s. The medium particles became floated after reaching minimum fluidization air velocity. When air flow became stable at the pre-determined rate, the coal particles were added to the top of the bed. After giving certain amount of time (as specified for each run), the air supply was switched off and the stratified particles (coal and medium particles) were permitted to settle down and distributed in different layers along the height of the bed based on their densities. The bed height then was divided into four or more layers and the stratified particles collected from each layer. The sample collections were done manually using a metal scoop. The coal particles in each layer were separated from the medium using an 850 µm opening size sieve. Finally, the weight of the coal particles in each layer was recorded and yield of each layer as a percentage of total sample

weight and also cumulative yield from top to the bottom of the bed were calculated. Moreover, samples were analyzed for ash content and petrographic composition. Only samples obtained from the best run for each size fraction were sent for maceral content analysis. In addition, coal samples were analyzed for phosphorus content. In order to measure the separating density of the layers, the collected coal samples from the top layers also were subjected to sink float test using CsCl (aq) as the heavy liquid medium.

4.1.4 Effect of bed height, fluidization time and coal load on separation efficiency - Fording River sample

The focus of this project is to investigate the effect of particle size on the vitrinite upgrading and ash and phosphorus removal from clean coal for both samples using ADMFB. However, in order to optimize the operating conditions of fluidized bed, the effect of bed height and fluidization time on ash rejection of coal particles in fine fractions of Fording River sample were also investigated. In order to study the effect of bed height on ADMFB performance, two different sand bed heights (20 and 30 cm) were tested. Sample collecting zones for tests with bed height = 20 cm are shown in Fig 4.3.

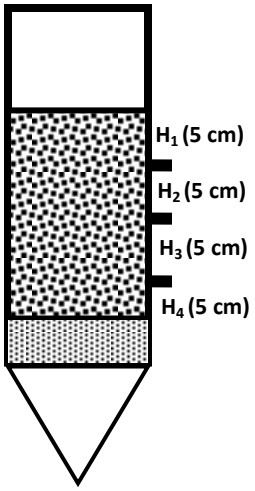

Fig 4.3 Sample collecting zones along the bed for bed height = 20 cm

In order to investigate the effect of fluidization time on the efficiency of ash removal, the fluidization tests were also carried out with fluidization time T = 8 minutes and T = 3 min tests. Bed layers of 5 cm thickness were collected from top to the bottom of the bed. In case of top 5 cm layer, it was also divided into two separate layers (top layer thickness = 2 cm). All collected samples for both tests were analyzed for the ash content based on the ASTM D3174-02.

In order to compare the efficiency of separation at different bed heights and fluidization times and for different size fractions, the separation efficiency (E_p) for Air dense medium fluidized bed is used which is defined as (Choung, Mak, & Xu, 2006):

$$E_p = \frac{\rho_{75} - \rho_{25}}{2} \qquad (4-2)$$

Where, ρ_{75} and ρ_{25} are the specific gravity values on yield vs. density curve where 25% and 75% of the feed material is considered as refuse. Generally, E_p value of equal or less than 0.1 is considered as an efficient separation for ADMFB (Choung et al., 2006). In order to study the effect of coal load on ADMFB performance, three different coal loads (300 g, 100 g and 50 g) have been added to the fluidized bed at constant silica sand weight (9kg). For the finest size fraction (1.00 – 2.36 mm), coal load of 25 g also has been tested. For the finest size fraction (1.00 – 2.36 mm), coal loads of 50 g and 25 g also have been tested.

3.2 Results and discussion

3.2.1 Bed density

The average density of the bed can be calculated using equation (4 – 3) (Prashant et al. 2010):

$$\rho = (1 - \varepsilon)\rho_s + \varepsilon\rho_f \qquad (4-3)$$

Where: ε is the bed void, ρ is the bed density, ρ_s is the density of solid and ρ_f is the density of fluid. Assuming: ε = 0.4, ρ_f = 1.1839 kg/m^3 and ρ_s = 2620 kg/m^3, separation density was obtained as: ρ = 1570 kg/m^3

4.2.2 Batch ADMFB tests - intermediate fractions of Fording River (< 4.75 mm)

4.2.2.1 Sink-float analysis for intermediate fractions of Fording River sample

The washability curves were plotted for intermediate fractions (1 - 2.36, 2.36 - 3.35 and 3.35 - 4.75 mm) of Fording River sample in Fig 4.4. As seen from washability curves, the 1.38 - 1.80 g.cm^{-3} density ranges is characterized with reasonably high yield and extremely low ash content. This observation indicates the possibility of efficient ash removal by physical separation at density of 1.80 g.cm^{-3}. the ash content of the float fractions increases with increase in size in all density cuts. The yield and ash content data for sink-float tests in each size fraction have been listed in table 1 - 3 in Appendix A.

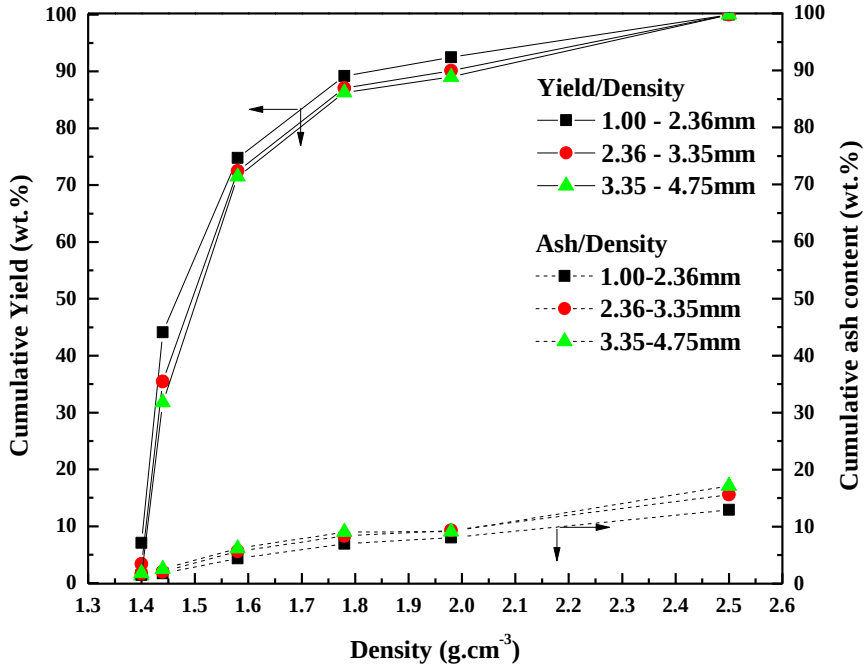

Fig 4.4 Washability curves for intermediate fractions of Fording River coal

4.2.2.2 Effect of bed height on separation efficiency

4.2.2.2.1 Bed height = 20 cm

Fig 4.5 shows the cumulative yield and ash content versus density at the bed height of 20 cm for intermediate fractions of Fording River sample. It has been observed that ρ_{50} (the density cut-point on yield vs. density curve where 50% of the feed material is considered as refuse) reduces from 1.76 g.cm^{-3} to 1.72 g.cm^{-3} with Increase in size from 1.00 - 2.36 mm to 3.35 - 4.75 mm size fraction. Furthermore, efficiency of ash separation improves with increase in size. For 3.35 - 4.75 mm size fraction, the ash content of the clean coal (separated at density of 1.70 g.cm^{-3}) is 8.15% which is substantially lower than ash content of the raw feed coal (around 17%).

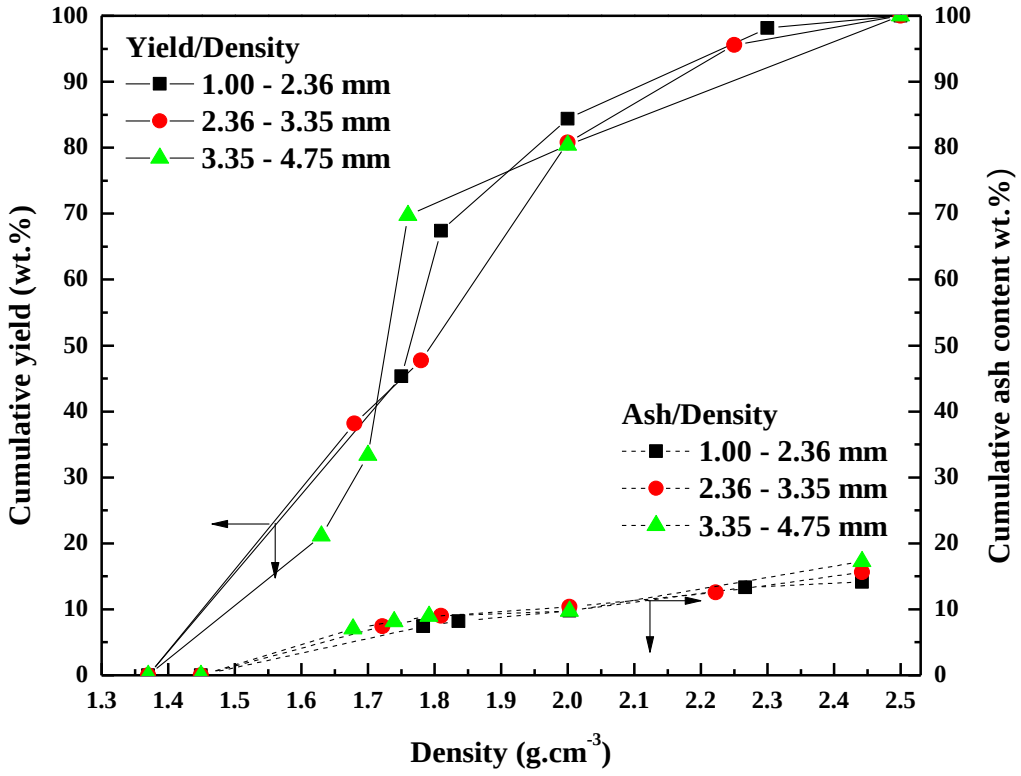

Fig 4.5 Cumulative yield and ash vs. density - intermediate fractions of Fording River sample at bed height = 20 cm

Using equation 4.2, E_p values are calculated for the intermediate size fractions and listed in Table 4.3. It can be seen that lowest E_p value obtained for 3.35 - 4.75 mm size fraction (E_p =

0.125). It is concluded that the ash rejection is somewhat more efficient in the largest size fraction, consistent with the findings of other researchers (Choung et al., 2006). Tables 4- 6 in Appendix A show the recovery and ash content for samples collected at each layer of bed height.

Table 4.3 E_p values for ADMFB tests at intermediate size fractions (bed height = 20 cm)

Size fraction (mm)	1.00 - 2.36	2.36 - 3.35	3.35 - 4.75
E_p	0.165	0.190	0.125

4.2.2.2.2 Separation at bed height (H) = 30 cm

As seen in Fig 4.6 and Tables 7 - 9 in Appendix A, the ash content of the top 5 cm layer of the bed is slightly larger than the "H = 20 cm" test. Moreover the yield of this layer is significantly lower than "H = 20 cm" test in all size fractions studied.

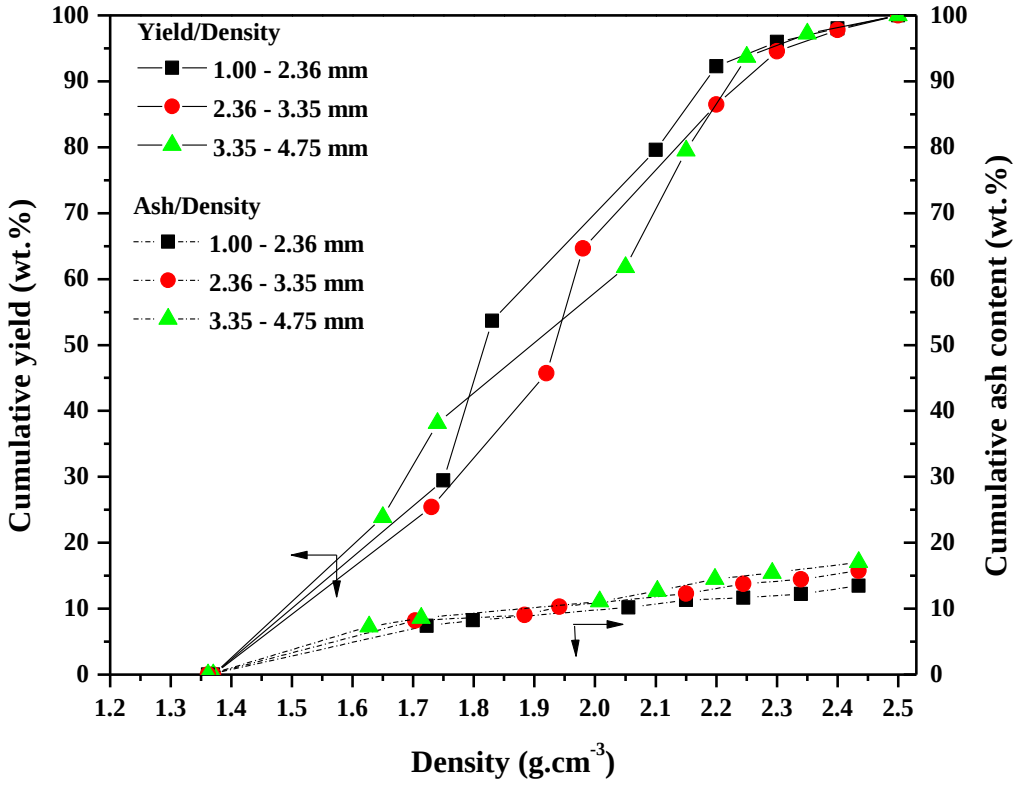

Fig 4.6 Cumulative yield and ash vs. density for intermediate size fractions for bed height = 30 cm

As shown in Table 4.4, E_p value is higher as we increase the bed height to 30 cm as compared with the bed height of H = 20 cm. It is concluded that increase in the bed height from 20 to 30 cm shows negative effect on separation efficiency. This finding may be attributed to the fact that coal particles have more space to move downward with increase in bed height.

Table 4.4 E_p values of ADMFB tests for intermediate size fractions at different bed heights

Size fraction (mm)	1.00 - 2.36	2.36 - 3.35	3.35 - 4.75
E_p (H = 30 cm)	0.185	0.175	0.235
E_p (H = 20 cm)	0.165	0.190	0.125

3.2.2.3 Effect of the fluidization time

As shown in Fig 4.7, the increase in the fluidization time significantly reduces the recovery of clean coal in top 5 cm layer of the bed for all size fractions as compared with the results in Fig 4.5 with the fluidization time of T = 3 minutes. This could be attributed to the fact that lighter coal particles which initially stayed in the top layer had more time to move downward through middle and bottom parts of the bed when fluidization time was increased. Consequently, the separating density for the first top 5 cm layer of the bed is around 2 $g.cm^{-3}$ which is significantly higher than "T = 3 minutes" experiments for all size fractions as shown in Fig 4.5. The recovery and ash content different bed layers at different fluidization time are listed in Tables 10 - 12 in Appendix A. As seen from these Tables, increase in fluidization time also leads to the remixing of coal particles and movement of lighter coal particles downward and heavier ones upward to the bed. The back mixing effect is more significant for the size fractions of 2.36 - 3.35 mm and 3.35 - 4.75 mm. As a result, no proper density-based stratification along the bed has been observed for those sizes. It can be concluded that increase in the fluidization time has negative impact on the efficiency of separation.

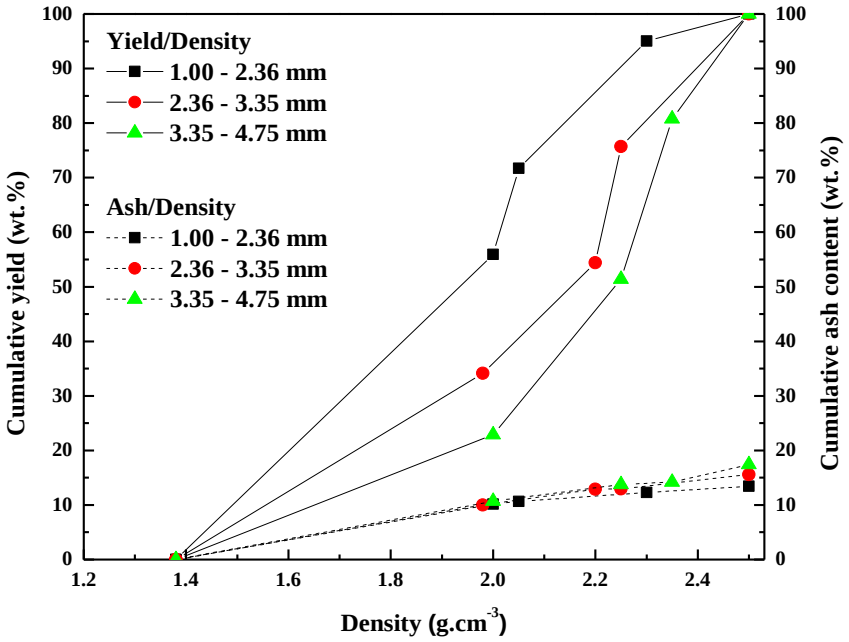

Fig 4.7 Cumulative yield and cumulative ash vs. density for intermediate size fractions at T = 8 min

4.2.2.4 Effect of feed coal load

In order to study the effect of feed coal load on the ADMFB performance, "T = 3 min and H = 20 cm" experiments have been repeated. But instead of constant coal load of 300 g, a different coal load (100 g) has been tested for all size fractions. Fig 4.8 displays the results of ADMFB tests for 100 g coal load for intermediate size fractions of Fording River sample. As seen from this Figure, reduction in the coal load results in separation of low ash coal from top layer especially in larger size fraction. For 3.35 – 4.75 mm size fraction, the ash content reduced from 17.1% in raw coal to 5.75% in top 2 cm layer of bed as compared with 7.05% for the same bed layer with coal load of 300 g. Consequently, separating density of the top layer for 3.35 – 4.75 mm is reduced from 1.64 $g.cm^{-3}$ to 1.55 $g.cm^{-3}$ by reduction in coal loading from 300 g to 100 g. For the finest size fraction (1.00 – 2.36 mm), the effect of change in the feed coal load to 50 g and 25 g also have been investigated. No significant change in the separating density of bed top layer has been observed for coal load of 50 g. In case of coal load = 25 g, clean coal with high

vitrinite content (70.2%) and lower separating density (roughly around 1.65 g.cm^{-3}) was obtained by sampling at top 1cm layer of the bed. However, this separation has been achieved in the expense of a much lower yield (around 19%) for the clean coal.

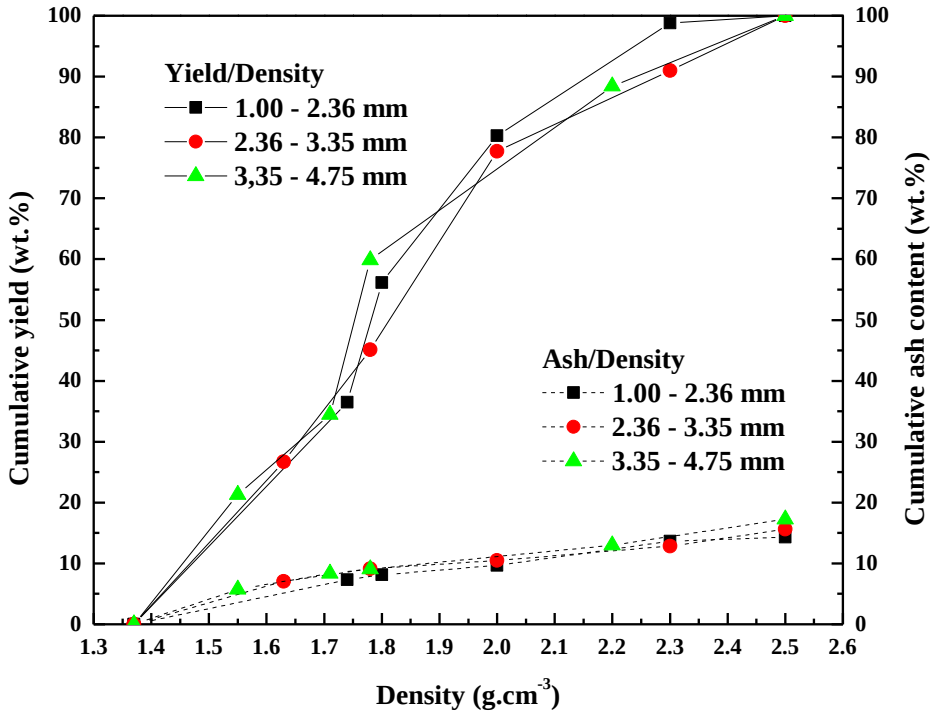

Fig 4.8 Cumulative yield and cumulative ash vs. density for H = 20 cm, T = 3 minutes and coal load = 100 g

4.2.2.5 Phosphorus removal for intermediate size fractions at T = 3 min. and H = 20 cm

In order to investigate the separation efficiency of ADMFB on the reduction of phosphorus content of Fording River coal, samples collected from 5 cm layer intervals along the bed height at "T = 3 min and H = 20 cm" conditions have been analyzed for the phosphorus content. As illustrated in Table 4.5, phosphorus is more concentrated in the bottom of the bed and specifically in the bottom 5 cm layer which is the heaviest density fraction of the coal samples in each size. As shown in Fig 4.9, the efficiency of phosphorus removal is much higher for the largest size (3.35 - 4.75 mm) as compared with smaller ones. An 80% clean coal recovery was

achieved for 3.35 – 4.75 mm size fraction while phosphorus content was reduced from 0.15% in raw coal to 0.09% in clean coal. High phosphorus rejection of this size fraction is attributed to the fact that not only phosphorus content of heavier density fraction (bottom layer of the bed) is higher in 3.35 - 4.75 mm but also the yield of this layer is significantly higher as compared with smaller size fractions. This could be explained based on washability characteristic of the coal. It can be easily observed that phosphorus is distributed through whole density range of coal. However it is more associated with heavier density fractions (gangue minerals). The extent of phosphorus inorganic affinity increases with increase in size. As a result, phosphorus can be reduced by gravity separation to reject the gangue minerals, but with the expense of lower yield.

Table 4.5 Phosphorus content of different bed layers for intermediate size fractions

Size fraction (mm)	Bed layers	Density range ($g.cm^{-3}$)	Phosphorus content (wt.%)
1.00 - 2.36	H1(top)	< 1.81	0.08
	H2	1.81 – 2.00	0.16
	H3	2.00 – 2.30	0.10
	H4(bottom)	> 2.30	0.22
2.36 - 3.35	H1(top)	< 1.78	0.06
	H2	1.78 – 2.00	0.07
	H3	2.00- 2.25	0.08
	H4(bottom)	> 2.25	0.37
3.35 - 4.75	H1(top)	< 1.70	0.12
	H2	1.70 - 1.76	0.05
	H3	1.76 – 2.00	0.13
	H4(bottom)	> 2.00	0.51

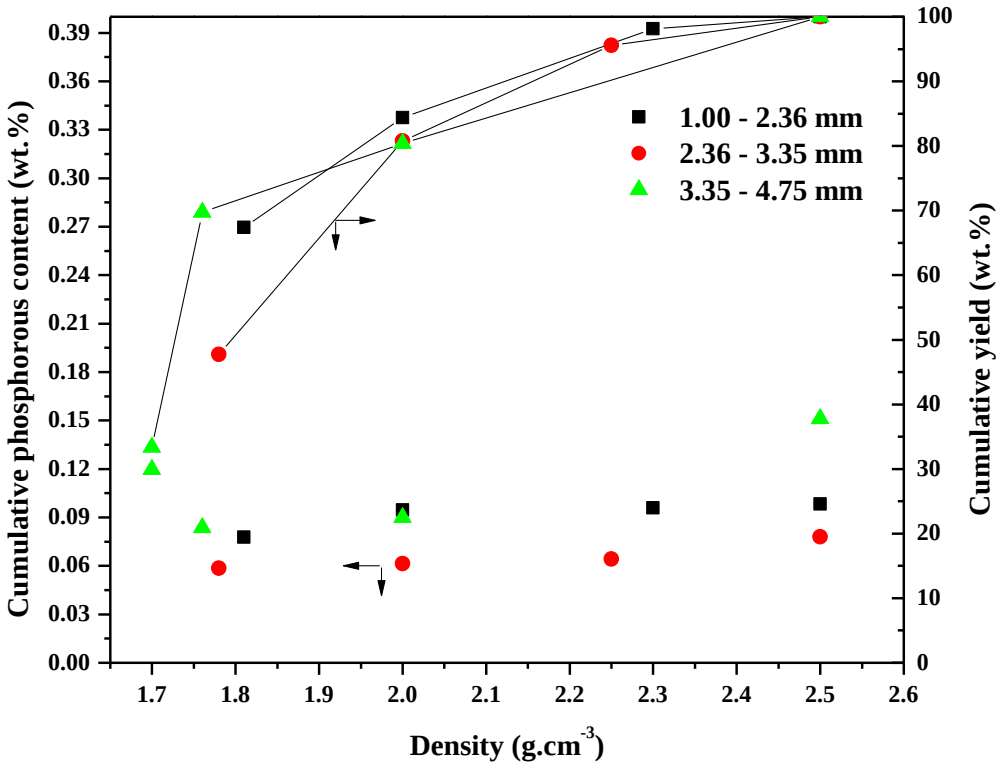

Fig 4.9 Cumulative phosphorus content vs. density for intermediate fractions of Fording River sample

4.2.2.6 Macerals content analysis for intermediate size fractions

In order to study the efficiency of ADMFB in upgrading the vitrinite content of the clean coal, the raw and clean coal in the intermediate size fractions from tests with coal load of 300 g and 100 g have been analysed for macerals distribution. The clean coal samples which were collected from top layer of the bed have been analysed for macerals distribution. As seen from Table 4.6, for coal load of 300 g, the vitrinite content of the clean coal from top layer of the bed is almost the same as the vitrinite content of the raw sample in the same size, indicating no upgrading in vitrinite content of the clean coal. For coal load of 100 g, vitrinite upgrading in clean coal is observed for all sizes except for the finest size fraction (1.00 - 2.36 mm). Best result is obtained for 3.35 – 4.75 mm size fraction with vitrinite upgrading from 45.0% in raw coal to 55.4% in the clean coal. Successful vitrinite upgrading for tests with coal load of 100 g can be attributed to

reduction in back mixing inside the top layer of the bed. As coal load decreases, the concentration of coal particles in the coal-sand mixture also reduces. Consequently, fewer number of heavy coal particles are attached to lighter coal particles and remain on the top of the bed. As a result, back-mixing of coal particles inside the top layer of the bed is minimized.

Table 4.6 Vitrinite content analysis for Fording River intermediate size fractions-ADMFB tests

Size fraction (mm)	Vitrinite content (raw coal)	Raw sample Reflectivity (%)	Coal load (g)	Clean coal vitrinite content	Clean coal Reflectivity (%)	Separating density ($g.cm^{-3}$)
1.00 - 2.36	59.0	1.20	300	60.9	1.18	1.80
			100	60.9	1.18	1.80
2.36 - 3.35	51.0	1.18	300	51.7	1.17	1.78
			100	54.5	1.19	1.63
3.35 – 4.75	45.0	1.18	300	-	-	1.70
			100	55.4	1.19	1.55

4.2.3 Batch ADMFB test for coarse fractions (> 4.75 mm) of Fording River sample

4.2.3.1 Sink-float analysis for coarse fractions of Fording River sample

Fig 4.10 shows the sink-float tests results for coarse fractions (> 4.75 mm) of Fording River sample. It can be easily observed that the yield of sink-float test for heavier densities (> 1.80 $g.cm^{-3}$) is significantly higher as compared with intermediate fractions of < 4.75 mm. It increases from roughly around 15% in 3.35 - 4.75 mm size fraction to 43% in +25 mm). Moreover, it is evident from this figure that ash content increases significantly with increase in density above 1.60 $g.cm^{-3}$. This finding indicates that separation at low density cut-points for coarse size fractions of Fording River sample is possible, but with the expense of lower yield. It can be noted that the ash content of the raw coal in coarse fractions varies from 27% for 4.75 - 13 mm to 39% for +25 mm size fraction while, the ash content of raw coal in intermediate size fractions varies from 13.82 wt.% for 1.00 – 2.36 mm to 17.2 wt.% for 3.35 – 4.75 mm size fraction.

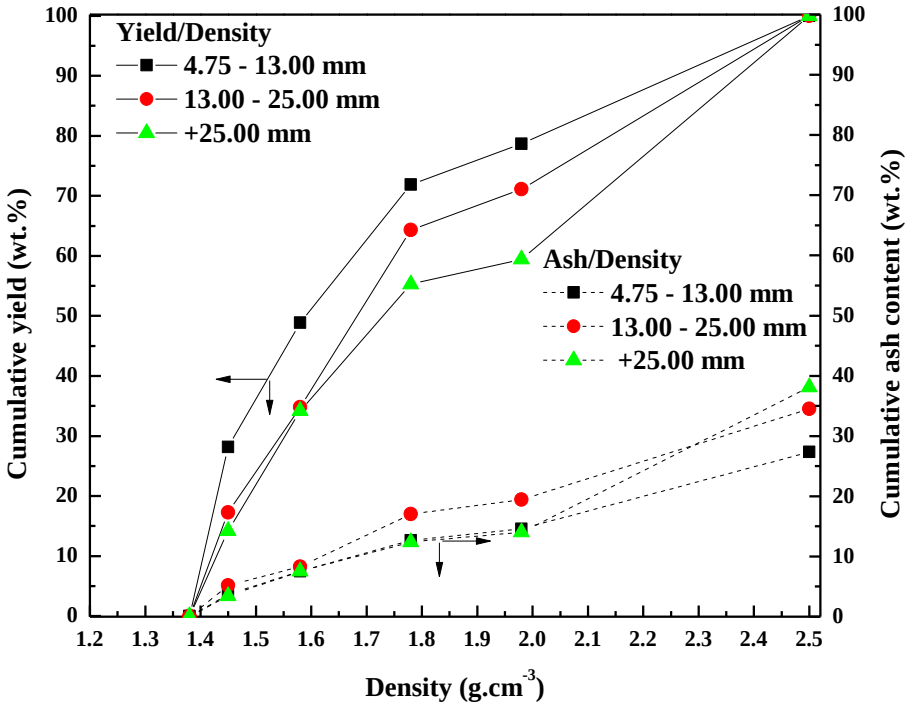

Fig 4.10 Washability curves for coarse fraction of Fording River sample

4.2.3.2 Ash separation efficiency for coarse fractions of Fording River samples

Fig 4.11 demonstrates the variation of cumulative yield and ash along the fluidized bed height as a function of the separation density for coarse fractions (> 4.75 mm) of Fording River sample. It is evident that the slope of the yield curve in the low density region of the bed is much lower for coarse fractions as compared with intermediate fractions (< 4.75 mm). This behavior can be attributed to the washability characteristics of coarse fractions where most of the coal concentrated in larger than 1.60 g.cm^{-3} density fraction. Similar to what observed by other researchers (Mak, 2007), the effect of back mixing is remarkably reduced by increasing particle size, resulting in the segregation of layers with lower densities. It has been established that for an efficient separation, coal and medium particles should be within different Geldart particle groups (Mak, Choung, Beauchamp, Kelly, & Xu, 2008). Since Geldart classification is also a function of particle size, coal and medium particles should have enough size difference to be in different

Geldart groups. As a result, increase in coal particle size improves the density segregation of coal particles. However the separation at the low density results in a lower yield. For example, ρ_{25} reduces from 1.62 g.cm^{-3} to 1.50 g.cm^{-3} with Increase in size from 4.75 - 13 mm to +25 mm size fraction.

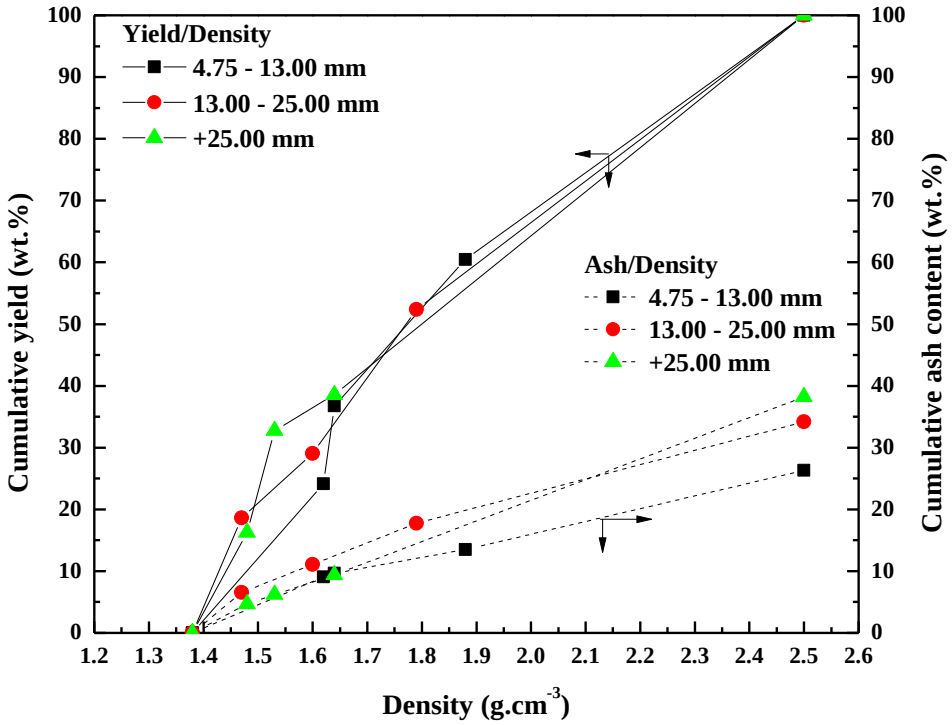

Fig 4.11 Cumulative yield and ash vs. density for coarse fractions of Fording River sample

4.2.3.3 Phosphorus removal for coarse fractions of Fording River sample using ADMFB

Table 4.7 lists the phosphorus content of coal samples collected from different layers along the bed height versus the density of the coal. Similar to the intermediate fractions, the lowest phosphorus content is in the low density fraction recovered from top 10 cm layer of the bed, indicating that the phosphorus is more associated with the inorganic part of the coal. However, for the intermediate size fractions, the phosphorus content increases with density; for the coarse fraction, no similar trend was observed. The variation of the phosphorus content as a function of

density in coarse fractions can be attributed to increase in heterogeneity of the coal. The total phosphorus content of the coal in > 13 mm size fraction is roughly around 0.13%, which is significantly higher than 4.75 – 13 mm size fraction with phosphorus content of 0.08%.

Table 4.7 Phosphorus content of different layers collected along the bed height for coarse size fractions

Size fraction (mm)	Bed layers	Density range ($g.cm^{-3}$)	Phosphorus content (wt.%)
4.75 - 13	H1(top)	< 1.62	0.04
	H2	1.62- 1.64	0.08
	H3	1.64- 1.88	0.04
	H4(bottom)	> 1.88	0.11
13 - 25	H1(top)	< 1.47	0.07
	H2	1.47 - 1.6	0.03
	H3	1.6 - 1.79	0.20
	H4(bottom)	> 1.79	0.16
+25	H1(top)	< 1.48	0.04
	H2	1.48 - 1.53	0.23
	H3	1.53 - 1.64	0.09
	H4(bottom)	> 1.64	0.14

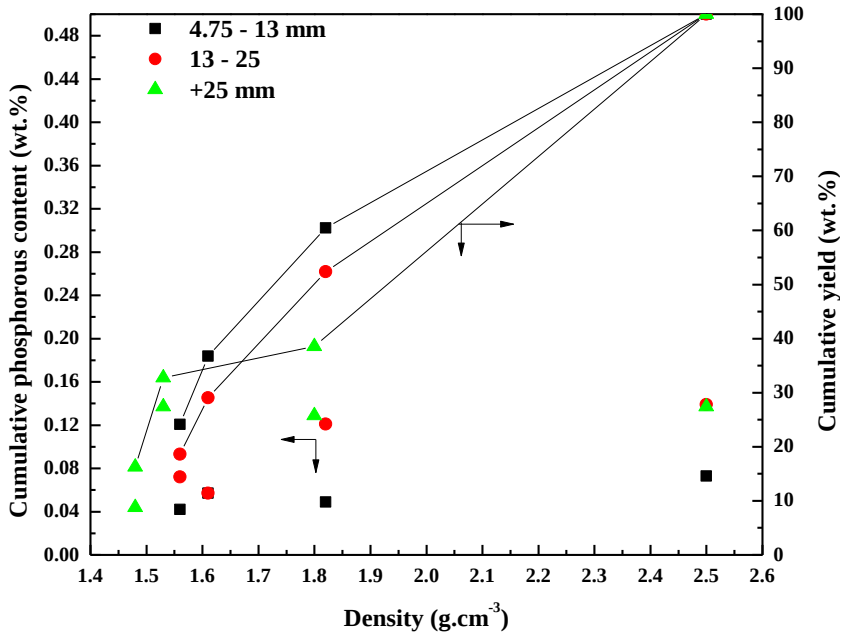

Fig 4.12 Cumulative phosphorus content vs. density for coarse fractions of Fording River sample. (Note that the first point in each curve in Fig 4.12 represents the sample recovered from top 5 cm layer of the bed. Second point represents the sample recovered from top 10 cm layer and so on.)

4.2.3.4 Vitrinite upgrading in clean coal

Table 4.8 presents the petrographic composition of clean coal collected from top of the bed for coarse fractions of Fording River sample. As seen from this table, the increase in size to above 13 mm significantly improves the vitrinite upgrading in the clean coal recovered from top of the fluidized bed. Moreover, the best results were obtained for 13 – 25 mm size fraction. This behavior can be attributed to the significant reduction in back mixing problem in larger sizes, which consequently results in much higher ash rejection to the tailing and a better segregation of coal particles. As seen from this table, the reactive portion of clean coal is remarkably higher than raw coal for all sizes. Fig 4.13 shows the comparison between raw feed coal and clean coal from ADMFB tests for the entire particle size range of Fording River sample. It can be easily observed that ADMFB is more efficient in vitrinite upgrading for coarse fractions as compared with intermediate fractions. Best result is obtained for 13 – 25 mm size fraction. Moreover, no separation is achieved for 1 – 2.36 mm.

Table 4.8 Petrographic composition of raw and clean coal of Fording River coarse size fractions-ADMFB tests

Size fraction (mm)	Separating density of clean coal ($g.cm^{-3}$)	Yield (wt.%)	Sample	Vitrinite (wt.%)	Liptinite (wt.%)	Inertinite (wt.%)	Mineral matter (wt.%)	Reactive portion* (wt.%)	Reflectivity (%)
4.75 – 13	1.64	36.77	Raw	42.70	0.70	41.70	14.90	56.20	1.14
			Clean	45.10	0.40	46.60	7.90	63.90	1.12
13 – 25	1.60	29.07	Raw	35.70	0.30	45.00	19.00	53.50	1.14
			Clean	51.58	0.34	43.08	5.00	68.26	1.13
+25	1.53	32.77	Raw	40.40	0.60	37.20	21.80	51.80	1.13
			Clean	44.70	1.00	49.50	4.80	60.40	1.19

*Reactive portion of coal which can be easily fluidized during coking process is the summation of liptinite, vitrinite and half of the semi-fusinite macerals in the coal.

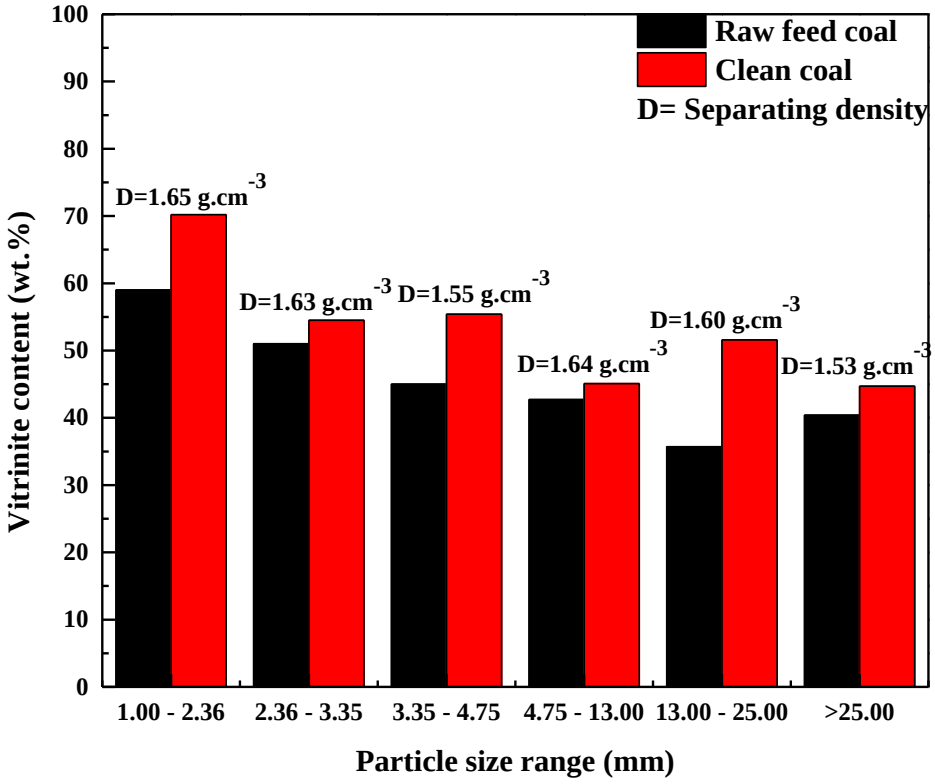

Fig 4.13 Comparison of vitrinite content in raw and clean coal for ADMFB tests of Fording River samples in different size fractions. Note that this figure shows best results obtained for each size fraction using different coal loads. For 1.00 – 2.36 mm, result for coal load of 25 g is used.

4.2.4 Batch ADMFB operation for Coal Mountain Operation sample

4.2.4.1 Sink-float analysis for Coal Mountain Operation sample

Fig 4.14 demonstrates the cumulative yield and ash content versus density for sink-float tests at different size fractions of Coal Mountain Operation sample. It should be noted that the yield of the sink-float at the density of 1.40 g.cm^{-3} is much higher in this sample in all sizes as compared with the Fording River sample. For densities less than 1.60 g.cm^{-3}, the ash content does not noticeably change with increase in particle size. However, for > 1.60 g.cm^{-3} density fraction, the ash content increases significantly with increase in size. The ash contents of all size fractions of

Coal Mountain Operation samples are remarkably higher as compared with the Fording River sample.

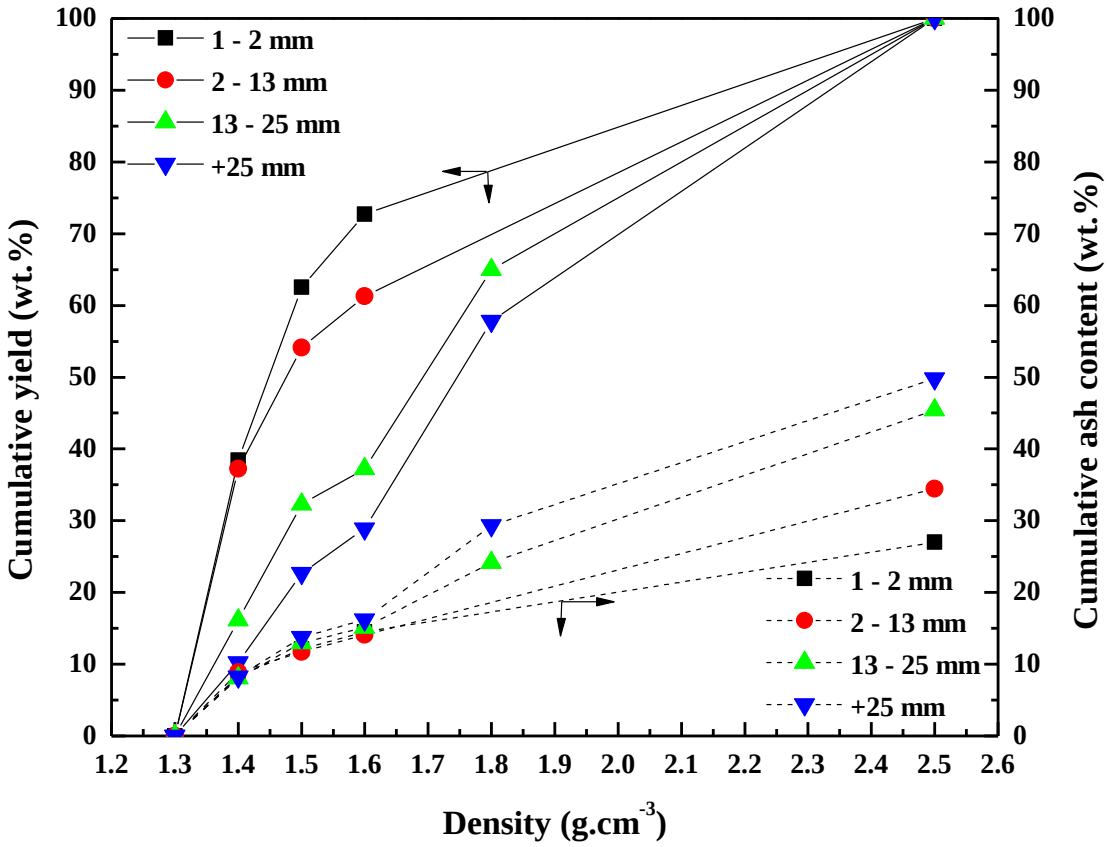

Fig 4.14 Washability curves for different size fractions of Coal Mountain Operation sample

Fig 4.15 compares the yield versus density curves for Fording River and Coal Mountain Operation samples at similar size fraction (1 – 2 mm). As seen from this figure, at any selected density in this curve, yield of sink float for Coal Mountain Operation sample is higher than Fording River sample. So it can be concluded that coal mountain operation sample is easier to wash as compared to Fording River sample especially at finer size fractions.

*The particle size range for Fording River sample in Fig. 4.15 is 1.00 – 2.36 mm which is the closest particle size range to 1 – 2 mm size fraction for Coal Mountain Operation sample.

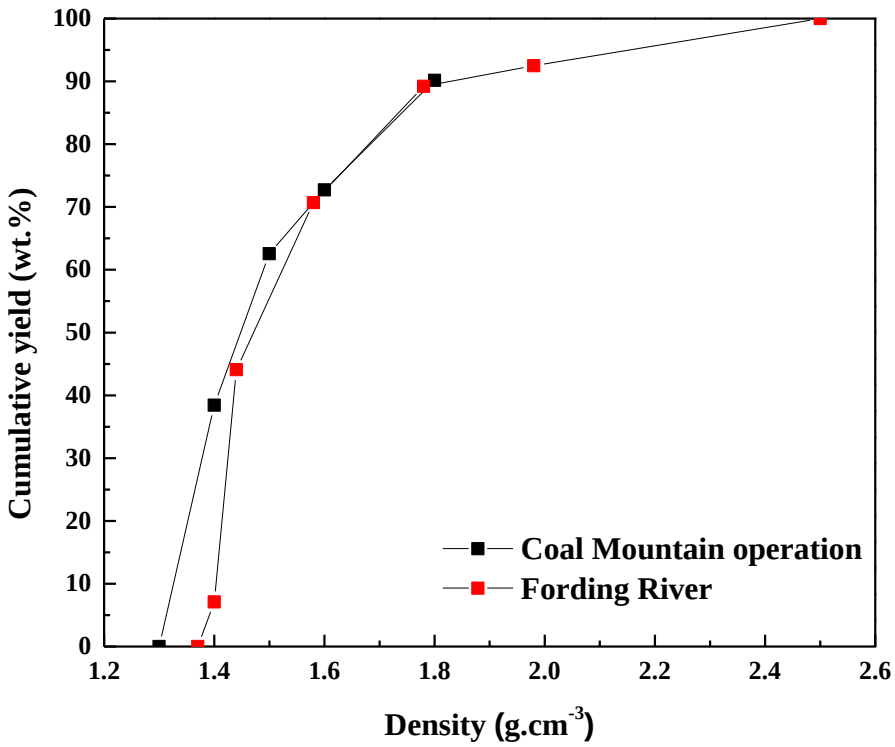

Fig 4.15 comparison of washability of Coal mountain operation and Fording River sample for 1 – 2 mm size fraction

4.2.4.2 Ash separation efficiency for different size fractions of Coal Mountain Operation sample

Fig 4.16 shows the change in the cumulative yield and ash content of the Coal Mountain Operation sample as collected from different layers along the fluidized bed height as a function of the density of the coal. Similar to Fording River sample, the cumulative yield was sharply increased in the low density range (< 1.60 $g.cm^{-3}$) for finer fractions (1 - 2 mm and 2 - 13 mm). The ash content of the bed top layer is drastically reduced with the particle size of above 13 mm. As already discussed, this behavior can be attributed to change in the washability characteristics of the coal with increase in size.

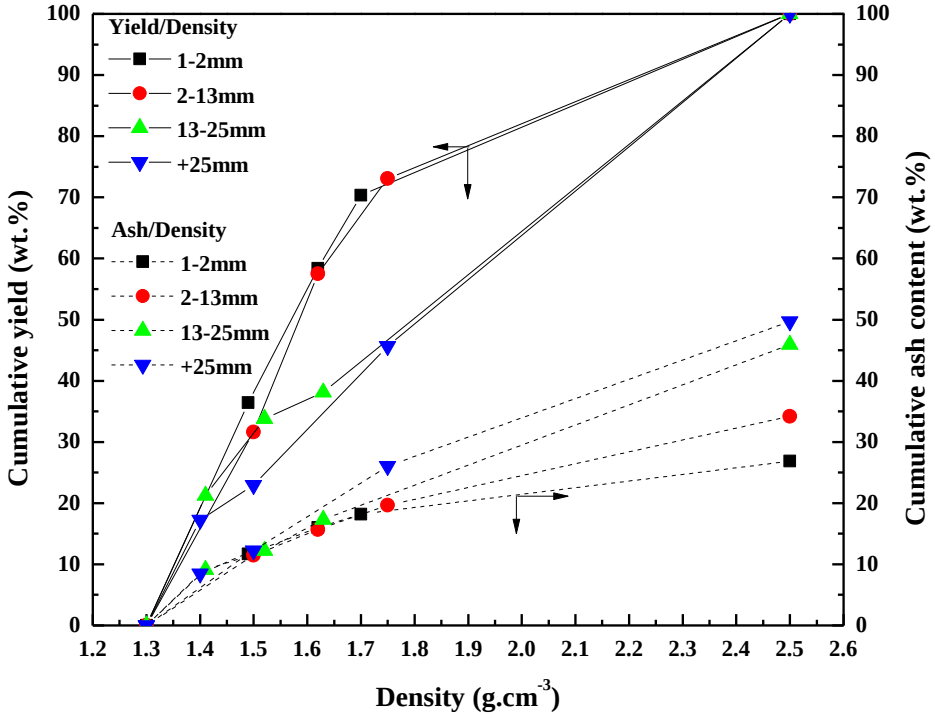

Fig 4.16 Cumulative yield and ash vs. density for ADMFB tests of different size fractions, Coal Mountain Operation

4.2.4.3 Vitrinite upgrading in clean coal

Table 4.9 shows the petrographic composition of clean coal recovered from top layer of the bed for different size fractions of Coal Mountain Operation sample. The separating density of clean coal recovered from top layer of the bed for all size fractions varies in the range of 1.49 – 1.52 $g.cm^{-3}$ which is remarkably lower as compared with Fording River samples. Despite of the Fording River sample, vitrinite upgrading in clean coal was observed for all < 25 mm size fraction, especially for fine fraction (1 - 2 mm). This behaviour can be attributed to two facts. First of all, vitrinite in Fording River sample is mainly concentrated in a narrow density range (1.38 - 1.45 $g.cm^{-3)}$ while for Coal Mountain Operation sample, vitrinite is distributed over a wider range of density and is less concentrated in the low density fraction. As a result, vitrinite upgrading can be achieved with separation at higher densities. Second reason is the difference in

ash content between these two samples. The ash content of the Coal Mountain Operation sample is considerably higher than Fording River sample. Therefore, the reduction in the ash content from raw coal to the clean coal is more significant for Coal Mountain Operation sample as compared with Fording River sample. Consequently, higher ash rejection for Coal Mountain Operation sample, results in higher vitrinite upgrading as compared with Fording River sample. As seen from Table 4.9, the vitrinite content of the clean coal in +25 mm size fraction is lower than the raw coal. A comparison between vitrinite content of raw feed coal and clean coal recovered from top of the bed for all sizes of Coal Mountain Operation samples is given in Fig 4.17. Table 27 in appendix A lists the reactive portion in raw and clean coal in all size fractions of Coal Mountain Operation sample.

Table 4.9 Petrographic composition of clean coal in different size fractions of Coal Mountain Operation sample-ADMFB tests

Size fraction (mm)	Separating density of clean coal ($g.cm^{-3}$)	Raw sample		Clean coal					
		Vitrinite (wt.%)	Reflectivity (%)	Yield (wt.%)	Vitrinite (wt.%)	Liptinite (wt.%)	Inertinite (wt.%)	Mineral matter (wt.%)	Reflectivity (%)
1 – 2	1.49	31.3*	1.08*	36.45	43.10	0.90	45.10	10.90	1.11
2 – 13	1.50	29.4	1.07	31.63	38.70	0.50	50.30	10.50	1.08
13 – 25	1.52	25.4	1.09	33.81	36.10	0.70	56.20	7.00	1.07
+25	1.50	30.3	1.07	26.65	22.30**	0.60	71.10	6.00	1.15

*Due to lack of raw sample data for 1 – 2 mm size fraction, the 0.7 – 2 mm size fraction data (given by mine owner) has been used as the nearest approximation. ** Data cannot be explained due to the complexity of coal composition in large size fraction.

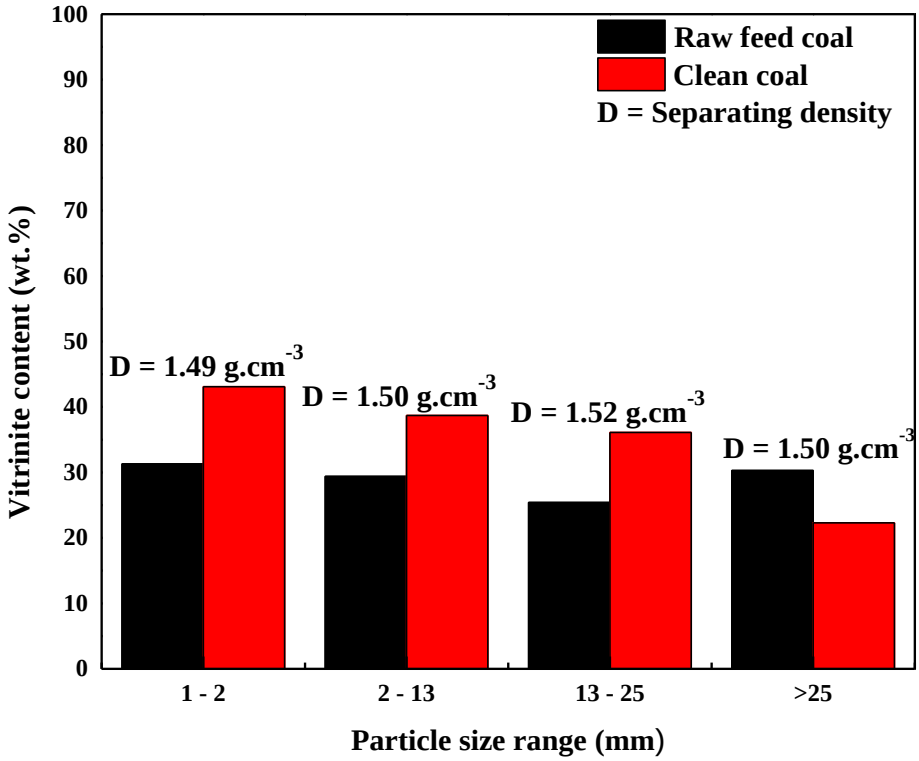

Fig 4.17 Comparison of vitrinite content in raw and clean coal for ADMFB tests in different size fractions of Coal Mountain Operation sample

Chapter5. Denver flotation cell

5.1 Experimental

5.1.1 Materials

5.1.1.1 Coal

Froth flotation was conducted for the fine size fractions of both Fording River and Coal Mountain Operation samples. Four size fractions of Fording River and Coal Mountain Operation samples (-75 µm, 75 - 212 µm, 212 – 425 µm and 425 - 600 µm) were used to study the effect of particle size on Denver cell flotation performance. The coal sample from Fording River with the size of 1000 - 600 µm was ground using a ball mill and then sieved to above-mentioned fractions. Dry coal samples are stored in a laboratory freezer at -18 °C to prevent oxidation.

5.1.1.2 Chemical additives

Sodium hydroxide solution was used to adjust the pulp pH during the experiments. MIBC and kerosene (both purchased from Fisher Scientific, Canada) were used as frother and collector respectively.

5.1.2 Experimental setup

Fig 5.1 shows the schematic diagram of the Denver cell used for the flotation tests. A one-liter flotation cell was used in flotation experiments. The air was introduced through the impeller shaft for the purpose of aeration. Air flow rate was measured using a Cole palmer rotameter (purchased from Fisher Scientific, Canada). The agitator was driven by 0.5 HP Baldor Industrial Motor. A tachometer was used to measure the Agitation speed of the flotation tests. The pH of feed pulp was measured using a portable pH meter from OAKTON Eutech Instruments.

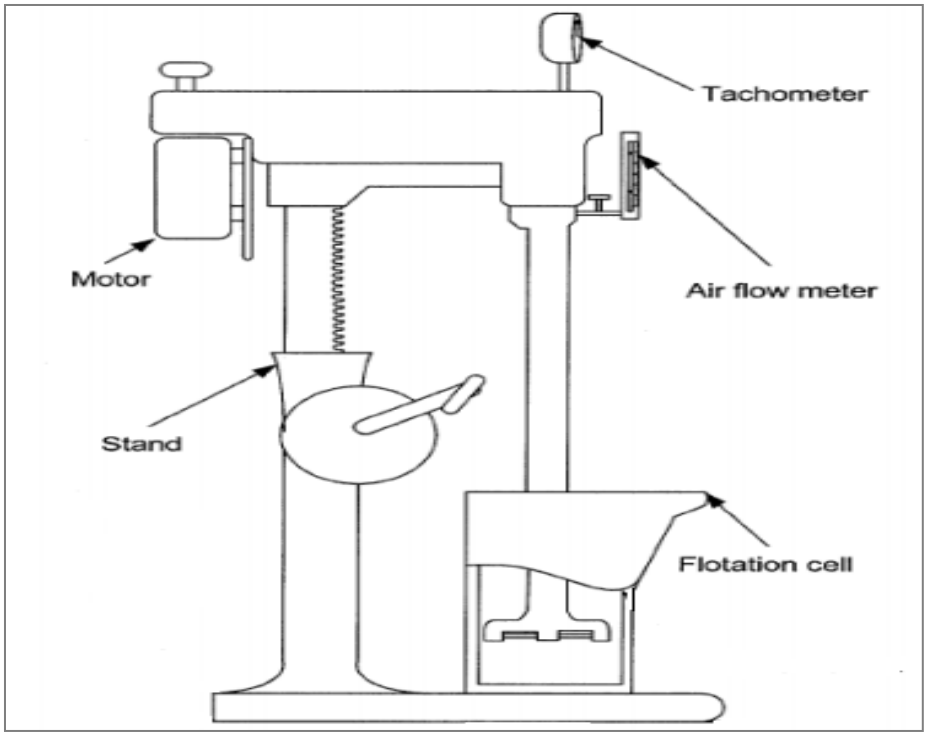

Fig 5.1.Schematic diagram of Denver Cell (L. Thomas, 2002)

5.1.3 Denver cell operation

5.1.3.1 Flotation tests for Fording River sample

In order to study the effect of pulp pHs on the vitrinite recovery, ash and phosphorus rejection, the flotation tests were conducted in 4 different pHs (7, 8, 9 and 11) and for three different size fractions (-75, 75 - 212 and 212 - 425) for Fording River sample. Flotation tests were performed for 425 - 600 μm size fraction only in slurry pH of 7 and 8 due to the very poor floatability of this fraction in high pHs. Prior to each test, 100 grams of coal sample and 1 liter of de-ionized water were mixed and agitated for 10 minutes using magnetic stirrer. The pulp pH was adjusted using sodium hydroxide solution and measured using a pH meter. The pulp was added to Denver cell and agitated for 15 minutes at 1500 rpm, followed by adding the frother (MIBC, 10 ppm). The pulp was then conditioned for an additional 5 minutes. Finally, a stream of air (flow rate 150 ml/min) was injected to the cell. Using a metal scope, the froth layer was collected by scrapping

it from top of the cell into a container until no more froth overflow observed. The air flow and agitator were switched off and collected concentrates and tailings were filtered, dried, weighed and stored for further analysis. All froth and tailing samples were analyzed for ash content using programmed electrical furnace based on the ASTM D3174-02. All froth samples were analyzed for the phosphorus content and petrographic vitrinite distribution. Due to the extremely hydrophobic nature of first coal sample, no collector was added to the pulp prior to flotation test for all experiments.

5.1.3.2 Flotation tests for Coal Mountain Operations sample

In order to study the effect of the particle size and collector dosage on the flotation recovery and ash rejection, the flotation tests were conducted for four different size fractions (< 75 μm, 75 - 212 μm, 212 - 425 μm and 425 – 600 μm). Prior to each test, 100 grams of coal sample and 1 liter of de-ionized water were mixed and agitated for 10 minutes using magnetic stirrer. The pulp was added to Denver cell and agitated for 5 minutes at 1500 rpm, followed by adding the collector (kerosene). The collector was added in five different collector dosages (0 ppm, 6 ppm, 8 ppm, 10 ppm, 15 ppm) for 212 - 425 μm and two collector dosages (0 ppm, 8 ppm) for the rest of the size fractions. The frother (MIBC, 10 ppm) was added to the pulp three minutes later after collector addition. The pulp was then conditioned for an additional 5 minutes. Finally, a stream of air (flow rate 150 ml/min) was injected to the cell. Using a metal scope, the froth layer was collected by scrapping it from top of the cell into a container until no more froth overflow was observed. The air flow and agitator were switched off and collected concentrates and tailings were filtered, dried, weighed and stored for further analysis. All froth and tailing samples were analyzed for ash content. The froth of 75 - 212 μm size (collector dosage: 8 ppm) and 212 - 425 μm size (collector dosage: 8 ppm) were analyzed for the petrographic distribution.

5.2 Results and discussion

5.2.1 Flotation tests for Fording River

5.2.1.1 Effect of pulp pH and particle size on ash separation efficiency

Fig 5.2 shows the results of the froth flotation tests at different pulp pHs for different size fractions of Fording River sample. For -75 µm and 75 – 212 µm size fractions, the increase in pulp pH significantly reduces the froth yield and ash content of the froth. However, for 212 - 425 µm fraction, the increase in pH up to 11 has less impact on both froth yield and the froth ash content. Similar trend has been observed for 425 – 600 µm size fraction at pH 7 to 9 (data for this size fraction is presented in Table 1 in appendix B). The reduction in the froth yield with increase in pH value for fine size fractions can be attributed to the decrease in coal hydrophobicity as a result of ionization of carboxylic groups on the surface (Liu, Somasundaran, Vasudevan, & Harris, 1994) which consequently reduces coal floatability. The significant reduction in froth ash content for -75 µm and 75 - 212 µm size fractions with increase in pH can be attributed to two facts. First of all, it has been experimentally established that increase in the pulp pH results in higher rejection of pyrite minerals to the tailing (Liu et al., 1994). Secondly, as already been discussed by (Jenson & Miller, 1992), the increase in pulp pH improves the dispersion of coal particles in the pulp. Table 1 in appendix B displays the froth yield and ash content of froth and tailing at different pulp pHs for all size fractions. Fig 5.3 shows the effect of particle size on flotation efficiency at neutral condition (pulp pH =7). Flotation efficiency index is a term that combines the effect of froth yield, froth ash content and tailing ash content into a single variable and is defined as (Cebeci, 2001):

$$F.E.I = \frac{A_T * W_C}{A_C} \qquad (5-1)$$

Where: $F.E.I$ is flotation efficiency index, W_C is the weight of clean coal, A_T is ash content of tailing and A_C is the ash content of the clean coal. It can be seen that the efficiency of separation increases with increase in particle size until it reaches a maximum at 212 - 425 µm and then decreases with further increase in size. The separation efficiency is poor in finest fraction (-75 µm) and in largest size fraction (425 – 600 µm) with a low ash rejection and a low froth yield. Lack of wash water in froth phase and shallow froth zone increase the probability of entrainment of fine minerals in froth zone (Zhou, 1996) and consequently results in low ash rejection for the finest fraction. Low froth yield of the largest size fraction is also due to the increase in particle-bubble detachment probability by increase in size (Mohns, 1998).

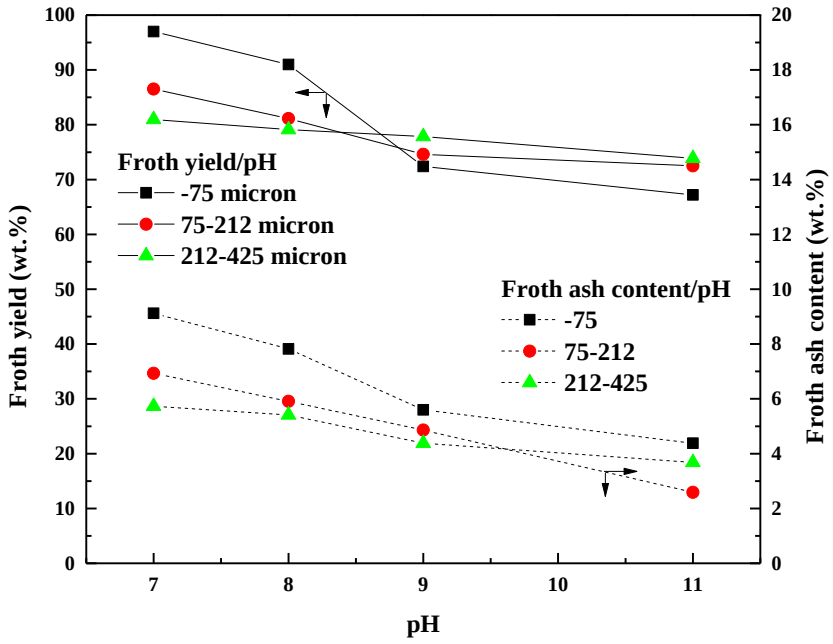

Fig 5.2 Effect of change in particle size and pulp pH on froth yield and ash content

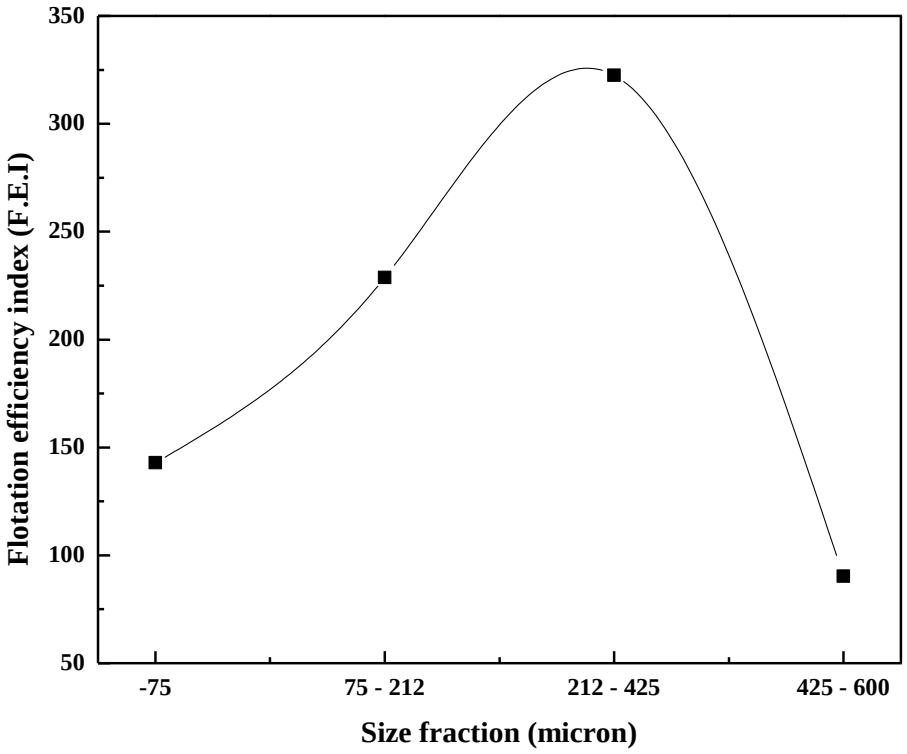

Fig 5.3 Effect of particle size on flotation efficiency at pulp pH = 7

5.2.1.2 Effect of pulp pH on phosphorus content removal

Fig 5.4 shows the comparison of phosphorus content in raw coal with flotation froth of the same size fraction at different pulp pHs for three different size fractions (-75, 75 - 212 and 212 -425 μm). Remarkable reduction in phosphorus content was achieved for all sizes at neutral pH of 7. Increase in the pulp pH to 9 seems to have a marginal effect on phosphorus content. Further increase in pH to 11 has almost no effect on phosphorus level in clean coal. It should be noted that the phosphorus content data for -75 μm size fraction at pH of 7 is not included in this figure due to the extremely high flotation yield of this size. As shown in Fig 5.5, the increase in the pulp pH to 9 also significantly increases the phosphorus rejection for all sizes. However, the further increase in pulp pH does not significantly increase the ash and phosphorus rejection.

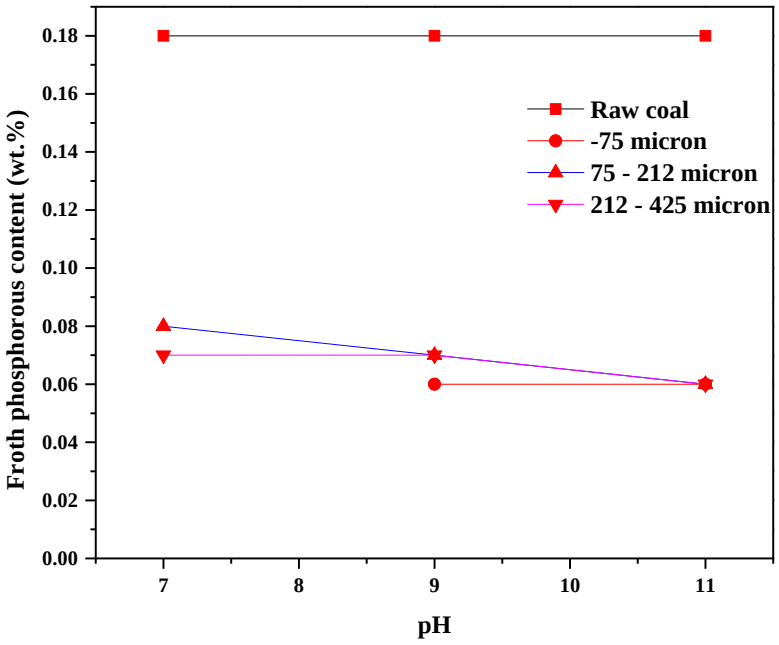

Fig 5.4 Effect of change in pulp pH on froth phosphorus content

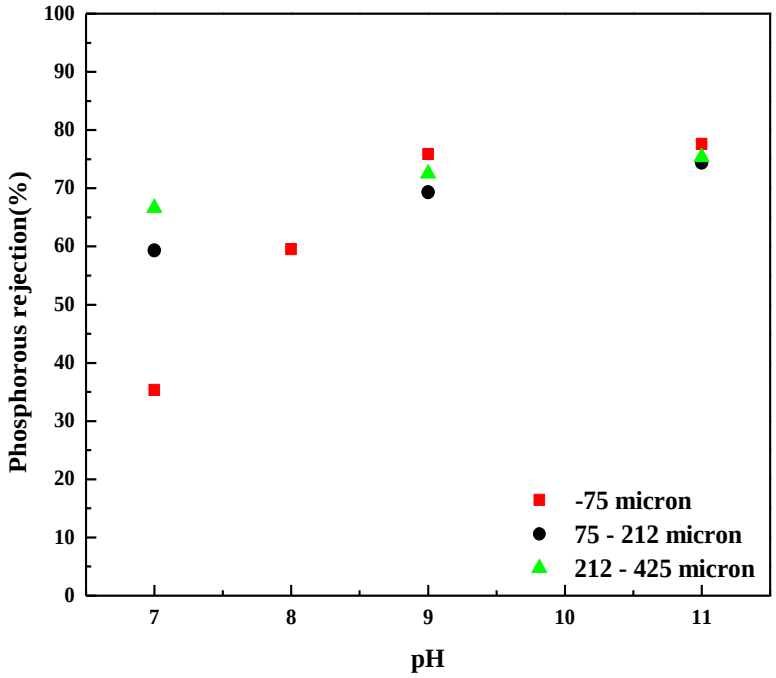

Fig 5.5 Effect of change in pulp pH on phosphorus rejection for fine fractions of Fording River sample

5.2.1.3 Effect of pulp pH on the maceral content of the froth for Fording River sample

Petrographic analysis of the froth collected at different pulp pH and for different size fractions of Fording River sample is listed in table 5.1. It is worthy to mention that the vitrinite content of the raw sample in the studied sizes varies between 65% for -75 µm to 62.5% for 212 - 425 µm. As seen from this table, the increase in pulp pH slightly improves the vitrinite content and reactive components of the froth for -75 µm and 75 - 212 µm size fractions. Increase in the coal pulp pH makes the electrostatic interaction energy between particle and bubble more repulsive as compared with neutral pH condition and reduces the floatability of less hydrophobic particles. Since inertinite is generally less hydrophobic than vitrinite, its floatability readily reduces by increase in pH and hence, the froth becomes more selective toward vitrinite rather than inertinite in higher pHs (Honaker, Mohanty, & Crelling, 1996). For 212 - 425 µm size, increase in pulp pH results in lower vitrinite content and higher inertinite content for the froth layer.

Table 5.1 Petrographic analysis of froth layer at different pulp pH for fine size fractions of Fording River sample

Size Fraction (µm)	Raw feed coal vitrinite content (wt.%)	Pulp Ph	Vitrinite (wt.%)	Inertinite (wt.%)	Reactive (wt.%)
-75	65.0	8	73.5	23.2	82.1
		9	74.3	22.4	82.2
		11	76.7	18.9	82.4
75 - 212	64.0	7	75.3	19.4	83.9
		9	78.4	18.4	86.5
		11	78.5	19.4	87.5
212 - 425	62.5	7	75.4	19.2	84.0
		9	71.5	25.3	81.9
		11	69.7	28.3	80.7

This behavior can be interpreted based on the vitrinite liberation. As discussed in first chapter, if macerals are liberated, then increase in pulp pH changes the ζ-potential and consequently

electrostatic interaction energy of the liberated macerals. As a result, it has been expected that increase in the pulp pH leads to increase in the vitrinite content and decrease in the inertinite content of the froth layer. However, the amount of vitrinite particles presented in the froth was significantly reduced with increase in particle size to above 212 µm.

5.2.1.4 Effect of flotation kinetics on ash removal and vitrinite upgrading -Fording River

Fig 5.6 displays the froth recovery as a function of flotation time. As seen from this figure, no froth is recovered after 27 minutes. Furthermore, sharpest increase in the froth recovery is happened beyond 13 minutes for both samples. Fig 5.7 shows the variation of froth yield and froth ash content with flotation time for the conducted experiments. For 75 - 212 µm size fraction, 46.2% froth yield is achieved at 6 minutes while the ash content is reduced from 10% in the raw coal to 3.2% in the froth. For 212 - 425 µm size fraction, 51% froth yield is achieved at T = 6 minutes while the ash content is reduced from 10% in the raw coal to 3.2% in the froth.

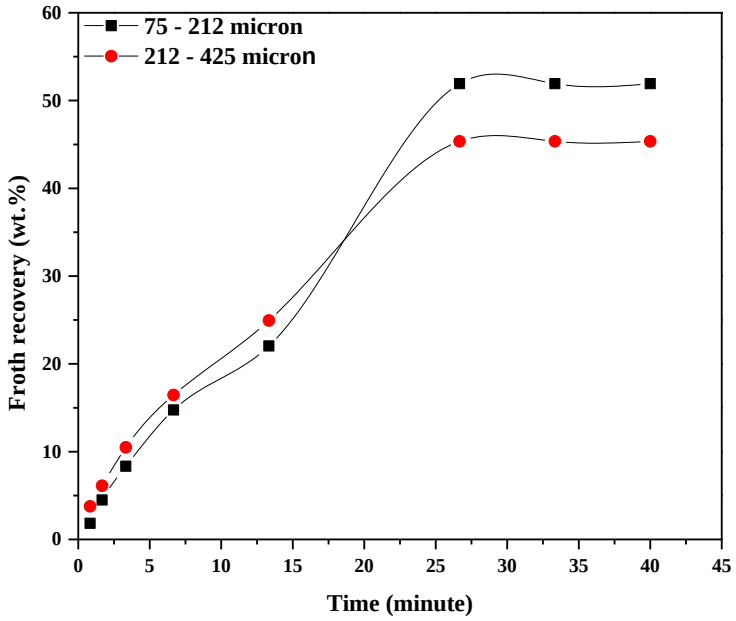

Fig 5.6 Froth recoveries vs. flotation time for fine fractions of Fording River sample

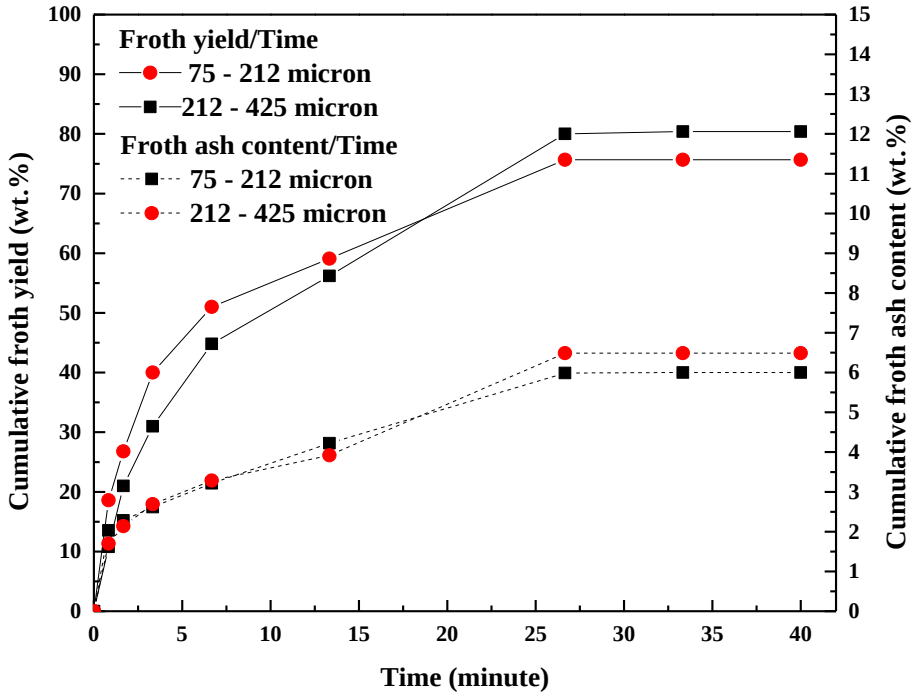

Fig 5.7 Cumulative froth yield and froth ash content vs. flotation time for fine fractions of Fording River sample

Table 5.2 displays the vitrinite content of the froth sample collected at T = 6 minutes as compared with vitrinite content of froth (over entire flotation time) and raw coal in the studied size fractions. As seen from this table, vitrinite content of the samples collected before T = 6 minutes is significantly higher than vitrinite content of the froth over entire flotation time. So it can be concluded that froth contains more vitrinite in first six minutes of flotation and afterwards the vitrinite content is dropped. This behaviour can be attributed to the fact that vitrinite macerals are more hydrophobic than other macerals. As a result, they quickly become floatable at the first couple of minutes of flotation.

Table 5.2 Effect of flotation kinetics on froth vitrinite content-Fording River

Size fraction (µm)	Raw coal vitrinite content (wt. %)	Froth vitrinite content over entire flotation time (wt. %)	Froth vitrinite content collected before T=6 minutes (wt. %)
75 - 212	64	75.3	79.8
212 - 425	62.5	75.4	81.2

5.2.2 Flotation tests for Coal Mountain Operation sample

5.2.2.1 Effect of collector dosage on froth ash content

In order to find the optimum dosage of collector, flotation tests were conducted for 212 - 425 µm size fraction at five different collector dosages (0 ppm, 6 ppm, 8 ppm, 10 ppm, 15 ppm). As shown in Fig 5.8, the froth yield of this size fraction increases with the collector dosage. However, the high collector dosage reduces the froth quality, and results in high ash content in the froth. This finding is in accordance with finding that reported by Naik, Reddy, & Misra (2005).

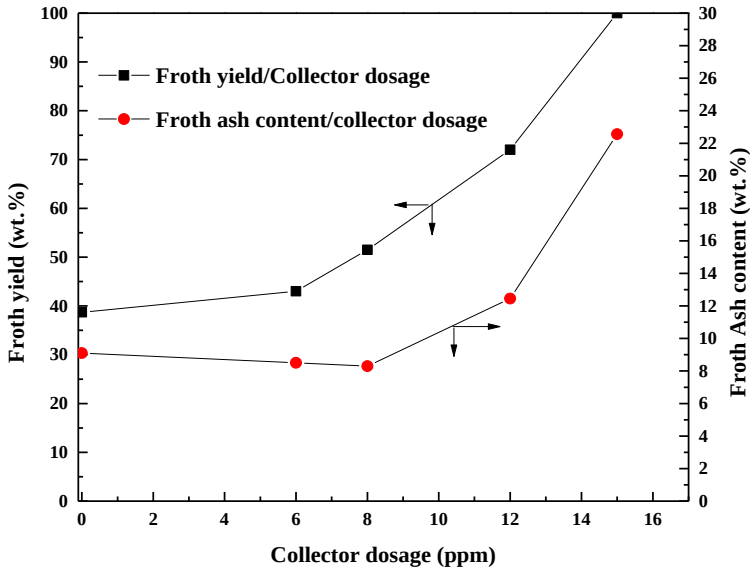

Fig 5.8 Effect of collector dosage on froth yield and ash content for 212 - 425 µm size fraction

Since the main aim of the froth flotation tests was to upgrade the vitrinite content of the coal, the collector dosage at 8 ppm was chosen for the flotation of coal sample in the 75 – 212 µm, 212 – 425 µm and 425 – 600 µm size fractions. For -75 µm, collector addition leads to flotation of all coal particles and almost no tailing is observed in this condition.

5.2.2.2 Effect of particle size on froth yield, froth ash content and froth vitrinite content

Table 5.3 shows the froth yield, ash and vitrinite content for the fine fractions of Coal Mountain Operation sample. Very small amount of tailing has been observed for the size fraction of -75 µm with and without addition of collector. Further attempt to increase the slurry pH to 11 does not improve the ash rejection for this size fraction. However, increase the size fraction to 75 - 212 µm significantly improves the coal particles dispersion and results in better ash separation. Increase in size up to 425 µm also significantly improves the ash rejection. However, the froth yield is also notably reduced with increase in particle size. Further increase in size fraction to 425 – 600 µm has negative effect on both froth yield and ash rejection.

Table 5.3 Froth flotation tests results for fine size fractions of Mountain Operation sample

Size fraction (µm)	Collector dosage (ppm)	Raw feed coal ash content (wt.%)	Raw feed coal vitrinite content (wt.%)	Froth recovery (wt. %)	Froth ash content (wt. %)	Froth vitrinite content (wt.%)
-75	0	22.26	34.9	96.0	22.00	-
-75	8			98.0	22.20	-
75 - 212	0	21.30	35.5	53.2	14.18	49.8
75 - 212	8			83.8	19.63	-
212 - 425	0	22.35	35.5	44.2	9.12	-
212 - 425	8			60.3	10.32	47.0
425 - 600	8	22.06	34.0	36.7	15.67	-

Table 5.3 also lists the vitrinite content of raw feed coal and the froth samples for flotation tests of fine fractions of Coal Mountain Operation sample. As shown in this table, vitrinite content of the froth is significantly higher than the raw coal for both size fractions. Efficiency of vitrinite

upgrading by flotation is slightly higher for 75 - 212 µm as compared with 212 – 425 µm. This behavior can be attributed to liberation of vitrinite macerals in smaller particle size. Complete petrographic analysis of froth for the studied size fractions is presented in Table 3 in Appendix B.

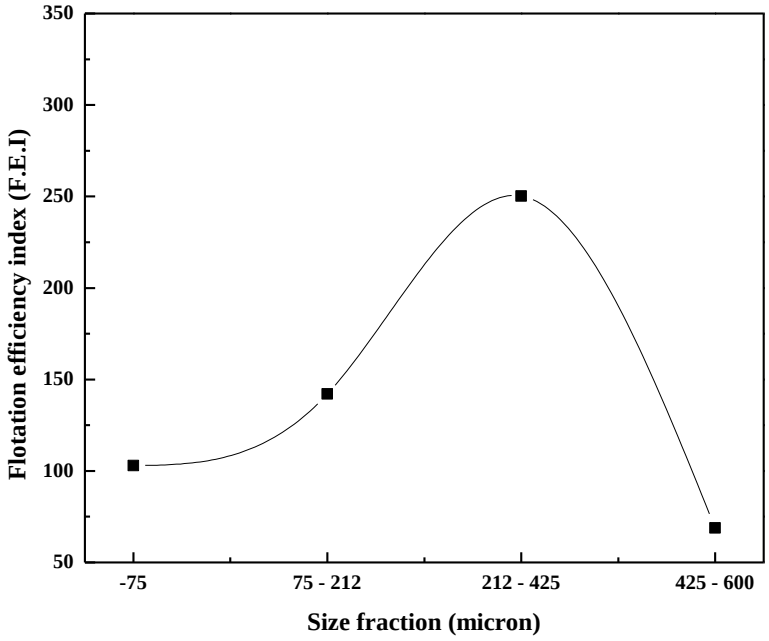

Fig 5.9 Effect of particle size on flotation efficiency index for collector dosage of 8 ppm

Fig 5.9 shows the effect of particle size on flotation efficiency index for the studied size fraction at collector dosage of 8 ppm. As seen from this figure, the flotation efficiency index increases with increase in size until it reaches a maximum at 212 – 425 µm and then decreases with further increase in size. It can be noted that the flotation efficiency index is smaller as compared with Fording River sample in all size fractions.

5.2.2.3 Flotation kinetics for Coal Mountain Operation sample

Fig 5.10 displays the froth recoveries as a function of flotation time for fine fractions of Coal Mountain Operation sample at constant collector dosage of 8 ppm and frother dosage of 10 ppm.

As seen from this figure, no froth is recovered after 13 minutes for 212 – 425 µm and after 26 minutes for 75 – 212 µm. Furthermore, sharp increase in the froth recovery is happened beyond 3 minutes for both samples.

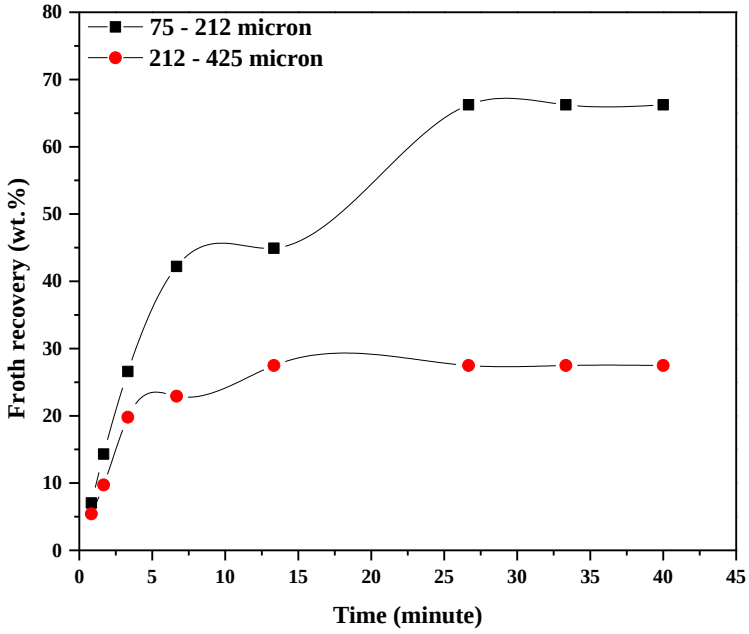

Fig 5.10 Froth recoveries and froth ash content vs. flotation time - Coal Mountain Operation

Fig 5.11 shows the variation of cumulative froth yield and ash content as a function of flotation time for 75 – 212 µm and 212 - 425 µm size fractions of Coal Mountain Operation sample. For 75 - 212 µm size fraction, 42.4% froth yield is achieved at T = 3 minutes while the ash content is reduced from 22% in the raw coal to 13.35% in the froth. For 212 - 425 µm size fraction, 50% froth yield is achieved at T = 3 minutes while the ash content is reduced from 23% in the raw coal to 8.8% in the froth.

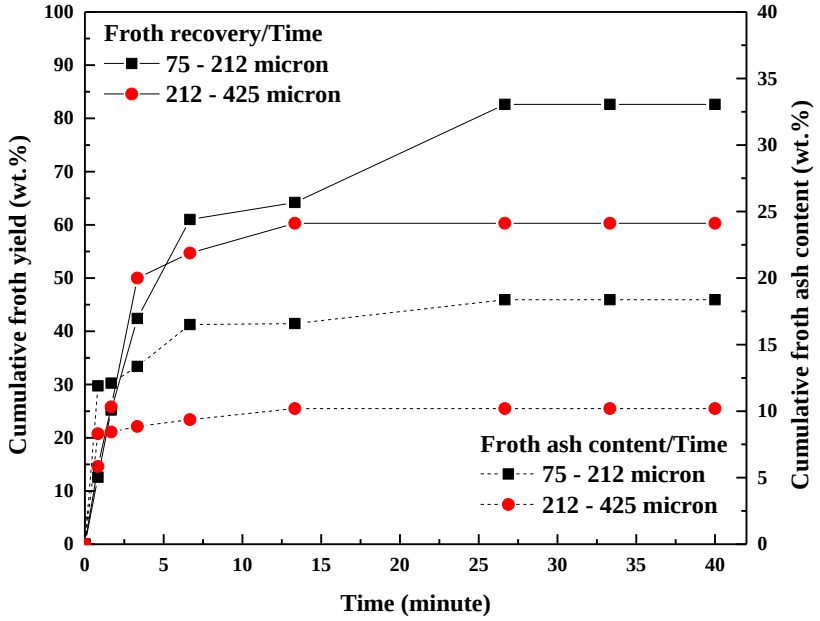

Fig 5.11 Froth yield and froth ash content vs. flotation time - Coal Mountain Operation

Table 5.4 displays the vitrinite content of the froth sample collected at T = 3 minutes as compared with vitrinite content of froth (over entire flotation time) and raw coal in the studied size fractions. Similar to Fording River sample, vitrinite content of the samples collected before T = 3 minutes is slightly higher than the ash content of the froth over entire flotation time. Again, this behaviour can be attributed to the higher hydrophobicity of vitrinite macerals as compared with the rest of the macerals. As a result, they quickly become floatable at the first couple of minutes of flotation.

Table 5.4 Effect of flotation kinetics on froth vitrinite content- Coal Mountain Operation

Size fraction (µm)	Raw coal vitrinite content (wt. %)	Froth vitrinite content over entire flotation time (wt. %)	Froth vitrinite content collected before T= 3 minutes (wt. %)
75 – 212	35.5	45.0*	45.0
212 – 425	35.5	47.0	49.0

* Estimated based on results obtained without adding collector

Chapter6. Conclusions

6.1 Analysis of petrographic composition and phosphorus distribution of density separated coal fractions for Fording River sample

Based on extensive size and density analysis on fine fraction of Fording River coal it can be concluded that:

- Vitrinite-rich density fraction of Fording River coal is 1.38 - 1.45 $g.cm^{-3}$.
- The recovery of vitrinite in this fraction significantly is increased by decrease in size below 425 μm due to liberation of macerals.
- Phosphorus in this coal is more associated with minerals rather than macerals.
- Density separation at density of 1.45 $g.cm^{-3}$ significantly reduces the phosphorus in the fine fractions of this coal (up to 35%).
- Further phosphorus removal is still necessary for this coal to meet the required phosphorus level (0.05 %) for use in blast furnaces

6.2 Air dense medium fluidized bed

Based on the result of the batch air dense medium fluidized bed experiments for Fording River and Coal Mountain Operation samples following conclusions can be derived:

- Clean coal with low ash content is obtained using this method for all sizes of both samples.

For Fording River sample:

- Increase in bed height (from 20 to 30 cm) and fluidization time (from 3 to 8 minutes) has negative effect on the ash separation efficiency of Fording River sample.

- Reduction in coal load (from 300 g to 100 g) for intermediate fractions reduces the back mixing and results in separation of coal fractions with low ash and high vitrinite content.
- An 80% clean coal yield is achieved for 3.35 – 4.75 mm size fraction while ash content is reduced from 17 wt. % in raw coal to 9.75% in clean coal.
- Good phosphorus rejection has been observed for all sizes.
- An 80% clean coal yield is achieved for 3.35 – 4.75 mm while phosphorus content is reduced from 0.15 wt. % in raw coal to 0.09 wt. % in clean coal.
- No significant vitrinite upgrading is observed for the 1 – 2.36 mm size fraction.
- Good vitrinite upgrading is achieved with reduction in coal loading from 300 g to 100 g for 2.36 – 4.75 mm but in expense of lower yield.
- Considerable vitrinite upgrading is achieved with the size fraction of larger than 13 mm, but in the expense of lower yield of the clean coal.

For Coal Mountain Operation sample:

- A 73% clean coal yield is achieved for 2 – 13 mm size fraction while the ash content was reduced from 32.4 wt. % in raw coal to 19.6 wt.% in clean coal.
- The vitrinite content of clean coal in < 25 mm size fraction is increased significantly.
- A 36.5 wt. % clean coal yield was achieved while the vitrinite content is increased from 31.3 wt. % in raw coal to 43.1 wt. % in clean coal for 1 – 2 mm size fraction.

- Contrary to Fording River sample, efficient separation of < 1.50 $g.cm^{-3}$ density fraction has been observed for Coal mountain Operation sample.

6.3 Denver cell froth flotation

Based on the result of the Denver cell flotation for fine coal fractions it can be concluded that:

I) Fording River sample:

- For 75 - 212 µm size fraction, 56.2% froth yield is achieved at T = 6 minutes while the ash content is reduced from 10% in the raw coal to 3.9% in the froth.
- For 212 - 425 µm size fraction, 51% froth yield is achieved at T = 6 minutes while the ash content is reduced from 10% in the raw coal to 3.2% in the froth.
- For 75 - 425 µm size fraction, froth yield of 53% is achieved at T = 6 minutes while the vitrinite content is increased from 64% in the raw coal to 80% in the froth.

- At neutral pH, the efficiency of ash rejection and vitrinite upgrading increases by increase in particle size up to 425 µm and then decreases.
- The effect of pulp pH on froth yield and ash rejection of 212 - 425 µm size fraction is less significant than smaller size fractions.
- Increase in pulp pH to 9 has a marginal effect on froth phosphorus content.
- Increase in pulp pH up to 11 has a positive effect on vitrinite upgrading for < 212 µm particle size and negative effect for 212 - 425 µm

II) Coal Mountain Operation sample

- For 75 - 212 µm size fraction, 42.4% froth recovery is achieved at T = 3 minutes while the ash content is reduced from 22% in the raw coal to 13.35% in the froth

- For 212 - 425 µm size fraction, 50% froth recovery is achieved at T = 3 minutes while the ash content is reduced from 23% in the raw coal to 8.8% in the froth
- The efficiency of ash rejection increases with particle size up to 425 µm and then decreases
- Significant vitrinite upgrading has been achieved for the particle size of 75 - 425 µm.
- No tailing is observed for < 75 µm size fraction due to agglomeration of fine coal particles.

6.4 Comparison of Fording River and Mountain Operation coals

Fording River sample

- Hard to wash – low ash content
- Coarse fractions (> 3 mm): Using ADMFB, Vitrinite can be upgraded from 41% to 50% by separation at density of 1.55 $g.cm^{-3}$ with yield of 35% while the ash content can be reduced from 27.5% to 9.0%.
- Phosphorus level can be reduced from 0.12% to 0.07% by separating at density of 1.55 $g.cm^{-3}$.
- Fine fraction (< 425 µm): Using froth flotation (6 minutes) vitrinite can be upgraded from 63% to 80% with yield of 50% while ash content can be decreased from 10% to 3%.

Coal Mountain Operation

- Easy to wash - high ash content

- Coarse fractions (> 1 mm): Using ADMFB, Vitrinite can be upgraded from 29% to 37% by separation at density of 1.55 $g.cm^{-3}$ with yield of 35% while the ash content can be reduced from 35.0% to 10.6%.

- Fine fraction (< 425 µm): Using froth flotation (3 minutes) vitrinite can be upgraded from 35% to 50% with yield of 50% while ash content can be reduced from 22% to 11%.

References

Al Taweel, A. M., Delory, B., Wozniczek, J., Stefanski, M., Andersen, N., & Hamza, H. A. (1986). Influence of the surface characteristics of coal on its flotability. *Colloids and Surfaces, 18* (1), 9-18.

Arnold, B. J., & Aplan, F. F. (1989). The hydrophobicity of coal macerals. *Fuel, 68* (5), 651-658.

Bowman, R. A. (1988). A rapid method to determine total phosphorus in soils. *Soil Science Society of America, 52*, 1301-1304.

Burchill, P., Howarth, O. W., Richards, D. G., & Sword, B. J. (1990). Solid-state nuclear magnetic resonance studies of phosphorus and boron in coals and combustion residues. *Fuel, 69* (4), 421-428.

Carr, A. J., & Jorgensen, J. G. (1975). An estimation of the effective reactive/inert ratio of semifusinite in western Canadian coals No. 141). Ottawa: CANMET.

Carter, M. R. (1993). Total and organic phosphorus. *Soil sampling and method of analysis* (pp. 121-123) CRC Press.

Cebeci, Y. (2001). The investigation of flotability improvement of yozgat ayridam lignite using various collectors. *Fuel, 81*, 281-289.

Chaudhary, P. N. (1999). Dephosphorization of high carbon ferromanganese using $BaCO_3$ based fluxes. Unpublished PhD, Department Of Metallurgical And Materials Engineering Iidian Institure Of Technology, Kharagpur,India.

Chen, Q., & Yang, Y. (2003). Development of dry beneficiation of coal in china. *Coal Preparation: A Multinational Journal, 23* (1-2), 3-12.

Choi, C., & Dyrkacz, G. R. (1989). Base-catalyzed separation of coal macerals. *Energy & Fuels, 3* (5), 579-585.

Choi, C., Dyrkacz, G. R., & Stock, L. M. (1987). Density separation of alkylated coal macerals. *Energy & Fuels, 1* (3), 280-286.

Choung, J., Mak, C., & Xu, Z. (2006). Fine coal beneficiation using an air dense medium fluidized bed. *Coal Preparation, 26* (1), 1-15.

Claassens, V. (2009). The release of mineral matter and associated phosphorus as a function of the particle size coal. *International Journal of Coal Preparation and Utilization, 29* (3), 99-111.

Díez, M. A., Alvarez, R., & Barriocanal, C. (2002). Coal for metallurgical coke production: Predictions of coke quality and future requirements for cokemaking. *International Journal of Coal Geology, 50* (1–4), 389-412.

Dwari, R. K., & Rao, K. H. (2007). Dry beneficiation of coal - A review. *Mineral Processing and Extractive Metallurgy Review, 28* (3), 177-234.

Dyrakacz, G. R., Bloomquist, C. A. A., Ruscic, L., & Horwitz, E. P. (1983). Some variations in properties of coal macerals elucidated by density gradient separation. *Preprints - American Chemical Society, Division of Fuel Chemistry, Volume 28, Number 1.* Seattle, WA, USA. *, 28* (1) pp. 93-96.

Dyrkacz, G. R. (1994). *Adventures in maceral separation* No. ANL/CHM/CP--81225; CONF-940301--15). IL (United States): Argonne National Lab.

Dyrkacz, G. R., & Bloomquist, C. A. A. (1992a). Use of continuous flow centrifugation techniques for coal maceral separation. 1. fundamentals. *Energy & Fuels, 6* (4), 357-374.

Dyrkacz, G. R., & Bloomquist, C. A. A. (1992b). Use of continuous flow centrifugation techniques for coal maceral separation. 2. multiple density fractionations of coals. *Energy & Fuels, 6* (4), 374-386.

Dyrkacz, G. R., Bloomquist, C. A. A., & Ruscic, L. (1984). High-resolution density variations of coal macerals. *Fuel, 63* (10), 1367-1373.

Dyrkacz, G. R., & Horwitz, E. P. (1982). Separation of coal macerals. *Fuel, 61* (1), 3-12.

Dyrkacz, G. R., Ruscic, L., & Fredericks, J. (1992). An investigation into the process of centrifugal sink/float separations of micronized coals. 1. some inferences for coal maceral separations. *Energy and Fuels, 6* (6), 720-742.

Dyrkacz, G. R., Bloomquist, C. A. A., & Horwitz, E. P. (1981). Laboratory Scale Separation Of Coal Macerals. *Separation Science and Technology, 16* (10), 1571-1588.

Falcon, R. M. S. (1978). Coal In South AFfrica - 2. The Application Of Petrography To The Characterization Of Coa. *Miner Sci Eng, 10* (1), 28-52.

Fan, M., Luo, Z., Tao, D., Zhao, Y., & Chen, O. (2009). Dry coal separation with a vibrated air-dense medium fluidized bed. *SME Annual Meeting and Exhibit and CMA's 111th National Western Mining Conference 2009*, Denver, CO. , *2*. pp. 714-717.

Garand, D. K. (1993). A study of operating variables in the column flotation of fine coal. (M.Sc., University of Alberta (Canada)). , 160.

Geldart, D. (1973). Types of gas fluidization. *Powder Technology, 7* (5), 285-292.

Geldart, D. (1986). Charactrization of fluidized powsers. *Gas fluidization technology* (pp. 41). New York: John Wiley and Sons.

Geldart, D., & Wong, A. C. Y. (1985). Fluidization of powders showing degrees of cohesiveness-II. experiments on rates of de-aeration. *Chemical Engineering Science, 40* (4), 653-661.

Gluskoter, H. J., Ruch, R. R., Miller, W. G., Cahill, R. A., & Dreher, G. B. K.,J.K. (1977). Occurrence and distribution of trace elements in coal No. 61801). Urbana,IL: Illinois State Geological Survey.

Gransden, J. F., Jorgensen, J. G., Manery, N., Price, J. T., & Ramey, N. J. (1991). Applications of microscopy to coke making. *International Journal of Coal Geology, 19* (1-4), 77-107.

Grieve, D. A. (1992). *Phosphorus in british columbia coking coals* B.C Ministry of Energy,Mines and petroleum Resources,Open File.

Gupta, R. (1990). Dry electrostatic beneficiation of illinois coal and eastern oil shales. (Ph.D., Illinois Institute of Technology). , 235.

Gupta, S., Shen, F., Lee, W. -., & O'Brien, G. (2012). Improving coke strength prediction using automated coal petrography. *Fuel, 94*, 368-373.

Harvey, R. D., & Ruch, R. R. (1984). Overview Of Mineral Matter In U. S. Coals. *Preprints of Papers - American Chemical Society, Division of Fuel Chemistry, Volume 29, Number 4.* Philadelphia, PA, USA. , *29.* (4) pp. 2-8.

Holuszko, M. E. (1979). Wettability and floatability of coal macerals as derived from flotation in methanol solutions. (MSc, Technical University of Silesia , Mining and Mineral Process Engineering, Poland) , 44.

Honaker, R. Q., Mohanty, M. K., & Crelling, J. C. (1996). Coal maceral separation using column flotation. *Minerals Engineering, 9* (4), 449-464.

Hower, J. C., Frankie, K. A., Wild, G. D., & Trinkle, E. J. (1984). Coal microlithotype response to froth flotation in selected western kentucky coals. *Fuel Processing Technology, 9* (1), 1-20.

Jenson, G. F., & Miller, J. D. (1992). *Selective flotation of fossil resin from western coal* No. DOE/PC/90178--T8). Pittsburgh ,U.S: U.S Department of Energy, Pittsburgh Energy Technology Center.

Jia, R., Harris, G. H., & Fuerstenau, D. W. (2000). An improved class of universal collectors for the flotation of oxidized and/or low-rank coal. *International Journal of Mineral Processing, 58* (1–4), 99-118.

Jiménez, A., Iglesias, M. J., Laggoun-Défarge, F., & Suárez-Ruiz, I. (1998). Study of physical and chemical properties of vitrinites. inferences on depositional and coalification controls. *Chemical Geology, 150* (3–4), 197-221.

Jin, H., Tong, Z., Schlaberg, H. I., & Zhang, J. (2005). Separation of fine binary mixtures under vibration in a gas-solid fluidized bed with dense medium. *Waste Management and Research, 23* (6), 534-540.

Karas, J., Pugmire, R. J., Woolfenden, W. R., Grant, D. M., & Blair, S. (1985). Comparison of physical and chemical properties of maceral groups separated by density dradient centrifugation. *International Journal of Coal Geology, 5* (4), 315-338.

Karner, F. R., Schobert, H. H., Falcone, S. K., & Benson, S. A. (1986). Elemental distribution and association with inorganic and organic components in North Dakota lignites. Mineral matter and ash in coal. *Developed from a Symposium at the 188th Meeting of the American Chemical Society.* Philadelphia, PA, USA. pp. 70-89.

Kawatra, S. K., & Eisele, T. C. (2001). Froth flotation. *Coal desulfurization: High-efficiency preparation methods* (pp. 124) Taylor & Francis.

Kleijn van Willigen, F., van Ommen, J. R., van Turnhout, J., & van den Bleek, C. M. (2005). Bubble size reduction in electric-field-enhanced fluidized beds. *Journal of Electrostatics, 63* (6-10), 943-948.

Laskowski, J. S. (1993). Frothers and flotation froth. *Mineral Processing and Extractive Metallurgy Review, 12* (1), 61-89.

Liu, D., Somasundaran, P., Vasudevan, T. V., & Harris, C. C. (1994). Role of pH and dissolved mineral species in pittsburgh no. 8 coal flotation system — I. floatability of coal. *International Journal of Mineral Processing, 41* (3–4), 201-214.

Luo, Z., Zhao, Y., Chen, Q., Fan, M., & Tao, X. (2002). Separation characteristics for fine coal of the magnetically fluidized bed. *Fuel Processing Technology, 79* (1), 63-69.

Luo, Z., Zhao, Y., Chen, Q., Tao, X., & Fan, M. (2004). Effect of gas distributor on performance of dense phase high density fluidized bed for separation. *International Journal of Mineral Processing, 74* (1-4), 337-341.

Luo, Z., Zhao, Y., Tao, X., Fan, M., Chen, Q., & Wei, L. (2003). Progress in dry coal cleaning using air-dense medium fluidized beds. *International Journal of Coal Preparation and Utilization, 23* (1-2), 13-20.

Luo, Z, Zhu, J., Fan, M.., Zhao, Y., & Tao, X. (2007). Low density dry coal beneficiation using an air dense medium fluidized bed. *Journal of China University of Mining and Technology, 17* (3), 306-309.

Mackowsky, M. (1983). Application Of Coal Petrology. *ICAM 81: Proceedings of the First International Congress on Applied Mineralogy.* Johannesburg, S Afr. (7) pp. 97-109.

Mak, C. (2007). Fine coal cleaning using an air dense medium fluidized bed. (M.Sc., University of Alberta (Canada)) , 106.

Mak, C., Choung, J., Beauchamp, R., Kelly, D. J. A., & Xu, Z. (2008). Potential of air dense medium fluidized bed separation of mineral matter for mercury rejection from alberta sub-bituminous coal,international journal of coal preparation and utilization.*28* (2), 115-132.

Miller, B. G. (2010). In Miller B. G. (Ed.), *Clean coal engineering technology* Elsevier.

Miller, J. D., Jensen, G. F., Yu, Q., & Yea, Y. (1992). *Selective flotation of fossil resins from western coals* No. DE-ACE907822-9OPC90178)U.S. Department of Energy.

Mohns, C. A. (1998). Effect of particle size on coal flotation kinetics. (M.Sc., Queen's University at Kingston (Canada)). *ProQuest Dissertations and Theses*,

Naik, P. K., Reddy, P. S. R., & Misra, V. N. (2005). Interpretation of interaction effects and optimization of reagent dosages for fine coal flotation. *International Journal of Mineral Processing, 75* (1-2), 83-90.

Natural Resources Canada. (2010). *About coal.* http://www.nrcan.gc.ca/energy/sources/

Nicholls, G. D. (1968). The geochemistry of coal-beuing strata. *Coal and coal-bearing strata,* (Murchison, D. and Westall, TS., Editors, Oliver md Boyd, La- don, ed., pp. 269-307). London: Oliver ANd Boyd.

Ofori, P., Firth, B., Obrien, G., McNally, C., & Nguyen, A. V. (2010). Assessing the hydrophobicity of petrographically heterogeneous coal surfaces. *Energy and Fuels, 24* (11), 5965-5971.

Pearson, D. E., & Price, J. T. (1985). Reactivity of inertinite (coal typing) of western Canadian coking coal. *Proceedings - 1985 International Conference on Coal Science.* Sydney, Aust. pp. 907-908.

Piñeres, J., & Barraza, J. (2011). Energy barrier of aggregates coal particle-bubble through the extended DLVO theory. *International Journal of Mineral Processing, 100* (1-2), 14-20.

Piñeres, J., & Barraza, J. (2012). Effect of pH, air velocity and frother concentration on combustible recovery, ash and sulphur rejection using column flotation. *Fuel Processing Technology, 97*, 30-37.

Podder, J., Hossain, T., & Mannan, K. M. (1995). An investigation into the thermal behaviour of bangladeshi coals. *Thermochimica Acta, 255* (0), 221-226.

Polat, M., Polat, H., & Chander, S. (2003). Physical and chemical interactions in coal flotation. *International Journal of Mineral Processing, 72* (1–4), 199-213.

Powell, M. A. (1987). *The inorganic geochemistry of two U.S coals, emery coal field, Utah and Powder River field, Wyoming*. Unpublished PhD, University of Western Ontario, London,Ontario.

Prashant, D., Xu, Z., Szymanski, J., Gupta, R., & Boddez, J. (2010). Dry cleaning of coal by a laboratory continuous air dense medium fluidized bed separator. *16th International Coal Preparation Congress, ICPC 2010*, Lexington, KY. pp. 608-616.

Ryan, B. D., & Grieve, D. A. (1996). Source and distribution of phosphorus in british columbia coal seams. *Geological Fieldwork, 1*, 277-294.

Sahu, A. K., Biswal, S. K., & Parida, A. (2009). Development of air dense medium fluidized bed technology for dry beneficiation of coal - A review. *International Journal of Coal Preparation and Utilization, 29* (4), 216-241.

Sahu, A. K., Tripathy, A., Biswal, S. K., & Parida, A. (2011). Stability study of an air dense medium fluidized bed separator for beneficiation of high-ash indian coal. *International Journal of Coal Preparation and Utilization, 31* (3-4), 127-148.

Schapiro, N., & Gray, R. J. (1964). The use of coal petrography in coke making. *Journal of the Institute of Fuel, 37*, 232-242.

Stepanov, Y. V., Gilyazetdinov, R. R., Popova, N. K., & Makhortova, L. A. (2005). Influence of composition of coal materials on coke quality. *Koks i Khimiya,* (7), 14-18.

Strassburger, J.H. (1969). Blast furnace - Theory and practice. (pp.337). New York: Gordon and Breach Science Publishers

Suárez-Ruiz, I., & Crelling, J. C. (2008). In Suárez-Ruiz I., Crelling J. C. (Eds.), *Applied coal petrology: The role of petrology in coal utilization* Academic Press.

Swaine, D. J. (1990). *Trace elements in coal*. London: Butterworths.

Thomas, L. (2002). Coal geology. (pp. 95) John Wiley & sons Ltd.

Tillman, D., Duong, D., & Harding, N. S. (2012). *Solid fuel blending: Principles, practices, and problems* Elsevier.

U.S Energy Information Adminstration. (2011). *International energy outlook 2011,coal section* No. DOE/EIA-0484(2011))

Van Houwelingen, J. A., & De Jong, T. P. R. (2004). Dry cleaning of coal: Review, Fundamentals and Opportunities. *GEOLOGICA BELGICA, 7* (3-4), 353-343.

Ward, C. R., Corcoran, J. F., Saxby, J. D., & Read, H. W. (1996). Occurrence of phosphorus minerals in australian coal seams. *International Journal of Coal Geology, 30* (3), 185-210.

Ward, C. (Ed.). (1984). *Coal geology and coal technology* (1st ed.) Blackwell Scientific.

Wei, L., Chen, Q., & Zhao, Y. (2003). Formation of double-density fluidized bed and application in dry coal beneficiation. *Coal Preparation: A Multinational Journal, 23* (1-2), 21-32.

Xu, Z., & Yoon, R. (1989). The role of hydrophobia interactions in coagulation. *Journal of Colloid and Interface Science, 132* (2), 532-541.

Xu, Z., & Yoon, R. (1990). A study of hydrophobic coagulation. *Journal of Colloid and Interface Science, 134* (2), 427-434.

Yang, D. C. (1990). Packed-bed column flotation of fine coal. PartII. technical — economic feasibility and scale-up Considerations. *Coal Preparation, 8* (1-2), 37.

Yu, Q., Bukka, K., & Miller, J. D. (1994). Chemistry of ozone conditioning in the selective flotation of macroscopic fossil resin from utah wasatch plateau coal. *Coal Preparation, 15* (1-2), 35-50.

Zhenfu, L., & Qingru, C. (2001a). Dry beneficiation technology of coal with an air dense-medium fluidized bed. *International Journal of Mineral Processing, 63* (3), 167-175.

Zhenfu, L., & Qingru, C. (2001b). Effect of fine coal accumulation on dense phase fluidized bed performance. *International Journal of Mineral Processing, 63* (4), 217-224.

Zhou, G. (1986). Continuous electrostatic beneficiation and surface conditioning of coal. (Ph.D., The University of Western Ontario (Canada)).

Zhou, Z. (1996). Gas nucleation and cavitation in flotation. (Ph.D., McGill University (Canada)). , 210.

Appendixes

Appendix A

Table A.1. Sink-float data for 1.00 - 2.36 mm size fraction-Fording River sample

Density (g/cc)	1.40	1.44	1.58	1.78	1.98	1.98 (sink)
Yield (wt.%)	7.10	36.99	26.60	18.52	3.29	7.50
Cumulative yield (wt.%)	7.10	44.09	70.69	89.21	92.50	100.00
Ash content (wt.%)	1.55	1.83	8.22	22.38	37.8	72.88
Cumulative ash content (wt.%)	1.55	1.78	4.20	7.97	9.03	13.82

Table A.2. Sink-float data for 2.36 - 3.35 mm size fraction-Fording River sample

Density (g/cc)	1.40	1.44	1.58	1.78	1.98	1.98 (sink)
Yield (wt.%)	3.33	32.10	35.04	16.61	3.06	9.86
Cumulative yield (wt.%)	3.33	35.43	70.47	87.08	90.14	100.00
Ash content (wt.%)	1.74	2.12	9.12	23.49	37.88	73.14
Cumulative ash content (wt.%)	1.74	2.08	5.58	8.99	9.97	16.02

Table A.3. Sink-float data for 3.35 - 4.75 mm size fraction-Fording River sample

Density (g/cc)	1.40	1.44	1.58	1.78	1.98	1.98 (sink)
Yield (wt.%)	1.34	31.80	39.70	14.80	2.70	11.00
Cumulative yield (wt.%)	1.34	31.80	71.50	86.30	89.00	100.00
Ash content (wt.%)	1.88	2.49	9.04	23.16	39.30	75.11
Cumulative ash content (wt.%)	1.88	2.56	6.16	9.07	9.14	17.15

Air dense medium fluidized bed (H = 20 cm)-Fording River sample

Table A.4. ADMFB tests data for 1.00 - 2. 36 mm size fraction-H = 20 cm-Fording River sample

Bed layer	Yield (wt.%)	Cumulative yield (wt.%)	Ash content (wt.%)	Cumulative ash content (wt.%)
H*(top 2 cm)	45.33	45.33	7.45	7.45
H1(top 5 cm)	67.42	67.42	8.19	8.19
H2	16.96	84.38	15.98	9.76
H3	13.78	98.16	35.15	13.32
H4	1.84	100	63.42	14.14

Table A.5. ADMFB tests data for 2.36 - 3.35 mm size fraction-H = 20 cm-Fording River sample

Bed layer	Yield (wt.%)	Cumulative yield (wt.%)	Ash content (wt.%)	Cumulative ash content (wt.%)
H*(top 2 cm)	33.18	38.18	7.44	7.44
H1(top 5 cm)	47.74	47.74	9.00	9.00
H2	33.06	80.80	12.40	10.39
H3	14.78	95.58	24.30	12.54
H4	4.42	100.00	81.24	15.60

Table A.6. ADMFB tests data for 3.35 - 4.75 mm size fraction-H = 20 cm-Fording River sample

Bed layer	Yield (wt.%)	Cumulative yield (wt.%)	Ash content (wt.%)	Cumulative ash content (wt.%)
H*(top 2 cm)	21.12	21.12	7.03	7.03
H1(top 5 cm)	33.37	33.37	8.15	8.15
H2	36.37	69.74	9.66	8.94
H3	10.68	80.42	15.02	9.75
H4	19.58	100.00	53.30	17.27

Air dense medium fluidized bed (H = 30cm) -Fording River sample

Table A.7. ADMFB tests data for 1.00 - 2.36 mm size fraction-H = 30cm-Fording River sample

Bed layer	Yield (wt.%)	Cumulative yield (wt.%)	Ash content (wt.%)	Cumulative ash content (wt.%)
H*(top 2 cm)	29.44	29.44	7.40	7.40
H1(top 5 cm)	53.68	53.68	8.26	8.26
H2	25.92	79.60	14.07	10.15
H3	12.69	92.29	18.65	11.32
H4	3.65	95.94	20.73	11.68
H5	2.06	98.00	37.86	12.23
H6	2.00	100.00	75.70	13.50

Table A.8. ADMFB tests data for 2.36 - 3.35 mm size fraction-H = 30cm -Fording River sample

Bed layer	Yield (wt.%)	Cumulative yield (wt.%)	Ash content (wt.%)	Cumulative ash content (wt.%)
H*(top 2 cm)	25.42	25.42	8.20	8.20
H1(top 5 cm)	45.70	45.70	9.05	9.05
H2	18.93	64.63	13.30	10.29
H3	21.86	86.49	18.20	12.29
H4	8.04	94.53	29.50	13.76
H5	3.23	97.76	33.77	14.42
H6	2.24	100.00	73.49	15.74

Table A.9. ADMFB tests data for 3.35 - 4.75 mm size fraction-H = 30cm -Fording River sample

Bed layer	Yield (wt.%)	Cumulative yield (wt.%)	Ash content (wt.%)	Cumulative ash content (wt.%)
H*(top 2 cm)	23.85	23.85	7.30	7.30
H1(top 5 cm)	38.15	38.15	8.57	8.57
H2	23.64	61.79	15.22	11.11
H3	17.69	79.48	18.20	12.69
H4	14.22	93.70	24.42	14.47
H5	3.49	97.19	40.40	15.40
H6	2.81	100.00	74.70	17.07

Air dense medium fluidized bed (T=8 minutes)-Fording River sample

Table A.10. ADMFB tests data for 1.00 - 2.36 mm size fraction-T = 8 minutes -Fording River sample

Bed layer	Yield (wt.%)	Cumulative yield (wt.%)	Ash content (wt.%)	Cumulative ash content (wt.%)
H1(top 5 cm)	55.91	55.91	10.15	10.15
H2	15.82	71.73	12.3	10.62
H3	23.29	95.02	17.5	12.31
H4	4.98	100.00	34.7	13.42

Table A.11. ADMFB tests data for 2.36 - 3.35 mm size fraction-T = 8 minutes -Fording River sample

Bed layer	Yield (wt.%)	Cumulative yield (wt.%)	Ash content (wt.%)	Cumulative ash content (wt.%)
H1(top 5 cm)	34.14	34.14	10.02	10.02
H2	20.25	54.39	17.72	12.89
H3	21.28	75.67	13.09	12.94
H4	24.33	100.00	23.76	15.58

Table A.12. ADMFB tests data for 3.35 - 4.75 mm size fraction-T = 8 minutes -Fording River sample

Bed layer	Yield (wt.%)	Cumulative yield (wt.%)	Ash content (wt.%)	Cumulative ash content (wt.%)
H1(top 5 cm)	22.90	22.90	10.69	10.69
H2	28.48	51.38	16.26	13.78
H3	29.41	80.79	14.98	14.22
H4	19.21	100.00	31.01	17.44

Sink-float data for coarse fractions of Fording River sample

Table A.13. Sink-float data for 4.75 - 13 mm size fraction- Fording River sample

Density (g/cc)	1.44	1.58	1.78	1.98	1.98 (sink)
Yield (wt.%)	28.17	20.71	23.02	6.79	21.31
Cumulative yield (wt.%)	28.17	48.88	71.90	78.69	100.00
Ash content (wt.%)	3.70	12.70	23.65	34.58	74.60
Cumulative ash content (wt.%)	3.70	7.51	12.68	14.57	27.36

Table A.14. Sink-float data for 13 - 25 mm size fraction- Fording River sample

Density (g/cc)	1.44	1.58	1.78	1.98	1.98 (sink)
Yield (wt.%)	17.28	17.51	29.54	6.79	28.88
Cumulative yield (wt.%)	17.28	34.79	64.33	71.12	100.00
Ash content (wt.%)	5.20	16.54	27.31	42.12	71.66
Cumulative ash content (wt.%)	5.20	8.33	17.04	19.44	34.52

Table A.15. Sink-float data for +25 mm size fraction- Fording River sample

Density (g/cc)	1.44	1.58	1.78	1.98	1.98 (sink)
Yield (wt.%)	14.20	19.97	21.12	4.18	40.53
Cumulative yield (wt.%)	14.20	34.17	55.29	59.47	100.00
Ash content (wt.%)	3.44	10.48	20.20	36.13	73.45
Cumulative ash content (wt.%)	3.44	7.55	12.38	14.05	38.13

ADMFB tests for coarse fractions of Fording River sample

Table A.16. ADMFB tests data for 4.75 – 13 mm size fraction- Fording River sample

Bed layer	Yield (wt.%)	Cumulative yield (wt.%)	Ash content (wt.%)	Cumulative ash content (wt.%)
H1(top 5 cm)	24.13	24.13	9.08	9.08
H2	12.65	36.78	10.84	9.68
H3	23.68	60.46	19.43	13.50
H4	39.54	100.00	45.95	26.33

Table A.17. ADMFB tests data for 13 - 25 mm size fraction- Fording River sample

Bed layer	Yield (wt.%)	Cumulative yield (wt.%)	Ash content (wt.%)	Cumulative ash content (wt.%)
H1(top 5 cm)	18.65	18.65	6.58	6.58
H2	10.43	29.08	19.14	11.08
H3	23.32	52.40	26.10	17.77
H4	47.60	100.00	52.27	34.19

Table A.18. ADMFB tests data for +25 mm size fraction- Fording River sample

Bed layer	Yield (wt.%)	Cumulative yield (wt.%)	Ash content (wt.%)	Cumulative ash content (wt.%)
H1(top 5 cm)	16.30	16.30	4.71	4.71
H2	16.47	32.77	7.69	6.20
H3	5.77	38.54	27.67	9.42
H4	61.46	100.00	56.26	38.21

Sink-float data for Coal Mountain Operation sample

Table A.19. Sink-float data for 1 - 2 mm size fraction- Coal Mountain Operation sample

Density (g/cc)	1.40	1.50	1.60	1.60 (sink)
Yield (wt.%)	38.44	24.10	10.17	27.29
Cumulative yield (wt.%)	38.44	62.54	72.71	100.00
Ash content (wt.%)	8.25	18.28	28.26	61.03
Cumulative ash content (wt.%)	8.25	12.10	14.52	27.00

Table A.20. Sink-float data for 2 - 13 mm size fraction- Coal Mountain Operation sample

Density (g/cc)	1.40	1.50	1.60	1.60 (sink)
Yield (wt.%)	37.26	16.86	7.19	38.69
Cumulative yield (wt.%)	37.62	54.12	61.31	100.00
Ash content (wt.%)	8.87	17.96	32.36	66.70
Cumulative ash content (wt.%)	8.87	11.70	14.12	34.46

Table A.21. Sink-float data for 13 - 25 mm size fraction- Coal Mountain Operation sample

Density (g/cc)	1.40	1.50	1.60	1.60 (sink)
Yield (wt.%)	21.17	11.04	7.65	62.36
Cumulative yield (wt.%)	21.17	32.21	39.86	100.00
Ash content (%)	8.41	17.92	28.18	63.84
Cumulative ash content (wt.%)	8.41	11.66	14.05	46.12

Table A.22. Sink-float data for +25 mm size fraction- Coal Mountain Operation sample

Density (g/cc)	1.40	1.50	1.60	1.60 (sink)
Yield (wt.%)	13.17	9.99	9.03	67.81
Cumulative yield (wt.%)	13.17	23.16	32.19	100.00
Ash content (wt.%)	8.23	19.19	29.93	64.43
Cumulative ash content (wt.%)	8.23	12.95	17.71	49.39

ADMFB tests for different size fractions of Coal Mountain Operation sample

Table A.23. ADMFB tests data for 1 - 2 mm size fraction- Coal Mountain Operation sample

Bed layer	Yield (%)	Cumulative yield (%)	Ash content (%)	Cumulative ash content (%)
H1(top 5 cm)	36.45	36.45	11.69	11.69
H2	21.91	58.36	23.12	15.98
H3	11.96	70.32	28.8	18.16
H4	29.68	100.00	47.43	26.85

Table A.24. ADMFB tests data for 2 - 13 mm size fraction- Coal Mountain Operation sample

Bed layer	Yield (wt.%)	Cumulative yield (wt.%)	Ash content (wt.%)	Cumulative ash content (wt.%)
H1(top 5 cm)	31.64	31.63	11.49	11.49
H2	25.88	57.52	20.82	15.68
H3	15.54	73.06	34.30	19.64
H4	26.94	100.00	73.68	34.20

Table A.25. ADMFB tests data for 13 - 25 mm size fraction- Coal Mountain Operation sample

Bed layer	Yield (wt.%)	Cumulative yield (wt.%)	Ash content (wt.%)	Cumulative ash content (wt.%)
H1(top 5 cm)	21.24	21.24	9.13	9.13
H2	12.58	33.82	17.52	12.25
H3	3.31	38.13	28.47	17.31
H4	61.87	100.00	65.55	45.92

Table A.26. ADMFB tests data for +25 mm size fraction- Coal Mountain Operation sample

Bed layer	Yield (wt.%)	Cumulative yield (wt.%)	Ash content (wt.%)	Cumulative ash content (wt.%)
H1(top 5 cm)	17.25	17.25	8.45	8.45
H2	5.67	22.92	21.96	12.21
H3	22.74	45.66	41.30	26.06
H4	54.34	100.00	69.49	49.68

Table A.27 Reactive portion* of raw and clean coal for ADMFB tests in different size fractions of Coal Mountain Operation sample

Size fraction (mm)	1 – 2	2 – 13	13 - 25	+25
Separating density of clean coal ($g.cm^{-3}$)	1.49	1.50	1.52	1.50
Raw coal reactive components (wt.%)	52.80**	48.20	48.00	49.50
Clean coal reactive components (wt.%)	62.00	56.40	57.30	51.60

*Reactive portion is the summation of liptinite, vitrinite and inert semi-fusinite macerals in coal. **Due to lack of raw sample data for 1 – 2 mm size fraction, the 0.7 – 2 mm size fraction data (given by TECK) has been used as the nearest approximation.

Appendix B

Denver cell flotation tests

Table B.1 Denver cell froth flotation for fine fractions-Fording River sample

Size fraction (μm)	pH	Yield (%)	Froth Ash content (%)	Tailing ash content (%)
-75	7	97.0	9.12	13.44
	8	91.0	7.82	17.96
	9	72.4	5.60	21.03
	11	67.2	4.38	24.10
75 – 212	7	86.5	6.93	18.33
	8	81.1	5.91	19.03
	9	74.6	4.86	22.51
	11	72.5	2.59	25.88
212 – 425	7	80.9	5.73	22.82
	8	79.1	5.41	23.43
	9	77.9	4.38	26.61
	11	73.9	3.68	29.87
425 - 600	7	55.4	8.10	13.20
	9	48.2	7.36	13.56

Table B.2 Effect of pH change on phosphorus rejection-Fording River

Size fraction(μm)	Raw sample phosphorus content (%)	pH	Froth phosphorus content (%)	Froth yield (wt.%)	Phosphorus rejection (%)
-75	0.18	7	0.12	97.0	35.33
		8	0.08	91.0	59.56
		9	0.06	72.4	75.87
		11	0.06	67.2	77.60
75 - 212	0.17	7	0.08	86.5	59.29
		9	0.07	74.6	69.28
		11	0.06	72.5	74.41
212 - 425	0.17	7	0.07	80.9	66.66
		9	0.06	77.9	72.51
		11	0.06	73.9	72.48

Table B.3 Maceral distribution of raw sample and froth for flotation tests fine fractions - Coal Mountain Operation sample

Size fraction (μm)	Sample	Vitrinite (wt.%)	Liptinite (wt.%)	Inertinite (wt.%)	Mineral matter (wt.%)
75 - 212	Raw	35.5	-	-	12.11
	Froth	49.80	0.20	42.30	7.70
212 - 425	Raw	34.00	-	-	12.21
	Froth	47.00	1.50	46.00	5.50

Appendix C

Air dense medium fluidized bed (feed coal load = 100 g, T=3 minutes) - Fording River

Table C.1. 1.00 – 2.36 mm size fraction

Bed layer	Yield (wt.%)	Cumulative yield (wt.%)	Ash content (wt.%)	Cumulative ash content (wt.%)
H*(top 2 cm)	36.48	36.48	7.33	7.33
H1(top 5 cm)	19.69	56.17	9.63	8.13
H2	24.12	80.29	13.20	9.66
H3	18.51	98.80	30.86	13.63
H4	1.20	100.00	69.33	14.29

Table C.2. 2.36 – 3.35 mm size fraction

Bed layer	Yield (wt.%)	Cumulative yield (wt.%)	Ash content (wt.%)	Cumulative ash content (wt.%)
H*(top 2 cm)	26.7	26.70	7.05	7.05
H1(top 5 cm)	18.42	45.12	12.12	9.11
H2	32.61	77.73	12.38	10.48
H3	13.28	91.01	26.70	12.83
H4	8.99	100	44.24	15.60

Table C.3. 3.35 – 4.75 mm size fraction

Bed layer	Yield (wt.%)	Cumulative yield (wt.%)	Ash content (wt.%)	Cumulative ash content (wt.%)
H*(top 2 cm)	21.3	21.30	5.75	5.75
H1(top 5 cm)	13.17	34.47	12.65	8.36
H2	25.38	59.85	10.10	9.05
H3	28.57	88.42	21.21	13.02
H4	11.58	100.00	49.78	17.27

Flotation kinetics study

Table.C.4. Flotation kinetic results for Fording River sample

Size fraction (µm)	Time (s)	Weight (g)	Weight. %	Cum wt%	Ash (wt.%)	Cum.ash (wt.%)
75 - 212	50	5.4	10.8	10.8	1.70	1.70
	100	5.1	10.2	21.0	2.60	2.14
	200	5.0	10	31.0	3.86	2.69
	400	6.9	13.8	44.8	4.62	3.29
	800	5.7	11.4	56.2	6.41	3.92
	1600	11.9	23.8	80.0	12.55	6.49
212 - 425	50	9.3	18.6	18.6	2.03	2.03
	100	4.1	8.2	26.8	2.85	2.28
	200	6.6	13.2	40.0	3.31	2.62
	400	5.5	11.0	51.1	5.42	3.22
	800	4.05	8.1	59.1	10.55	4.22
	1600	8.28	16.6	75.7	12.31	5.99

Table.C.5. Flotation kinetics results for Coal Mountain Operation sample

Size fraction (µm)	Time (s)	Froth weight (g)	Froth weight. %	Froth cumulative wt%	Froth Ash content (wt.%)	Cum.ash (wt.%)
75 - 212	50	6.3	12.6	12.6	11.9	11.9
	100	6.3	12.6	25.2	12.3	12.1
	200	8.6	17.2	42.4	15.2	13.36
	400	9.3	18.6	61.0	17.9	14.74
	800	1.6	3.2	64.2	18.0	14.90
	1600	9.22	18.44	82.64	24.6	17.07
212 - 425	50	7.3	14.6	14.6	8.3	8.3
	100	5.6	11.2	25.8	8.6	8.43
	200	12.1	24.2	50.0	9.3	8.85
	400	2.4	4.7	54.7	14.8	9.36
	800	2.8	5.6	60.3	18.2	10.19
	1600	0	0	60.3	0	10.19